The Simple Biosphere Model Version 4.2: SiB4

Technical Description

Katherine Haynes, Ian Baker, Scott Denning

Colorado State University
Fort Collins, Colorado
February 2020

Contents

List of Figures

List of Tables

1 Introduction

1.1 Overview

The Simple Biosphere Model Version 4 (SiB4) is a mechanistic, prognostic land surface model (LSM) that integrates heterogeneous land cover, environmentally responsive prognostic phenology, dynamic carbon allocation, and cascading carbon pools from live biomass to surface litter to soil organic matter (Haynes et al., 2019a; Baker et al., 2013; Lokupitiya et al., 2009; Sellers et al., 1996a). By combining biogeochemical, biophysical, and phenological processes, SiB4 predicts vegetation and soil moisture states, land surface energy and water budgets, and the terrestrial carbon cycle. Rather than relying on satellite data, SiB4 fully simulates the terrestrial carbon cycle by using the carbon fluxes to determine the above and belowground biomass, which in turn feeds back to impact carbon assimilation and respiration.

Every timestep (currently 10-minutes), SiB4 computes the terrestrial albedo, radiation budget, hydrological cycle, layered temperatures, and soil moisture, as well as the resulting energy exchanges, moisture fluxes, carbon fluxes, and carbon pool transfers. Photosynthesis depends directly on environmental factors (humidity, moisture, and temperature) and aboveground biomass; and carbon uptake is determined using enzyme kinetics (Farquhar et al., 1980) and stomatal physiology (Collatz et al., 1991, 1992). Carbon release occurs from autotrophic and heterotrophic respiration. Biomass growth and maintenance contribute to autotrophic respiration, and heterotrophic respiration depends on moisture, temperature, and the amount of dead plant material in the surface and soil carbon pools.

To calculate the carbon pools, the net assimilated carbon is allocated to the live pools. The phenology stage, combined with temperature and moisture environmental adjustments, dictates the fraction of carbon allocated to each live carbon pool. Carbon is transferred between the pools using totals of sub-hourly (timestep) amounts that vary with assimilation rate, day length, moisture, temperature, and pool size. Once the pools are updated, the land surface state and relative properties are revised; and the new values are used for assimilation and respiration, completing the carbon cycle and providing self-consistent predicted vegetation states, soil hydrology, carbon pools, and land-atmosphere exchanges.

SiB4 has been evaluated around the globe using a variety of metrics, including carbon and energy fluxes from the Fluxnet network, satellite solar-induced fluorescence (SIF) and soil moisture, and both remotely-sensed and site-level leaf area index (LAI) and biomass (Cheeseman et al., 2018; Curry et al., 2016; Haynes et al., 2019b; Smith et al., 2018). SiB4 is found to improve model predictions over grasslands, and the start of the growing season is well-captured across all vegetation types. In these studies, SiB4 is shown to have too long of a growing season compared to observations, with senescence being delayed by several weeks in some locations. In response to these findings, new respiration and transfer methods described in this document are expected to improve senescence predictions.

1.2 History

Over the past three decades, SiB has undergone substantial developments and improvements. SiB began as a simple but realistic biosphere model developed for calculating the transfer of energy, mass, and momentum between the land vegetation and the atmosphere (Sellers et al., 1986). The original land-surface parameterization scheme utilized two distinct vegetation layers with prescribed physical and physiological properties; and the model had seven prognostic physical-state variables: two temperatures, two interception water stores, and three soil moisture stores. The framework of SiB is shown in Figure 1.1, which illustrates the transfer pathways for latent and sensible heat flux. This version was coupled to general circulation models to improve their lower boundary conditions (Sato et al., 1989a).

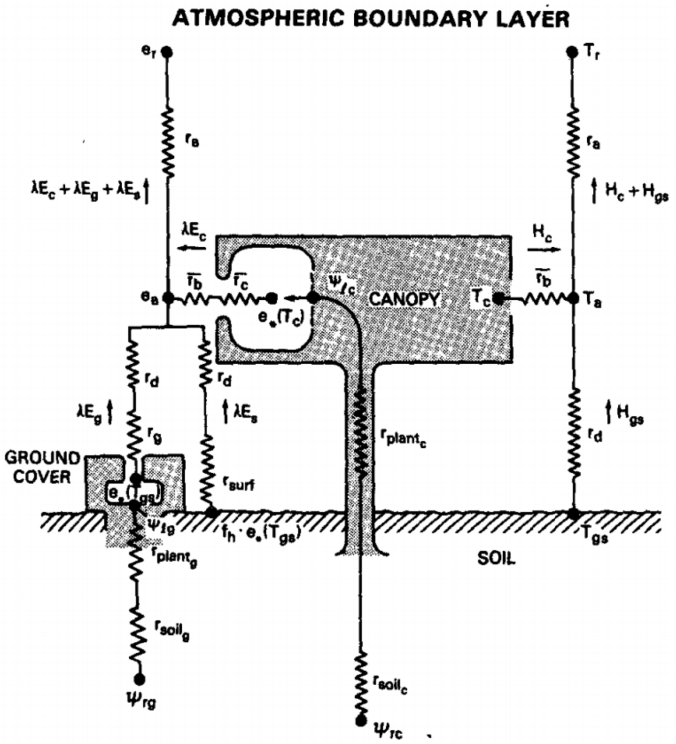

Figure 1.1: Framework of the Simple Biosphere Model (SiB) (Sellers et al., 1986). The transfer pathways for latent and sensible heat flux are shown on the left- and right-hand side of the diagram, respectively. Radiation and intercepted water treatment is omitted for clarity.

The first significant modification to SiB was to add ecosystem metabolism and satellite data to produce a more realistic model of photosynthesis and canopy conductance (SiB2) (Sellers et al., 1996a; Sellers et al, 1996b). The SiB2 structure is shown in Figure 1.2. To provide a consistent description of energy exchange, evapotranspiration, and carbon exchange by plants, SiB uses eco-physiological functionality to utilize photosynthesis and plant water relationships (Sellers et al., 1997). The prediction of photosynthetic carbon assimilation uses enzyme kinetics relationships developed by Farquhar et al. (1980). The vegetation behavior is coupled to the surface energy budget via predicted stomatal conductance using the Ball-Berry equation (Collatz et al., 1991, 1992; Randall et al., 1996; Sellers et al., 1996a). The leaf-level

predictions are integrated to represent vegetation canopies using satellite data (Sellers et al, 1996b). Remotely sensed vegetation indices specify time-varying phenological properties, and these data are converted to leaf physiological properties utilized by SiB from robust theoretical relationships (Sellers et al., 1992). The SiB2 carbon fluxes are annually balanced so that the annual soil respiration equals the annual carbon uptake from photosynthesis, with temporal variability in soil respiration arising from respiration rate dependencies on both temperature and moisture (Denning et al., 1996a; Raich & Nadelhoffer, 1989).

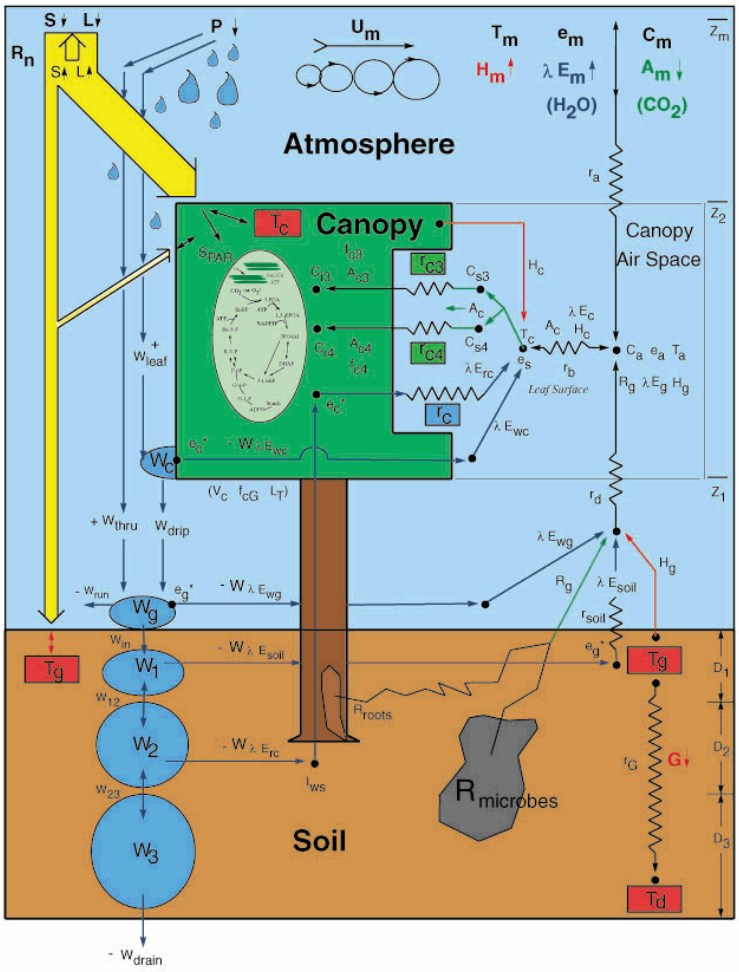

Figure 1.2: SiB2 (Sellers et al., 1996a).

Building on SiB2, a number of modifications were added to create SiB3. For more realistic flux calculations, the surface energy budget was revised to include prognostic temperature, moisture, and CO_2 in the canopy air space (CAS) (Vidale & Stöckli, 2005). Model hydrology was improved by adopting the Community Land Model soil/snow sub-model, where soil temperature and moisture are calculated for ten co-located soil layers and up to five snow layers (Dai et al., 2003). All snow and soil layers have explicit treatment of liquid water and ice, and the root profile in the soil is dependent upon vegetation type and exponentially decreases from the surface down to the bottom soil layer (Jackson et al., 1996). Finally, Suits et al. (2005) added the capability to model carbon isotope discrimination, biogeochemical

fractionation, and the recycling of stable carbon isotopes. An updated depiction of SiB3 is shown in Figure 1.3.

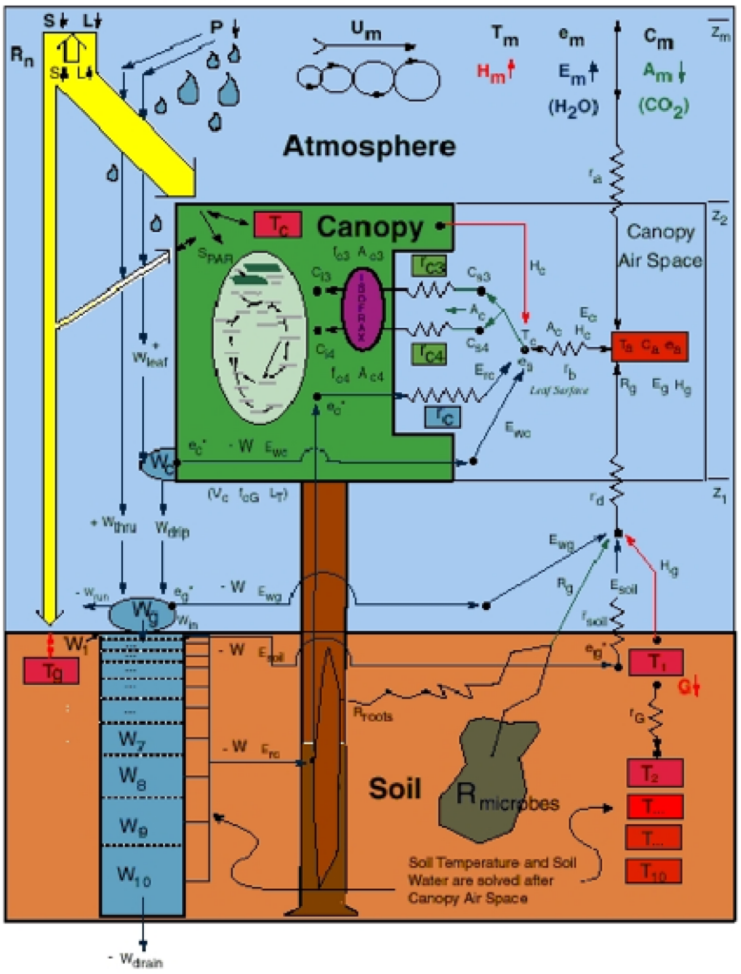

Figure 1.3: SiB3.

For SiB3, three important changes were made to improve the photosynthesis. First, to simulate a more realistic response of photosynthesis to drought, the soil water stress was modified to link the water stress to an effective root density (Baker et al., 2008, 2013). The transpirational load shifting to deep layers when the surface layers dry out is simulated by directly calculating the stress for each soil layer using volumetric water content scaled between field capacity and wilting point. The total water stress is then calculated by weighting the stress at each layer by the corresponding rooting fraction. Second, to include a photosynthetic response to frost, the temperature stress was modified to include a simple approximation of frost stress (Baker, 2011). And third, respiration was partitioned into autotrophic and heterotrophic components to help improve the annual cycle of carbon uptake and release (Schaefer et al., 2002).

As SiB developed, it branched out to different versions that each added new modeling capabilities to address concerns and uncertainties in the carbon cycle. The first concern, and one of the most variable aspects of the carbon cycle, is the timing of carbon uptake

and release. Plant physiological processes control vegetation phenology, and these processes depend on surface climatic conditions such as temperature, moisture and light (Larcher, 2002; Scheifinger et al., 2002). Seasonal and interannual climatic variations influence the timing of plant development, which in turn influences the temporal variability in ecosystem productivity (Baldocchi & Wilson, 2001; Richardson et al., 2010). Prognostic phenology models, which predict the timing of phenological events, can be used to investigate the relationship between climate variables, plant development, and carbon fluxes, in addition to providing continuous estimates of the biophysical state (Jolly et al., 2005; Stöckli et al., 2008).

To address this concern, a branch of SiB added the capability to predict vegetation phenology and leaf state, rather than relying on satellite products (SiBPP) (Stöckli et al., 2008, 2011). SiBPP predicts the growing season timing, as well as the leaf area index (LAI), using a combination of three climate and weather based factors: temperature, light and water vapor. Optimal parameters for the growth-determinant factors were obtained by using a data assimilation framework to perform a reanalysis of remotely sensed global vegetation phenology. SiBPP removes the dependency on satellite data and is a first step to mitigating some deficiencies of phenological models, providing a useful tool in understanding the processes controlling phenology.

Another highly variable aspect of the terrestrial carbon cycle is the magnitude of the fluxes, which is controlled not only by biological and physical processes, but also by the plant biomass and carbon pools. The assimilation of carbon by photosynthesis is directly related to the size of the leaf pool, and the release of carbon by respiration is directly related to the magnitudes of the carbon pools. Without including carbon pools, the magnitude of the leaf pool is typically prescribed from vegetation indices, such as the LAI or normalized vegetation difference index (NDVI) (Huntzinger et al., 2012). For respiration, if the carbon pools are not explicitly calculated, then models typically annually balance the carbon fluxes, making the assumption that on an annual basis the carbon released from respiration equals the carbon taken up during photosynthesis (Denning et al., 1996a). Modeling carbon pools is a key requirement for predicting carbon sources and sinks, understanding plant carbon allocation, and investigating the impacts of carbon pool changes due to disturbances such as herbivory, land cover change and fires (Schaefer et al., 2008; Randerson et al., 1996).

To simulate carbon pools in addition to carbon fluxes, a version of SiB has been coupled to the biogeochemistry from the Carnegie-Ames-Stanford Approach (CASA) model (SiB-CASA) (Schaefer et al., 2008, 2009)). SiB-CASA contains a scheme for carbon allocation, transformation and decomposition based on CASA (Potter et al., 1993; Randerson et al., 1996). Carbon from photosynthesis is allocated to live carbon pools (storage, leaves, stems, and roots), with the leaf pool being prognosed from LAI derived from remotely sensed Normalized Difference Vegetation Index (NDVI). Once in live pools, the carbon then flows through a series of dead pools (surface litter, woody debris, root litter, soil organic matter). Throughout this carbon sequence, microbes are interacting with the carbon to release carbon back into the atmosphere via heterotrophic respiration. The biophysical processes on short time timescales from SiB, combined with the biogeochemical processes on longer timeframes from CASA, make SiB-CASA suitable for a variety of research applications to study processes affecting carbon storage and fluxes.

In addition to varying temporally, carbon and energy fluxes and biomass pools vary spatially from different vegetation coverage. Croplands cover a substantial fraction of the land surface area and are significant contributors to spatial heterogeneity because they are managed ecosystems with unique dynamics, characterized by high net primary productivity during a short growing season. To better estimate the time-varying exchanges of carbon, water, and energy for croplands, a version of SiB contains a crop phenology module to specifically simulate corn, soybeans and wheat (SiBcrop) (Lokupitiya et al., 2009). SiBcrop predicts crop phenology using a carbon allocation scheme based on growing degree-days (GDD). In addition to simulating land-atmosphere exchanges for these species, SiBcrop also predicts crop biomass and yield. Modeling specific crops better predicts the onset and end of the growing season, carbon and energy exchanges, and biomass over croplands (Corbin et al., 2010b; Lokupitiya et al., 2009).

Original LSMs have difficulty capturing spatial heterogeneity: they typically have coarse spatial resolution and a single vegetation classification applying to the entire grid cell. The land cover type of each grid cell is chosen from a limited number of vegetation biomes, which include a variety of different species that coexist. As models increase in complexity and shift from global scale to regional and local applications, the use of a single biome over a coarse grid cell becomes limiting. To include land cover heterogeneity, LSMs include surface tiling or patches, offering flexibility in the representation of heterogeneous land surface processes (Avissar & Pielke, 1989; Essery et al., 2002). To capture land cover heterogeneity, a version of SiB coupled to a mesoscale model implemented patches to represent multiple land use classes within a single grid cell (SiB-RAMS) (Corbin et al., 2008; Wang et al., 2007).

To compile the different versions of SiB, incorporate the latest developments in land surface modeling, and innovate a new method for predicting phenology and the terrestrial carbon cycle, the latest version of SiB (SiB4) consistently combines carbon fluxes and carbon pools in a predictive framework. The new features in SiB4 can be summarized as follows:

(i) Using plant functional types (PFTs), (Section 2.2.1),

(ii) Incorporating carbon pools (Section 2.2.3),

(iii) Using patches to represent heterogeneity, (Section 2.2.5),

(iv) Introducing prognostic phenology,
- Dynamic seasonal stages (non-crop PFTs, Section 8)
- Defined seasonal stages (crop PFTs, Section 9)

(viii) Including disturbance,
- Fire (Section 10.1)
- Grazing (Section 10.2)

(v) Adding variable carbon pool allocation (Section 11.1),

(vii) Including new autotrophic respiration processes (Section 11.2),

(vi) Adding litterfall mechanisms (Section 11.3.2), and

(ix) Closing the terrestrial carbon cycle (Section 12).

With these updates, SiB4 uses a single mathematical framework to predict self-consistent land-atmosphere exchanges of carbon, water, energy, radiation, and momentum; carbon storage in cascading pools of biomass and organic matter; water storage in snow and soil column layers; and vegetation properties such as albedo, LAI, and fraction of photosynthetically active radiation (FPAR). An overview of SiB4 is shown in Figure 1.4. While still including the biogeochemical processes shown in Figure 1.3, SiB4 predicts the terrestrial carbon cycle by unifyied fluxes, interactive carbon pools, and prognostic phenology, removing the dependence on remotely-sensed vegetation states. By using a single set of equations to represent ecosystem processes rather than specifying specific vegetation properties, ecosystem characteristics emerge in SiB4, such as co-located vegetation and precipitation gradients and variable root to shoot ratios.

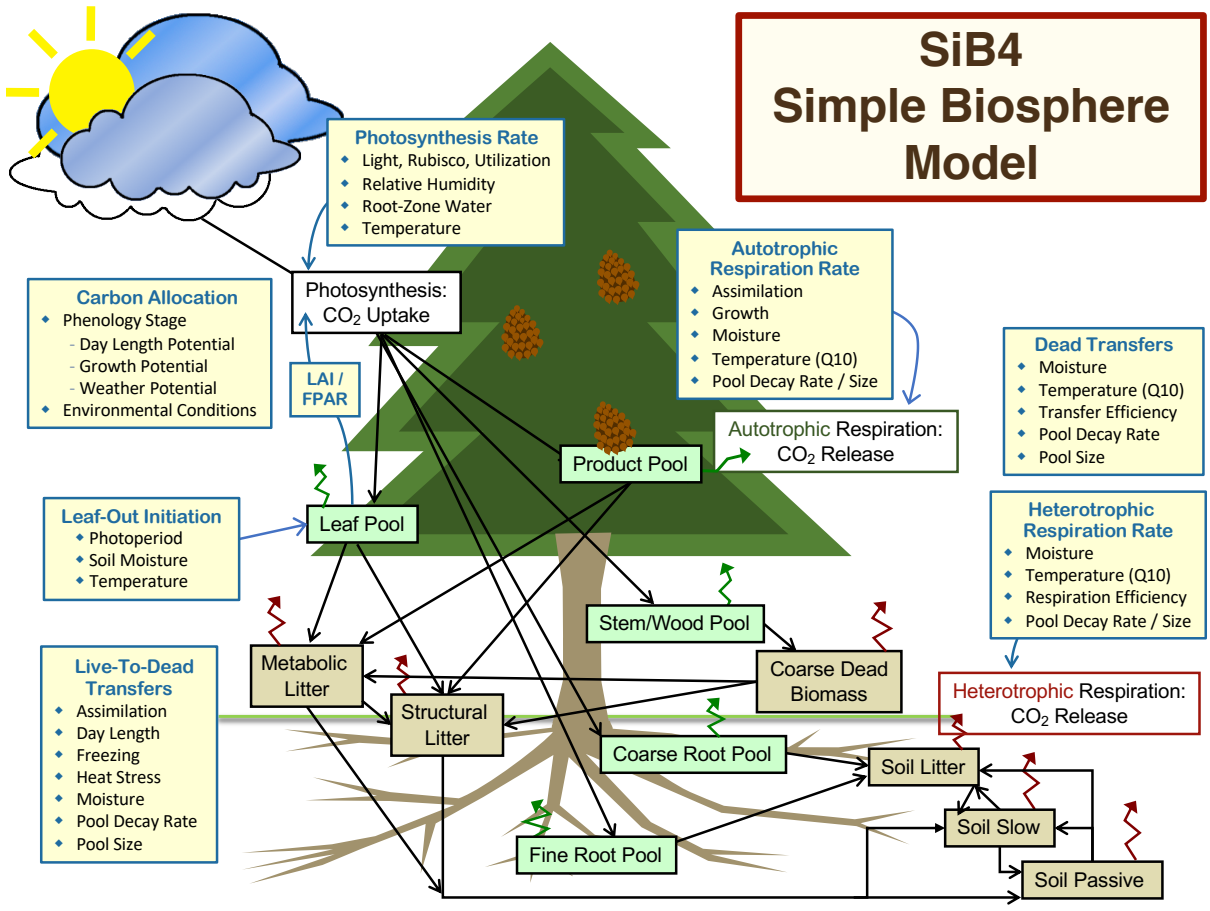

Figure 1.4: SiB4 (Haynes et al., 2019a).
White boxes show the land-atmosphere exchanges of carbon via photosynthesis and respiration. Green boxes show the live carbon pools, tan boxes show the dead carbon pools, and black lines show the flow of carbon. Green lines show the release of carbon into the atmosphere via autotrophic respiration, and burgundy lines show the carbon release from heterotrophic respiration. Yellow boxes show the predominant influences on the carbon fluxes and pools.

1.3 Applications

Since its creation, several different versions of SiB have been developed, and it has been used in a variety of studies across a wide range of spatial and temporal scales. SiB has been implemented into General Circulation Models to predict land surface boundary conditions (Sato et al., 1989a; Randall et al., 1996). In addition to providing surface properties and energy fluxes, SiB has been updated to predict carbon fluxes that can be used to generate atmospheric CO_2 concentrations (Denning et al., 1996a,b); and these resulting atmospheric CO_2 concentrations can be analyzed to reveal processes driving atmospheric CO_2 distributions (Corbin et al., 2008; Denning et al., 1999; Parazoo et al., 2008, 2012). Additionally, global carbon fluxes from SiB have been used as input data for atmospheric inversions aimed at locating and quantifying carbon sources and sinks and improving global carbon budget estimates (Law et al., 2008; Lokupitiya et al., 2008; Patra et al., 2008).

In addition to simulating carbon and energy fluxes, SiB has the capability to simulate other carbon-related constituents that can be used to aid our understanding of biophysical processes. With the capability of simulating carbon isotopes, SiB has been used in global fractionation studies to investigate terrestrial carbon exchange (Suits et al., 2005; Ballantyne et al., 2011; van der Velde et al., 2014). With the capability of simulating carbonyl sulfide (OCS), SiB has been used in global studies to investigate constraints on differential responses of photosynthesis and respiration to environmental forcing (Berry et al., 2013; Glatthor et al., 2015; Kuai et al., 2015; Wang et al., 2016). Finally, with the capability of simulating solar-induced chlorophyll fluorescence (SIF), SiB has been used to investigate the relationship of SIF to gross primary production (GPP) and the utility of SIF to constrain GPP (Baker et al., 2014; Cheeseman et al., 2018).

Scaling down to regional studies, SiB has been used for studying land-atmosphere interactions for a variety of different vegetation types across a wide range of climates. On continental scales, SiB has been used to investigate photosynthesis across North America and Africa (Baker et al., 2010; Williams et al., 2008; Williams & Hanan, 2011). In the tropics, studies have used SiB to investigate tropical forests across a range of hydrological regimes throughout Amazonia (Baker et al., 2008, 2013; Harper et al., 2014). In temperate regions, studies focusing on grasslands and crops across central North America have used SiB to investigate land-atmosphere exchanges of energy and carbon (Hanan et al., 2005; Lokupitiya et al., 2016). And in high latitudes, SiB has been used to study carbon storage and fluxes in permafrost regions (Schaefer et al., 2011; Sulman et al., 2012; Schaefer & Jafarov, 2016).

In addition to being used offline, SiB has also been used in combination with atmospheric transport models. SiB has been coupled to a mesoscale model in order to focus on diurnal and synoptic-scale land-atmosphere interactions, atmospheric circulations, and resulting atmospheric CO_2 concentrations (Denning et al., 2003; Lu et al., 2005; Nicholls et al., 2003; Wang et al., 2007). A regional scale atmosphere-ecosystem model coupled to SiB has also been used to evaluate the space and time impacts on U.S. atmospheric CO_2 concentrations from fossil fuel emissions (Corbin et al., 2010a) and from crops (Corbin et al., 2010b). Finally, SiB has been utilized in conjunction with regional inverse models to obtain regional carbon budgets across the North American mid-continent (Lauvaux et al., 2012; Ogle et al., 2015; Schuh et al., 2013), and in studies investigating North American carbon sources and sinks (Butler et al., 2010; Schuh et al., 2010; Zupanski et al., 2007).

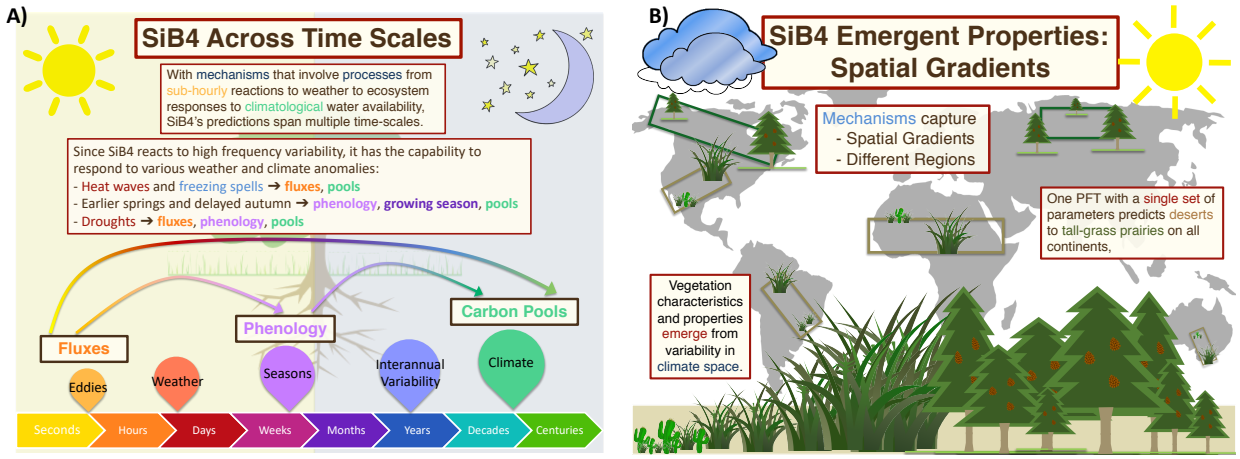

Figure 1.5: Future Applications.
A) Studies across timescales. **B)** Studies across spatial scales.

Combining new innovations with the established photosynthesis, radiation, and hydrology processes, SiB4 is a tool that can be used in a wide variety of studies. Unifying carbon fluxes and pools via phenology not only closes the terrestrial carbon cycle, but also yields predictions that span multiple time scales. Utilizing biogeochemical mechanisms to capture sub-hourly vegetation reactions to weather, phenological mechanisms to capture seasonal behavior, and climatological mechanisms to capture long-term vegetation responses to climate, SiB4 predicts ecosystem behavior across time scales from minutes to centuries (Figure 1.5A). Being a global model that reacts to high frequency variability, SiB4 has the capability to respond to weather and climate anomalies, and thus can be used in studies of the impacts of heat waves, freezing spells, and short-term drought on ecosystems around the world. By using prognostic phenology, SiB4 can be included in growing season length studies to investigate the impact of earlier springs and delayed autumns on ecosystems, including changes in land-atmosphere fluxes, live biomass, and carbon pools. Finally, SiB4 can be used to investigate anomalies that persist through seasons or for years, such as long-term drought.

SiB4 has the capability of simulating emergent ecosystem behaviors in both time and space because it uses a single mechanistic framework to capture overarching biological strategies held in common as vegetation responds to changes in the environment. Spatial gradients emerge as vegetation responds to shifts in climate, and SiB4 can be used as a tool to study these emergent properties (Figure 1.5B). For example, with a single set of parameters, SiB4 predicts C4 grasslands ranging from desert to tall-grass prairies to productive tropical pastures; and evaluating their response to varying climatic conditions can yield insights on ecosystem behaviors and processes. Additionally, in SiB4 vegetation characteristics emerge from relationships developed across climates, and analyzing these properties can lead to further knowledge and understanding of ecosystem dynamics. For example, the root-shoot ratio in SiB4 is not prescribed, but instead emerges as a long-term property from daily changing carbon allocation. By viewing root-shoot ratios as emergent properties from different patterns in carbon allocation, evaluating this metric yields insight into allocation patterns prevalent not only for different vegetation types and for different regions, but also for ecosystem responses to climate and perturbations in time or space.

2 Model Structure

2.1 Soil and Snow

2.1.1 Structure

SiB4 uses ten soil layers and up to five snow layers. The number of snow layers (nsl) is variable. All soil column variables extend from the deepest layer (layer 10) to the top layer (layer 1), and if present the snow variables extend from the level closest to the ground (layer 0) to the top layer (layer -5). The soil layers are calculated at the beginning of a simulation. The depth ($Node_z$) of soil layer i is given by

$$Node_{z(i)} = f_s \left(e^{0.5(i-0.5)} - 1 \right), \tag{1}$$

where i varies from 1 to $nsoil$ and f_s is a soil layer vertical scaling factor currently set to 0.073. The thickness (Dz) of each layer i is given by

$$Dz_i = \begin{cases} 0.5 \left(Node_{z(1)} + Node_{z(2)} \right) & i\text{=}1 \\ 0.5 \left(Node_{z(i+1)} + Node_{z(i\text{-}1)} \right) & i\text{=}2,\ ...,\ nsoil\text{-}1 \\ Node_{z(nsoil)} - Node_{z(nsoil\text{-}1)} & i = nsoil \end{cases} \tag{2}$$

And the interface depth ($Layer_z$) for any layer i is given by

$$Layer_{z(i)} = \begin{cases} 0.5(Node_{z(i)} + Node_{z(i+1)}) & i\text{=}1,\ ...,\ nsoil\text{-}1 \\ Node_{z(i)} + 0.5(Dz_{nsoil}) & i\text{=}nsoil \end{cases} \tag{3}$$

The soil structure information for SiB4 is shown in Table 2.1, and the soil column structure variables are listed in Table B1.

Although the soil layers are set at the start of a simulation, the depth of the snow layers can change, thus Dz is a prognostic variable whose calculation is discussed in Section 5. Once the thickness of the snow layers is determined, the node depth and interface depth of snow layer i are given by

$$Node_{z(i)} = Layer_{z(i)} - 0.5Dz_i \tag{4}$$

$$Layer_{z(i-1)} = Node_{z(i)} - 0.5Dz_i \tag{5}$$

This calculation is performed for the current number of snow layers given by nsl.

Level	$\mathbf{Layer_z}$ (m)	$\mathbf{Node_z}$ (m)	Dz (m)
1	0.05114	0.02073	0.05114
2	0.13167	0.08154	0.08053
3	0.26444	0.18180	0.13277
4	0.48335	0.34709	0.21890
5	0.84426	0.61960	0.36091
6	1.43930	1.06891	0.59505
7	2.42037	1.80969	0.98106
8	4.03787	3.03104	1.61750
9	6.70467	5.04470	2.66681
10	10.0246	8.36465	3.31996

Table 2.1: Soil Layer Information.

2.1.2 Soil Properties

Soil sand and clay fractions, along with longwave and shortwave reflectivity, are required input. This information is specified per grid cell and does not vary with depth. Upon the start of a simulation, SiB4 calculates basic soil properties using relationships from Clapp & Hornberger (1978), Cosby et al. (1984), and Lawrence et al. (2008). Since these equations use both sand/clay fractions and percentages, first temporary variables save the soil texture variables as percentages, such that $Clay_P = 100 \cdot Clay_{Frac}$ and $Sand_P = 100 \cdot Sand_{Frac}$. Using these, the calculations for the soil properties are provided below, and these variables are listed in Table B2.

$$Poros = 0.489 - 0.00126 Sand_P \tag{6}$$

$$BD_{Dry} = 2700(1 - Poros) \tag{7}$$

$$K_{Sat} = \frac{0.0070556 \cdot 10^{(-0.884 + 0.0153 Sand_P)}}{1000.} \tag{8}$$

$$C_{Solid} = \frac{2.128 Sand_{Frac} + 2.385 Clay_{Frac}}{Sand_{Frac} + Clay_{Frac}} \cdot 10^6 \tag{9}$$

$$TK_{Dry} = \frac{0.135 BD_{Dry} + 64.7}{2700. - 0.947 BD_{Dry}} \tag{10}$$

$$TK_{Mineral} = \left(\frac{8.8 Sand_{Frac} + 2.92 Clay_{Frac}}{Sand_{Frac} + Clay_{Frac}} \right)^{(1 - Poros)} \tag{11}$$

$$TK_{Sat} = TK_{Mineral} \cdot 0.57^{Poros} \tag{12}$$

$$Bee = 2.91 + 0.159 Clay_P \tag{13}$$

$$PH_{Sat} = \frac{-10 \cdot 10^{(1.88 - 0.0131 Sand_P)}}{1000.} \tag{14}$$

$$FC = Poros \left(\frac{-1.53061}{PH_{Sat}} \right)^{\frac{-1}{Bee}} \tag{15}$$

$$WP = Poros \left(\frac{-153.061}{PH_{Sat}} \right)^{\frac{-1}{Bee}} \tag{16}$$

$$W_{Opt} = 100 \left(-0.08 Clay_{Frac}^2 + 0.22 Clay_{Frac} + 0.59 \right) \tag{17}$$

$$W_{Sat} = 0.25 Clay_{Frac} + 0.5 \tag{18}$$

$$Z_m = -2 Clay_{Frac}^3 - 0.4491 Clay_{Frac}^2 + 0.2101 Clay_{Frac} + 0.3478 \tag{19}$$

$$W_{Exp} = \left(\frac{W_{Opt}}{100} \right)^{Z_m} \tag{20}$$

2.2 Vegetation

2.2.1 Plant Functional Types

Biomes represent biotic communities that are characterized by the prevailing climate, rather than by vegetation behavior or ecological functionality; thus, they are arbitrary products of classification rather than natural units with clearly defined and related mechanisms (Whittaker, 1956; Bonan et al., 2002). Since biomes represent communities rather than processes, representing vegetation as biomes becomes inconsistent between the model resolution and the plant level with decreasing spatial resolutions. An alternative method commonly used to classify land surface vegetation is to use plant functional types (PFTs), which group plants according to their function and physical, physiological, and phenological characteristics. Using PFTs rather than biome classifications is useful in LSMs because they reduce the complexity of species diversity and instead utilize leaf-level eco-physiological relationships (Wullschleger et al., 2014).

SiB4's PFTs (Table 2.2) group natural vegetation by plant size (tree, shrub, or grass), by leaf shape (needleleaf or broadleaf), and by foliage longevity (evergreen or deciduous). Since tundra environments are known to have difficult and unique growing conditions, both shrubs and grasses have been separated by climate. SiB4 includes a modified version of the crop phenology model developed by Lokupitiya et al. (2009), and thus has maize, soybeans and winter wheat.

Each of the PFTs belongs to one of six groups: barren, needleleaf forest, broadleaf forest, shrub, grass, or crop. Combining PFTs together into groups with similar leaf type and structure provides a useful reference for PFTs with similar characteristics that share group-specific processes. Each PFT also belongs to one of four types: bare ground, evergreen,

Ref.	PFT Name	Abbr.	Type	Group
1	Desert and Bare Ground	DBG	1	1
2	Evergreen Needleleaf Forest	ENF	2	2
4	Deciduous Needleleaf Forest	DNF	3	2
5	Evergreen Broadleaf Forest	EBF	2	3
8	Deciduous Broadleaf Forest	DBF	3	3
11	Shrubs (Non-Tundra)	SHB	3	4
12	Tundra Shrubs	SHA	3	4
13	Tundra Grassland	C3A	3	5
14	C3 Grassland	C3G	3	5
15	C4 Grassland	C4G	3	5
17	C3 Generic Crop	C3C	4	6
18	C4 Generic Crop	C4C	4	6
20	Maize	MZE	4	6
22	Soybeans	SOY	4	6
24	Winter Wheat	WWT	4	6

Table 2.2: Plant Functional Types (PFTs).

deciduous, or crop. These types are based on leaf persistence, foliar phenological patterns, and seasonal behavior, and their values are used as references for phenological processes that are type-specific.

2.2.2 Root Profiles

The root profile in the soil exponentially decreases from the surface down to the bottom soil layer. The root fraction ($Root_F$) in each soil layer depends on the plant function type, such that

$$Root_{Tot} = \frac{(1 - e^{-K_{Root} \cdot Layer_{z(nsoil)}})}{K_{Root}} \tag{21}$$

$$Root_F = \frac{(e^{-K_{Root} \cdot Z_2} - e^{-K_{Root} \cdot Z_1})}{(K_{Root} \cdot Root_{Tot})} \tag{22}$$

where $Root_{Tot}$ is the total roots in the soil column and K_{Root} is a PFT-dependent root density extinction coefficient. In addition to specifying the root extinction, SiB4 has an additional parameter to specify the maximum rooting depth ($Root_D$). There will not be any roots below this specified depth, and the rooting fractions will be redistributed to move any necessary roots. Sample rooting fractions for the EBF and C4G PFTs are shown in Table 2.3.

Level	**Node$_z$** (m)	**Root$_F$ EBF**	**Root$_F$ C4G**
1	0.02073	0.08326	0.24516
2	0.08154	0.11729	0.27011
3	0.18180	0.16153	0.25119
4	0.34709	0.19823	0.16347
5	0.61960	0.20163	0.06044
6	1.06891	0.15149	0.00926
7	1.80969	0.07024	0.00036
8	3.03104	0.01529	0.00000
9	5.04470	0.00103	0.00000
10	8.36465	0.00001	0.00000

Table 2.3: Sample Root Profiles.

2.2.3 Carbon Pools

For carbon storage, SiB4 uses eleven pools, which are updated daily at midnight local time (LST) and listed in Table 2.4. Similar to SiB-CASA, the flow of carbon between the pools in SiB4 is based on a system of first-order, linear differential equations (Schaefer et al., 2008, 2009). There are five live carbon pools in SiB4 ($nlpool = 5$), three of which are aboveground and compose the plant canopy ($ncpool = 3$). The leaf pool (leaf) contains leafy biomass. The stem/wood pool (stwd) holds the structural aboveground biomass: for grasses and crops this represents stems, while for forest and shrub PFTs this is wood. The product pool (prod) contains seed and flower carbon for non-crop PFTs and the yield for crops.

Number	Carbon Pool	Abbr.	Type	Location	Levels
1	Leaf	leaf	Live	Canopy	1
2	Fine Root	froot	Live	Soil	10
3	Coarse Root	croot	Live	Soil	10
4	Stem/Wood	stwd	Live	Canopy	1
5	Product	prod	Live	Canopy	1
6	Coarse Dead Biomass	cdb	Dead	Surface	1
7	Metabolic Litter	metl	Dead	Surface	1
8	Structural Litter	strl	Dead	Surface	1
9	Soil Litter	slit	Dead	Soil	10
10	Soil Slow	slow	Dead	Soil	10
11	Soil Armored	arm	Dead	Soil	10

Table 2.4: Carbon Pools.

The roots are broken into two separate pools: fine (froot) and coarse (croot). The fine roots take up water and nutrients and are shorter lived, while the coarse roots have a woody structure with a longer turnover time. Using these definitions, forest and shrub PFTs have both fine and coarse roots; however, grasses and crops only have fine roots. Both fine and coarse roots have the same distributions throughout the soil column.

While many LSMs with carbon pools explicitly include live storage carbon (e.g. SiB-CASA, CLM), SiB4 does not separate out the storage of nonstructural carbohydrates necessary for plant maintenance and growth. The lack of storage carbon measurements, the high variability of pool sizes between species (Poorter et al., 2015), and the uncertainty of carbon allocation to carbon pools (De Kauwe et al., 2014; Malhi et al., 2011) justifies a simpler approach. The carbon required for the maintenance of all live pools is removed directly from the pool itself. During the growing season, the carbon for growth comes directly from the carbon taken up during photosynthesis. For deciduous and grass PFTs, the carbon necessary for leaf-out is stored in the minimal leaf pool.

The non-living carbon in SiB4 is divided into six pools ($ndpool = 6$), three at the surface and three in the soil. The surface pools consist of two litter pools: a metabolic pool (metl) with a fast soil turnover rate and a more slowly decaying pool (strl). There is also an aboveground pool for coarse dead biomass (cdb). For grass PFTs, this pool stores the carbon in standing dead grass; for forests and shrubs, this pool represents the coarse woody debris, which stores the carbon in non-living wood. Belowground there are three non-living carbon pools: a soil litter pool (slit) to store the non-living roots and quickly over-turning soil carbon, a slow soil carbon pool (slow) to contain humus and other recalcitrant organic material, and an armored pool (arm) containing organic material bound to clay with long turnover times. Once in the soil, there is recycling of carbon amongst the soil carbon pools.

2.2.4 Vegetation Properties

SiB4 calculates a variety of vegetation properties that are used for hydrology, phenology, photosynthesis, and radiation. These properties are updated daily at midnight LST and are listed in Table B3.

The current leaf state is represented by the leaf area index (LAI), which is calculated from the canopy pools using a specific leaf area (SLA), such that

$$LAI = Pool_{LAI} \cdot SLA \tag{23}$$

$$Pool_{LAI} = \begin{cases} \text{Leaf} & \text{non-grass PFTs} \\ \text{Leaf} + \text{Stwd} + \text{Prod} & \text{grass PFTs} \end{cases} \tag{24}$$

where SLA is a parameter set to global-mean values from PFT-specific studies. In calculating LAI, for grasslands and crops, all three canopy pools are summed, while for forest and shrub PFTs the LAI represents only the leaf pool. The LAI is bounded such that

$$LAI_{Min} \leq LAI \tag{25}$$

where LAI_{Min} is a parameter indicating the required minimal storage of carbon in the leaf pool for seasonal regrowth.

2.2.5 Land Cover Heterogeneity

To include land cover heterogeneity, SiB4 uses tiles of up to ten different PFTs per site or grid cell, each with separate areal fractions. The areal coverage of PFTs is prescribed from satellite imagery. The weather driver data is defined per grid cell, whereas all soil and vegetation variables are saved per PFT tile. Figure 2.1 shows a pictoral representation of this setup in SiB4.

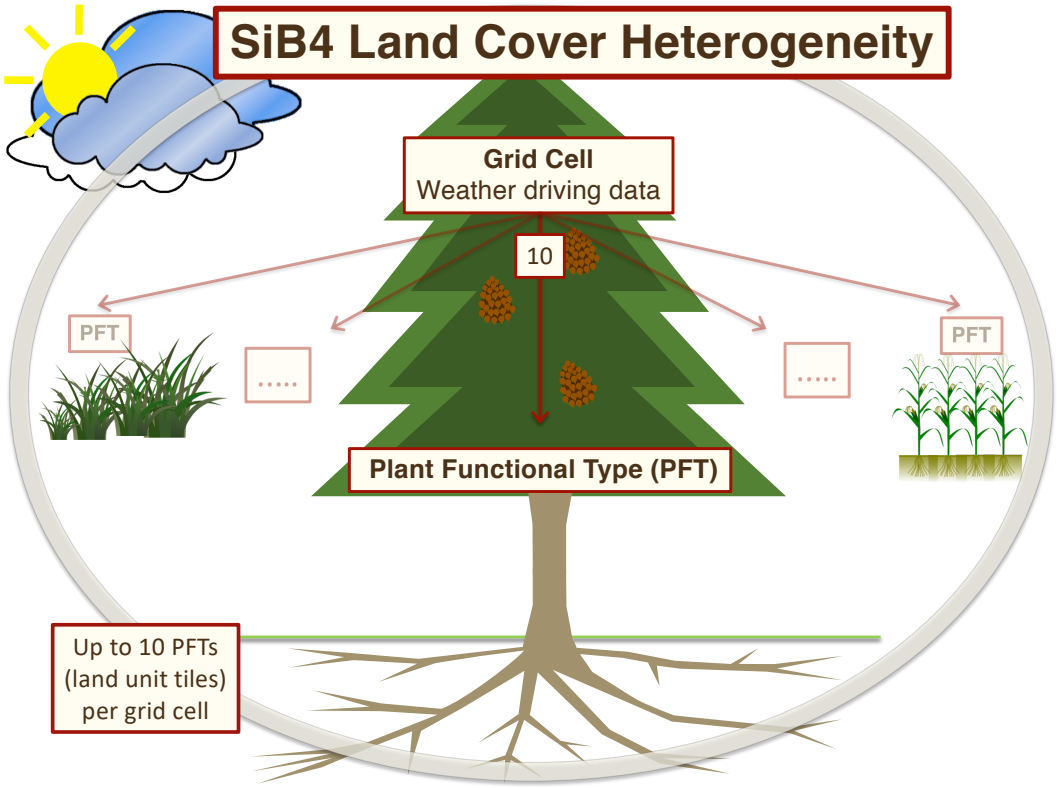

Figure 2.1: PFT Tiles.

2.3 Input Variables

SiB4 has five types of input variables: driver data, fire emissions, structural properties, parameters, and constants. These are all listed in Appendix A at the end of this document (Tables A1 - A15). Basic definitions for input variables are as follows:

1. **Meteorological Drivers** (Table A1).
2. **Fire Emissions** (Table A2).
3. **Structural Properties** (Table A3).
4. **Aerodynamic Parameters** (Table A4).
5. **Physiological Parameters** (Table A5).
6. **Dynamic Phenology Parameters** (Table A6).
7. **Defined Phenology Parameters** (Table A7).
8. **Fire Parameters** (Table A8).
9. **Grazing Parameters** (Table A9).
10. **Allocation Parameters** (Table A10).
11. **Autotrophic Respiration Parameters** (Table A11).
12. **Senescence Parameters** (Table A12).
13. **Heterotrophic Respiration Parameters** (Table A13).
14. **Physical Constants** (Table A14).
15. **Specified Constants** (Table A15).

The meteorological drivers and fire emissions change in time and space, and thus grid cell values are read as often as the temporal resolution of the data source, which is typically hourly. Every model timestep these drivers and emissions are interpolated values between the provided times. The structural properties, parameters, and constants are constant in time, thus are only read in at the beginning of a simulation. The structural properties and parameters are both defined at the PFT level; however, the structural properties vary in space, while the parameters are single values per PFT applied globally. The constants are single values that do not change over time.

To be as versatile as possible, nearly every number used in any SiB4 relationship is a parameter, be it a driver, PFT-varying parameter, or a specified constant. While SiB4 includes numerous parameters, they are primarily used to represent mechanisms, and all of them can be grouped either into physical quantities or values required to define relationships. For example, a linear bounded relationship uses five parameters. These parameters should not be thought of as individual values that must be specified, but instead as groups of numbers that quantify a relationship. The parameters that represent biogeochemical processes, such as carbon allocation, are set from global mean values published from field campaigns and *in situ* studies. The parameters that use previously published mechanisms, such as the Q_{10} temperature-respiration response, use literature values. Finally, the parameters that use relationships are set by performing sensitivity studies for each PFT and evaluating the fluxes against eddy-covariance towers and the LAI to remotely-sensed values. Since SiB4 is designed to allow the parameters to change in recognition that global mean values may not be optimal for regional or site-specific studies, parameter ranges are provided.

2.4 Prognostic Variables and Governing Equations

SiB4 has prognostic equations for four vertical levels: canopy, canopy air space (CAS), ground surface, and soil/snow. The canopy and water interception variables are described by Sellers et al. (1996a). SiB4 uses a prognostic canopy air space that is described by Vidale & Stöckli (2005), allowing for the storage of heat, water, and carbon at that level and providing a more explicit representation of canopy processes. For the soil/snow, SiB4 follows the Community Land Model (CLM) approach outlined in Lawrence et al. (2018), where soil temperature and soil moisture are calculated for 10 co-located soil layers and up to 5 snow layers. Finally, SiB4 includes 11 prognostic carbon pools as described by Haynes et al. (2019a), where the soil pools include carbon storage for each of the 10 soil layers. Each of these referenced papers provide full descriptions and evaluations of these processes. Additionally, Baker (2011) provides derivations of these, including the numerical technique used to perform timestepping.

This section briefly provides the basic equations of the SiB4 prognostic variables, which are listed in Table B4. The net radiation terms are discussed more in Section 3; fluxes of heat, water vapor, and CO_2 are discussed more in Section 4, interception and soil moisture are discussed more in Section 5; and carbon pools are discussed more in Sections 8, 9, 10, 11, and 12.

Canopy Temperature

$$c_c \frac{\delta T_c}{\delta t} = Rn_c - H_c - \lambda E_c - \xi_{cs} \tag{26}$$

where

c_c = canopy effective heat capacity (J m^{-2} s^{-1})

T_c = canopy temperature (K)

Rn_c = absorbed net radiation (W m^{-2})

H_c = canopy sensible heat flux (W m^{-2})

λ = latent heat of vaporization (J kg^{-1})

E_c = canopy evapotranspiration rate (kg m^{-2} s^{-1})

ξ_{cs} = energy from canopy interception phase changes (W m^{-2})

CAS Temperature

$$c_a \frac{\delta T_a}{\delta t} = -H_a + H_c + H_g \tag{27}$$

CAS Water Vapor

$$c_a \frac{\delta e_a}{\delta t} = -E_a + E_c + E_g \tag{28}$$

CAS CO_2

$$c_a \frac{\delta pco2_a}{\delta t} = -F_{CO2a} + F_{CO2c} + F_{CO2g} \tag{29}$$

where

c_a = CAS effective heat capacity (J m^{-2} s^{-1})

T_a = CAS temperature (K)

H_a = CAS sensible heat flux (W m^{-2})

H_g = surface (top soil/snow layer) heat flux (W m-2)

E_a = CAS evapotranspiration rate (kg m^{-2} s^{-1})
E_g = surface evapotranspiration rate (kg m^{-2} s^{-1})
$pco2_a$ = CAS CO_2 partial pressure (Pa)
F_{CO2a} = CAS carbon flux (μmol m^{-2} s^{-1})
F_{CO2c} = canopy carbon flux (μmol m^{-2} s^{-1})
F_{CO2g} = surface carbon flux (μmol m^{-2} s^{-1})

Surface Temperature

$$c_g \frac{\delta T_{D,g}}{\delta t} = Rn_g - H_g - \lambda E_g - \frac{2\pi C_D}{\tau_D}(T_{D,g} - T_D) - \xi_{gs} \quad (30)$$

Soil/Snow Temperature

$$c_d \frac{\delta T_D}{\delta t} = \frac{\delta}{\delta z}\left[\lambda \frac{\delta T}{\delta z}\right] \quad (31)$$

where
c_g = surface effective heat capacity (J m^{-2} s^{-1})
$T_{D,g}$ = surface (top soil/snow layer) temperature (K)
Rn_g = surface absorbed net radiation (W m^{-2})
c_D = soil effective heat capacity (J m^{-2} s^{-1})
τ_D = daylength (s)
T_D = soil/snow temperature (K)
ξ_{gs} = energy from ground interception phase changes (W m^{-2})

Canopy Interception

$$\frac{\delta capacc_{liq,snow}}{\delta t} = P - D_d - D_c - E_{ci}/\rho \quad (32)$$

Ground Interception

$$\frac{\delta capacg}{\delta t} = D_d + D_c - E_{gi}/\rho \quad (33)$$

where
$capacc_{liq}$ = canopy surface liquid (kg m^{-2})
$capacc_{snow}$ = canopy surface ice (kg m^{-2})
$capacc_g$ = ground surface liquid (kg m^{-2})
P = precipitation rate (Pr_{cu} + Pr_{ls}, $m\ s^{-1}$)
D_d = canopy throughfall rate (m s^{-1})
D_c = canopy drainage rate (m s^{-1})
E_{ci} = evaporation rate from canopy stores
E_{gi} = evaporation rate from ground stores
ρ = density of water (kg m^{-3})

Soil Moisture

$$\frac{\delta\theta}{\delta t} = \frac{\delta q}{\delta z} - e \tag{34}$$

$$\theta_i = \frac{WWW_{Liq,i}}{\Delta z_i \rho_{Liq}} + \frac{WWW_{Ice,i}}{\Delta z_i \rho_{Ice}} \tag{35}$$

where θ = volumetric soil water content (liquid and ice) (mm^3 water/mm^3 soil)
$WWW_{Liq,i}$ = soil/snow liquid water per layer i (kg/m^2)
$WWW_{Ice,i}$ = soil/snow ice per layer i (kg/m^2)
q = soil water flux (kg/m^2/s)
z = height above some datum in soil column (mm, positive upwards)
e = sink term (evapotranspiration loss, mm water/mm soil/s)
ρ_{Liq} = density of liquid water (kg/m^3)
ρ_{Ice} = density of ice (kg/m^3)

Following CLM, the vertical soil moisture transport is governed by infiltration, surface and sub-surface runoff, gradient diffusion, gravity, and canopy transpiration through root extraction. When soils freeze, the hydraulic conductivity of the soil is greatly decreased, leading to nearly impermeable soil ice layers.

Canopy Conductance

$$\frac{\delta g_c}{\delta t} = -k_g(g_c - g_c inf) \tag{36}$$

Stomatal Resistance

$$\frac{\delta rst}{\delta t} = g_c^{-1} \tag{37}$$

where g_c = canopy conductance (m/s)
k_g = time constant (1/s)
g_{cinf} = estimate of g_c as $t \to \infty$ (m/s)
rst = stomatal resistance

Live Carbon Pools

$$\frac{\delta C_{lpool}}{\delta t} = G_{Assim} + G_{Seed} - L_{Fire} - L_{Grz} - L_{GResp} - L_{Hrvst} - L_{MResp} - L_{Trans} \tag{38}$$

Dead Carbon Pools

$$\frac{\delta C_{dpool}}{\delta t} = G_{Grz} + G_{Hrvst} + G_{Transl} + G_{Transd} - L_{Fire} - L_{Resp} - L_{Trans} \tag{39}$$

where C_{lpool} = live carbon pools (mol C m^{-2})
C_{dpool} = dead carbon pools (mol C m^{-2})
G_{Assim} = gain from photosynthesis (mol C m^{-2} s^{-1})
G_{Seed} = gain from seed (mol C m^{-2} s^{-1})
G_{Grz} = gain from grazing transfers (mol C m^{-2} s^{-1})

G_{Hrvst} = gain from harvest transfers (mol C m^{-2} s^{-1})
G_{Transl} = gain from live pool transfers (mol C m^{-2} s^{-1})
G_{Transd} = gain from dead pool transfers (mol C m^{-2} s^{-1})
L_{Fire} = loss from fire (mol C m^{-2} s^{-1})
L_{Grz} = loss from grazing (mol C m^{-2} s^{-1})
L_{GResp} = loss from growth respiration (mol C m^{-2} s^{-1})
L_{Hrvst} = loss from harvest (mol C m^{-2} s^{-1})
L_{MResp} = loss from maintenance respiration (mol C m^{-2} s^{-1})
L_{Resp} = loss from heterotrophic respiration (mol C m^{-2} s^{-1})
L_{Trans} = loss from transfer to dead pools (mol C m^{-2} s^{-1})

2.5 I/O

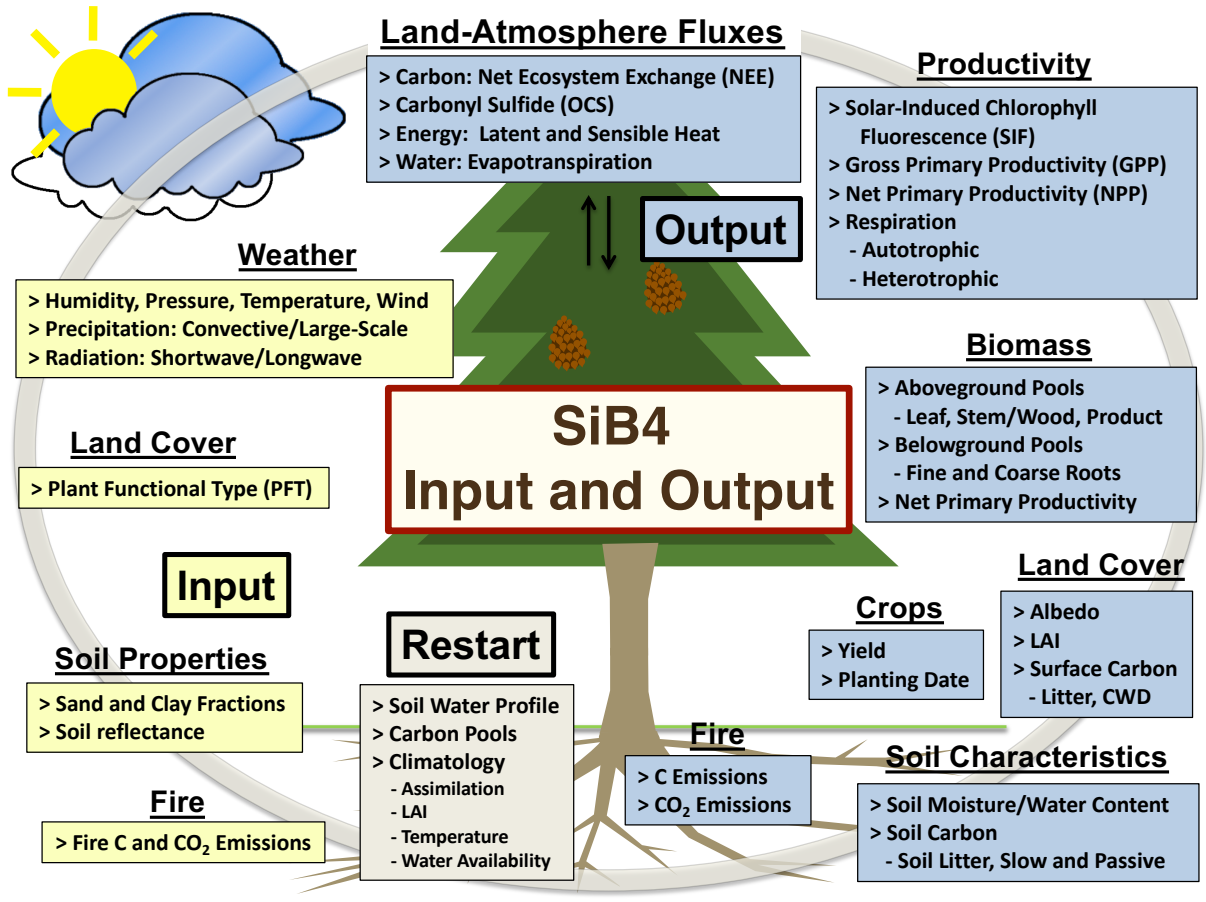

Figure 2.2: SiB4 Input and Output.
The required SiB4 input (yellow boxes), restart information (grey box), and the predominant output (blue boxes).

Figure 2.2 shows the inputs and major outputs of SiB4. One of the main features of SiB4 is the capacity to prognose both phenological timing and biomass. This predictive capability removes the requirement of remotely sensed vegetation data, which has three significant benefits:

1. It is no longer necessary to obtain satellite products depicting the leaf state for the desired simulation time.

2. Evaluation of SiB4 can utilize a variety of satellite products, including the vegetation data formerly used as input.

3. SiB4 can be used in a variety of forward-in-time studies, including weather prediction, land-atmosphere feedback investigations, and climate sensitivity experiments.

Simultaneous prediction of phenology and carbon pools reduces the input data for SiB4. Rather than using data that requires significant processing while limiting the simulation times, SiB4 only has three input requirements: 1) weather data, 2) a PFT map indicating the vegetation type, and 3) basic soil properties, including sand/clay fractions and reflectivity. All of these input data have a variety of sources and can either be obtained in advance, determined real-time, or easily predicted and then provided.

For initialization, SiB4 requires soil water profiles, carbon pools, and climate-based constants (Figure 2.2, gray box). These values can either be specified or calculated during a spin-up simulation. Ingesting carbon pools that contain sources and sinks enables SiB4 to produce unbalanced fluxes that can be used for a variety of applications, including more accurately simulating the atmospheric CO_2 growth rate. In contrast, performing a spin-up simulation will result in self-consistent carbon pools and fluxes. Spin-up simulations are typically run for at least ten years to create climatologically-based values that are less sensitive to weather pattern anomalies. The resulting carbon pools from a spin-up run are the steady-state pool values, which are obtained by iterating over the specified years until equilibrium is reached. The equilibrium requirement is satisfied if all carbon pools at either the start or end of the simulation are within 1% of the calculated equilibrium pools. If any of the initialization data are not provided, SiB4 will use default PFT-specific values.

SiB4 predicts numerous quantities that can be evaluated against a variety of data (Figure 2.2, blue boxes). In addition to carbon, energy, and water fluxes, SiB4 includes the simulation of COS that was developed in SiB3 (Berry et al., 2013). SiB4 also includes the simulation of solar-induced chlorophyll fluorescence (SIF) from SiB3 (Baker et al., 2014). Since SiB4 prognoses both the phenology and the resulting biomass, the output contains consistent predictions of carbon fluxes, biomass, surface carbon pools, and soil carbon reservoirs, as well as the associated land cover characteristics and soil hydrology.

2.6 Runtime Options

To run SiB4, users need to set all of the simulation specifications in the namelist (*namel_sibdrv*). There are eight lists with control options, each of which is listed and described here.

1. Control List

   - nsib: Nnumber of points in the simulation
   - starttime: Day of year to start simulation
   - startyear: Year to start simulation
   - endtime: Day of year to stop simulation
   - endyear: Year to stop simulation
   - dtsib: Model timestep, in seconds
   - restart_dtsib: Restart output interval (at least daily)
   - qp_dtsib: QP output interval (typically monthly)
   - pbp_dtsib: PBP output interval (typically daily)
   - hr_dtsib: HR output interval (typically hourly)
     For all of the output intervals:
     Values greater than zero are output frequencies with units of seconds.
     Values less than zero are output frequencies with units of months.

2. IO List

   - pft_info: File containing PFT information
   - pool_info: File containing pool information
   - aero_file: File containing aerodynamic properties
   - pgdd_file: File containing defined phenology parameters
   - pstg_file: File containing dynamic phenology parameters
   - phys_file: File containing physiological parameters
   - pool_file: File containing pool respiration and transfer parameters
   - vs_file: File containing vegetation structure
   - ic_file: File containing initial conditions and restart values
     If this file is not specified or does not exist, the model will start with default values.
   - dr_path: Directory containing driver data
   - fire_path: Directory containing fire emissions
   - out_path: Directory for model output
   - out_info: File containing output specifications and information
   - out_rinfo: File containing restart specifications and information

3. Spinup List

   - spinup: Flag to perform a spinup simulation
     A spinup simulation will continue until either:
     Pools are within the threshold equilibrium values
     Maximum number of iterations have been run
   - spinup_default: Flag to use default initial conditions for spinup
     For the defaults:
     All pools are zero except a minimal leaf pool
     Soil moisture starts at saturation
   - spinup_numyrs: Number of years to perform before equilibrium calculations
     Note that for spinup runs, entire years are simulated starting January 1 of the startyear.
   - spinup_maxiter: Maximum number of iterations in a spinup
   - spinup_threshold: Input/output ratio threshold required to stop spinup
   - spinup_writediag: Flag to follow output choices during spinup (false saves only equilibrium files)
   - spinup_writetxtf: Flag to write equilibrium pool information to a text file

4. Subgrid List

   - minlon: Minimum longitude for setting a subgrid
   - maxlon: Maximum longitude for setting a subgrid
   - minlat: Minimum latitude for setting a subgrid
   - maxlat: Maximum latitude for setting a subgrid

5. Point-By-Point (PBP) List

   - npbp: Number of points to be saved in PBP output
     Following this value, a list of corresponding lon/lat pairs (degress) is expected.
     If npbp is set to -1, then all points will be saved in the PBP output.

6. Balance List

   - badtc_print: Print canopy temperatures?
   - badtc_stop: Stop simulation for bad canopy temperatures?
   - canb_print: Print canopy balance values?
   - canb_stop: Stop simulation if canopy balance fails?
   - carbonb_print: Print carbon balance information?
   - carbonb_stop: Stop simulation if carbon balance fails?
   - carbonb_thresh: Carbon balance thresholds
   - fireb_print: Print fire balance information?

- fireb_stop: Stop simulation if fire balance fails?
- fireb_thresh: Fire balance threshold
- snocmbn_print: Print snow combine information?
- snocmbn_stop: Stop if snow combine water balance fails?
- snocmbn_thresh: Snow combine balance threshold
- bnum_allow: Number of allowable energy/water balance sequential offenses
- energyb_print: Print energy balance values?
- energyb_stop: Stop if energy balance fails?
- energyb_thresh: Energy balance threshold
- waterb_print: Print water balance values?
- waterb_stop: Stop if water balance fails?
- waterb_thresh: Water balance threshold

7. Print List

    - print_avec: Print avec/bvec values (matrix solver for fluxes)
    - print_driver: Print driver data values?
    - print_fire: Print fire emissions?
    - print_harvest: Print harvest information?
    - print_pftinfo: Print PFT information?
    - print_pooll: Print live pool values?
    - print_soil: Print soil properties?
    - print_sscol: Print soil/snow layer information?
    - print_veg: Print vegetation values?
    - print_stop: Stop simulation after printing information?

8. Switch List

    - cornsoy_switch: Flag to annually alternate corn and soybeans
    - fire_switch: Flag to use fire emissions
    - grazing_switch: Flag to use grazing
    - green_switch: Flag to use greenness fraction
    - eqclear_switch: Flag to clear equilibrium variables at start of simulation
    - leapyr_switch: Flag for using leap years (False == constant 365 days)
    - updatelst_switch: Flag to update carbon pools at 0 LST (rather than 0 GMT)

3 Radiation

This section provides an overview of the radiation scheme in SiB4. Further details, including complete equations, can be found in Sellers (1985) and Sellers et al. (1996a). All radiation variables are listed in Table B5.

3.1 Solar Radiation Characteristics

The cosine of the solar zenith angle (μ) is

$$\mu = sin\phi\ sin\delta - cos\phi\ cos\delta\ cosh \tag{40}$$

where h is the solar hour angle, δ is the solar declination angle, and ϕ is the latitude. Equation 40 assumes all angles have been converted to radians.

The solar hour angle is

$$h = \frac{\pi}{180} hr_{ang} \tag{41}$$

$$hr_{ang} = 360 LST_{Frac} - 180 \tag{42}$$

$$LST_{Frac} = \frac{Sec_{Day}}{86400} + \frac{lon}{360} \tag{43}$$

where hr_{ang} is the local time hour angle, LST_{Frac} is the local time expressed in a day fraction from 0 to 1, Sec_{Day} is the current second of the day, 86400 is the number of seconds per day, and lon is the longitude in degrees.

For the solar declination angle, both the sine and cosine are calculated such that

$$sin\delta = sin\left(\frac{\pi}{180} dec_{max}\right) \cdot sin(lon_{Earth}) \tag{44}$$

$$cos\delta = \sqrt{(1 - (sin\ \delta)^2} \tag{45}$$

where dec_{max} is a physical parameter and lon_{Earth} is the true longitude of the Earth.

The true longitude of the Earth is counted from the vernal equinox, and is incremented daily for each day following the equinox such that

$$lon_{Earth} = \sum_{day=1}^{neqnx} \frac{t_1 + 2(t_2 + t_3) + t_4}{6} \tag{46}$$

$$t_1 = \pi_{day}\ Asc(lon_{Earth})\ \pi_{day} \tag{47}$$

$$t_2 = \pi_{day}\ Asc(lon_{Earth} + 0.5 t_1) \tag{48}$$

$$t_3 = \pi_{day}\ Asc(lon_{Earth} + 0.5 t_2) \tag{49}$$

$$t_4 = \pi_{day}\ Asc(lon_{Earth} + t_3) \tag{50}$$

where $neqnx$ is the number of days since the vernal equinox ($eqnx = 80$), t_1, t_2, t_3, and t_4 are angle increments, and Asc is a correction calculated based on the angle around the Sun traversed since the beginning of the year. This is expressed mathematically as

$$Asc = reccn(1 - eccn \cdot cos(\alpha - \pi_{peri}))^2 \quad (51)$$

$$reccn = \frac{1}{(1 - eccn^2)^{1.5}} \quad (52)$$

where $eccn$ is the eccentricity physical constant, π_{peri} is a solar zenith angle physical constant, and α is the input angle.

3.2 Solar Radiation Components

Incoming solar radiation is partitioned into visible and near-infrared (NIR) components, both of which are further divided into direct (beam) and diffuse estimates. Using the surface incident shortwave radiation from driver data (SW_{Dwn}) and the current sun angle (μ), the components are calculated as:

$$cloud = \frac{rad_{c5} \cdot \mu - SW_{Dwn}}{rad_{c4} \cdot \mu} \quad (53)$$

$$dirad = 0.0683 + \frac{0.0604}{\mu - 0.0223 + 1.e^{-10}} \quad (54)$$

$$dirad = dirad + (1 - dirad) \cdot cloud \quad (55)$$

$$vnrad = \frac{rad_{c1} - cloud \cdot rad_{c2}}{(rad_{c1} - cloud \cdot rad_{c3}) + (rad_{c1} - cloud \cdot rad_{c2})} \quad (56)$$

$$radvbc = (1 - dirad) \cdot vnrad \cdot SW_{Dwn} \quad (57)$$

$$radvdc = dirad \cdot vnrad \cdot SW_{Dwn} \quad (58)$$

$$radnbc = (1 - dirad) \cdot (1 - vnrad) \cdot SW_{Dwn} \quad (59)$$

$$radndc = dirad \cdot (1 - vnrad) \cdot SW_{Dwn} \quad (60)$$

where $cloud$, $dirad$, and $vnrad$ are local variables. The radiation components $radvbc$, $radvdc$, $radnbc$, and $radndc$ are the visible beam radiation, visible diffuse radiation, NIR beam radiation, and NIR diffuse radiation, respectively.

3.3 Radiative Transfer Model

3.3.1 Overview

SiB4 calculates the interception, reflection, transmission, and absorption of radiation by vegetation and soil using the two-stream approximation model from SiB2 and described in Sellers et al. (1996a). The fundamental equations were presented by Dickinson (1983), modified by Sellers (1985), and summarized in Sellers et al. (1996a). The radiative transfer equations are solved for each of the four solar radiation components, with a simplified calculation for the exchanges of thermal infrared radiation. In solving the two-stream approximation model for the canopy-ground system (Sellers, 1985), canopy reflectances, absorbances, and transmittances are specified and the radiation absorbed by the canopy and soil from each incident component is calculated. Using the Stefan-Boltzmann law assuming radiative equilibrium, the net radiation is calculated from the absorbed radiation and the component temperatures.

3.3.2 Original Equations

The radiative transfer in vegetative canopies can be described using a two-stream approximation method solving the equations:

$$-\bar{\mu}(dI\uparrow/dL) + [1-(1-\beta)\omega]I\uparrow - \omega\beta I\downarrow = \omega\bar{\mu}K\beta_o e^{-KL} \quad (61)$$

$$\bar{\mu}(dI\downarrow/dL) + [1-(1-\beta)\omega]I\downarrow - \omega\beta I\uparrow = \omega\bar{\mu}K(1-\beta_o)e^{-KL} \quad (62)$$

where $I\uparrow$ and $I\downarrow$ are the upward and downward diffuse radiative fluxes normalized by the incident flux; $\bar{\mu}$ is the average inverse diffuse optical depth per unit leaf area; β and β_o are the upscatter parameters for the diffuse and direct beams; ω is the scattering coefficient; K is the optical depth of the direct beam per unit leaf area; and L is the cumulative leaf area index. Values of the parameters K and $\bar{\mu}$ are functions of canopy geometry and leaf angle distribution, and values of β and β_o are functions of canopy geometry and phytoelement optical properties.

To solve these equations, boundary conditions appropriate to a vegetative canopy covering a reflective soil surface are applied such that

$$I\downarrow = 0 \quad \text{at} \quad L = 0 \quad (63)$$

$$I\uparrow = \rho_s[I\downarrow + e^{-KL_T}] \quad \text{at} \quad L = L_T \quad (64)$$

where ρ_s is the soil reflectance and L_T is the total leaf area index. The solution of these equations yields

$$I\downarrow = \alpha_1 e^{-KL} + \alpha_2 e^{-\alpha_3 L} + \alpha_4 e^{\alpha_3 L} \quad (65)$$

$$I\uparrow = \alpha_5 e^{-KL} + \alpha_6 e^{-\alpha_3 L} + \alpha_7 e^{\alpha_3 L} \quad (66)$$

where α_1 through α_7 are algebraic combinations of the coefficients in Equations (61) and (62). These calculations are performed for each of the four solar radiation components, with slightly different simplified calculations for the exchanges of diffuse and direct beam radiation. Similar calculations are used to calculate the exchanges of thermal infrared radiation.

Using the calculated radiative fluxes, the solar radiation absorbed by the canopy (F_c) and ground (F_g) are given by

$$F_c = V[1 - I\uparrow_c - I\downarrow_g (1-\rho_s) - e^{-KL_T/V}(1-\rho_s)]F_\wedge \quad (67)$$

$$F_g = \{(1-V)(1-\rho_s) + V[I\downarrow_g (1-\rho_s) + e^{-KL_T/V}(1-\rho_s)]\}F_\wedge \quad (68)$$

where V is the canopy cover fraction, $F_\wedge$ is the incident radiant solar energy, $I\uparrow_c$ is the diffuse flux leaving the top of the canopy, and $I\downarrow_g$ is the diffuse flux leaving the base of the canopy. The net absorbed thermal radiation by the canopy ($F_{T,c}$) and ground ($F_{T,g}$) are

$$F_{T,c} = F_{T,0}V\delta_T - 2\sigma_s T_c^4 V\delta_T + \sigma_s T_g^4 V\delta_T \quad (69)$$

$$F_{T,g} = F_{T,0}(1 - V\delta_T) + \sigma_s T_c^4 V\delta_T - \sigma_s T_g^4 \quad (70)$$

where $F_{T,0}$ is the incident thermal infrared radiation (TIR, diffuse), $V\delta_T$ is the fraction of incident TIR absorbed by the canopy (with $\delta_T = 1 - e^{-L_T/V\bar{\mu}}$), and σ_s is the Stefan-Boltzmann constant. Finally, the net radiative fluxes for the canopy (Rn_c) and ground (Rn_g) are

$$Rn_c = \sum_{\wedge=V,N,T} F_{\wedge,c} \quad (71)$$

$$Rn_g = \sum_{\wedge=V,N,T} F_{\wedge,g} \quad (72)$$

where V, N, and T are the visible, near-infrared, and thermal wavelength intervals.

3.4 Radiation Calculations

3.4.1 Albedo

Following the notation above and published by Sellers (1985), the albedo is divided into four contributions: visible beam ($albedo_{VisB}$), visible diffuse ($albedo_{VisD}$), near-infrared beam ($albedo_{NIRB}$), and near-infrared diffuse ($albedo_{NIRD}$). The albedo components are given by

$$albedo_{VisB} = (1 - VCover) * albedoG_{Vis} + VCover * albedoC_B \quad (73)$$

$$albedo_{VisD} = (1 - VCover) * albedoG_{Vis} + VCover * albedoC_D \quad (74)$$

$$albedo_{NIRB} = (1 - VCover) * albedoG_{NIR} + VCover * albedoC_B \quad (75)$$

$$albedo_{NIRD} = (1 - VCover) * albedoG_{NIR} + VCover * albedoC_D \quad (76)$$

$$albedoG_{Vis} = Soref_{Vis} * (1 - snow_{gvfc}) + 0.8 * fmelt * snow_{gvfc} \quad (77)$$

$$albedoG_{NIR} = Soref_{NIR} * (1 - snow_{gvfc}) + 0.4 * fmelt * snow_{gvfc} \quad (78)$$

$$albedoC_B = h1/bot + h2 + h3 \quad (79)$$

$$albedoC_D = h7 + h8 \quad (80)$$

where $albedoG_{Vis}$ is the visible ground albedo, $albedoG_{NIR}$ is the NIR ground albedo, $albedoC_B$ is the beam canopy albedo, $albedoC_D$ is the diffuse canopy albedo, $VCover$ is the fraction of vegetation cover, $snow_{gvfc}$ is the snow vertical ground coverage (0 to 1 fraction), $fmelt$ is the snow melting fraction, and $h1$, $h2$, $h3$, $h7$, $h8$, and bot are all constants determined from the two-stream approximation model.

3.4.2 Radiation Absorption Factors

The albedos can be combined with the vegetation coverage and canopy transmittances to calculate canopy and ground radiation absorption factors ($radfacc$ and $radfacg$). These factors can be used to scale the incoming radiation fluxes in order to calculate the radiation absorbed, and are given by

$$\begin{aligned}
radfacc_{VisB} &= VCover * [(1 - albedoC_B) - Tran1_{Vis} * (1 - albedoG_{Vis}) \\
&\quad -Tran3_{Vis} * (1 - albedoG_{Vis})] \qquad (81)\\
radfacc_{VisD} &= VCover * [(1 - albedoC_D) - Tran2_{Vis} * (1 - albedoG_{Vis})] \qquad (82)\\
radfacc_{NIRB} &= VCover * [(1 - albedoC_B) - Tran1_{NIR} * (1 - albedoG_{NIR}) \\
&\quad -Tran3_{NIR} * (1 - albedoG_{NIR})] \qquad (83)\\
radfacc_{NIRD} &= VCover * [(1 - albedoC_D) - Tran2_{NIR} * (1 - albedoG_{NIR})] \qquad (84)\\
radfacg_{VisB} &= (1 - VCover) * (1 - albedoG_{Vis}) \\
&\quad +VCover * [(Tran1_{Vis} * (1 - albedoG_{Vis}) + Tran3_{Vis} * (1 - albedoG_{Vis})] \qquad (85)\\
radfacg_{VisD} &= (1 - VCover) * (1 - albedoG_{Vis}) \\
&\quad +VCover * Tran2_{Vis} * (1 - albedoG_{Vis}) \qquad (86)\\
radfacg_{NIRB} &= (1 - VCover) * (1 - albedoG_{NIR}) \\
&\quad +VCover * [Tran1_{NIR} * (1 - albedoG_{NIR}) + Tran3_{NIR} * (1 - albedoG_{NIR})] \qquad (87)\\
radfacg_{NIRD} &= (1 - VCover) * (1 - albedoG_{NIR}) \\
&\quad +VCover * Tran2_{NIR} * (1 - albedoG_{NIR}) \qquad (88)
\end{aligned}$$

where $Tran1_{Vis,NIR}$, $Tran2_{Vis,NIR}$ and $Tran3_{Vis,NIR}$ are canopy transmittances that depend on various coefficients including the scattering coefficient, leaf projection, vegetation greenness, saturation capacity depth, snow coverage, and solar zenith angle.

3.4.3 Absorbed Radiation

The absorption of radiation by the canopy ($radc3c$) and ground ($radc3g$) are given by

$$\begin{aligned}
radc3c &= \sum_i [radfacc_i * radn_i] + dlwbot * egc \qquad (89)\\
radc3g &= \sum_i [radfacg_i * radn_i] + dlwbot * (1 - egc) \qquad (90)
\end{aligned}$$

where i=$VisB$, $VisD$, $NIRB$, and $NIRD$; $radfacc_i$ and $radfacg_i$ are the corresponding absorption coefficients calculated in the previous section (Section 3.4.2); $radn_i$ are the appropriate incoming radiation components (Section 3.2); $dlwbot$ is the incoming downwelling longwave radiation; and egc is the effective ground cover for thermal radiation. These values account for the incident visible and NIR fluxes.

3.4.4 Net Radiation

The net radiation is calculated from physical laws combined with current losses from the canopy ($closs$), ground ($gloss$), and snow ($sloss$). The losses are given by

$$closs = 2 * egc * \sigma_s * T_c^4 - egc * \sigma_s * T_{sfc}^4 \quad (91)$$

$$gloss = \sigma_s * T_g^4 - egc * \sigma_s * T_c^4 \quad (92)$$

$$sloss = \sigma_s * T_s^4 - egc * \sigma_s * T_c^4 \quad (93)$$

where T_c is the canopy temperature, T_g is the ground temperature, T_s is the snow temperature, and T_{sfc} is the gound temperature if no snow is present, or the snow temperature if there is snow cover. Using these losses and the absorbed radiation, the canopy, ground, and snow net radiation ($radtc$, $radtg$, and $radts$) are given by

$$radtc = radc3c - closs, \quad (94)$$

$$radtg = radc3g - gloss, \text{ and} \quad (95)$$

$$radts = radc3g - sloss. \quad (96)$$

4 Land-Atmosphere Exchanges

Fluxes of heat, water, and carbon use the resistance formulation described in detail in Sellers et al. (1996a) and Vidale & Stöckli (2005). In this approach, exchanges are expressed in terms of differences as

$$\text{flux} = \frac{\text{potential difference}}{\text{resistance}}, \tag{97}$$

and the resistances are the integrals of inverse conductances over a path between specified potential difference endpoints. These fluxes are explicit functions of the atmospheric boundary conditions (Table A1), the prognostic temperature and water stores, three aerodynamic resistances (r_a, r_b, and r_d), the prognostic leaf surface resistance (r_c), and the empirical soil surface resistance (r_{soil}). Using a backward-differencing scheme, SiB4 solves the set of equations for the governing equations. The predicted resistances are used to calculate the heat fluxes and the prognostic temperature changes. The predicted conductances (inverse of resistance) are used to calculate the moisture fluxes (transpiration and soil evaporation), which are used to update the prognostic moisture stores. This section briefly discusses the land-atmosphere exchange processes included in SiB4, which are illustrated in Figure 1.3, and the variables used in this section are listed in Tables B3, B6, and B7.

4.1 Aerodynamic Resistances

The aerodynamic resistance model in SiB4 was originally documented in Sellers et al. (1986). This scheme was modified to describe height-varying leaf-area densities, more accurately representing the wind profile throughout the canopy by Sellers et al. (1989). SiB4 uses this improved turbulent transfer scheme, which is described in detail in Sellers et al. (1996a) and shown in Figure 4.1.

Different turbulence regimes exist between each of the layers, as shown in Figure 4.1. Above the canopy, a turbulent transition layer extends from the top of the canopy (z_2) to a specified height above the canopy (z_t). In this layer, shear stress is assumed to be constant and momentum transfer varies linearly with height. Above z_t, the conventional log-linear wind profile is assumed to be valid. Within the canopy, shear is extracted from the airflow, making the momentum transfer a linear function of local wind speed. The canopy is divided into upper and lower segments, and leaf area density is assumed to increase linearly with height from the lower canopy bound (z_1) to an inflection height (z_c), after which it decreases linearly with height to z_2. Below the canopy, a log-linear wind profile with constant shear stress dependent on the ground roughness length (z_s) links the soil surface to the flow at z_1. The full equation set describing the turbulent transfer profile are provided in Appendix B of Sellers et al. (1996a), and they yield wind speed profiles and transfer coefficients that are used to calculate the aerodynamic resistances.

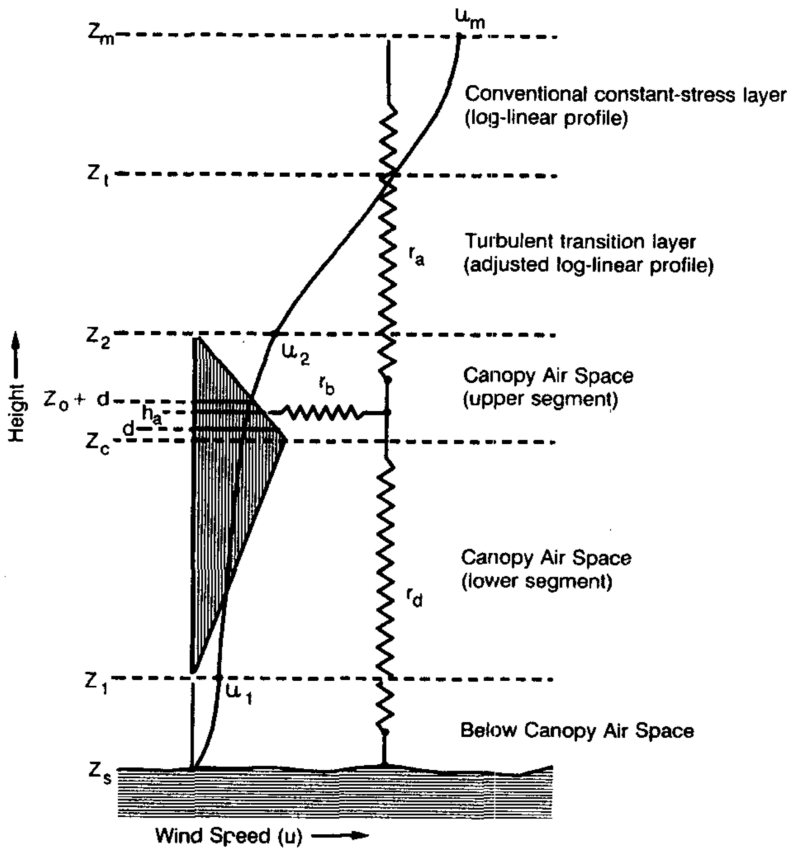

Figure 4.1: SiB Turbulent Transfer Regimes (Sellers et al., 1996a).

SiB4 has three aerodynamic resistances: the atmospheric reference level to canopy air space (CAS) resistance (r_a), the CAS to canopy resistance (r_b), and the CAS to ground resistance (r_d). Following Sellers et al. (1996a), starting at the canopy to the CAS, r_b is given by

$$r_b = \frac{C_1}{(u_2)^{\frac{1}{2}}} = \left[\int_{z_1}^{z_2} \frac{L_d (u)^{\frac{1}{2}}}{p_s C_s} dz \right]^{-1} \quad \text{neutral conditions} \tag{98}$$

$$= \left[\frac{(u_2)^{\frac{1}{2}}}{C_1} + \frac{L_T}{890} \left(\frac{T_c - T_m}{l_w} \right)^{\frac{1}{4}} \right]^{-1} \quad \text{nonneutral adjustment} \tag{99}$$

where C_1 = bulk canopy to CAS resistance coefficient $(\mathrm{m/s})^{-0.5}$
u_2 = wind speed at z_2 (m/s)
C_s = heat-mass transfer coefficient $(90(\mathrm{l}_w)^{0.5})$
l_w = leaf width (m)
L_d = leaf area density $(\mathrm{m}^2/\mathrm{m}^3)$
p_s = leaf shelter factor

The canopy source height is assumed to be equal to the height of r_b, and the resistance from the ground up to the CAS (r_d) is given by

$$r_d = \frac{C_2}{u_2} = \int_{z_s} h_a \frac{1}{K_s} dz \quad \text{neutral conditions} \tag{100}$$

$$= \frac{C_2}{u_2 \phi_H} \quad \text{nonneutral adjustment} \tag{101}$$

$$\phi_H = \left[1 + 9 \frac{(T_g - T_m)}{T_g u_2^2} z_2 \right]^{\frac{1}{2}} \tag{102}$$

where C_2 = ground to CAS resistance coefficient
K_s = heat-water vapor transfer coefficient, assumed equal to K_m (m^2/s)
h_a = canopy source height (m)

Above the canopy, the transfer between the CAS and the reference height is the integration of K_s over the distance from h_a to z_m, including within-canopy (h_a to z_2), turbulent transition layer (z_2 to z_t) and log-linear profile (z_t to z_m) segments:

$$r_a = \frac{C_3}{u_m} = \int_{h_a} z_m \frac{1}{K_s} dz = \left[\frac{1}{k} \log \left(\frac{z_m - d}{z_0} \right) \right]^2 \tag{103}$$

where C_3 is the aerodynamic CAS to reference height resistance coefficient.

4.2 Photosynthesis

Photosynthesis in SiB4 is thoroughly documented in Sellers et al. (1996a). SiB4 uses a physiologically-driven stomatal model that explicitly connects stomatal conductance and photosynthesis (Figure 4.2), and the stomatal model of Ball (1988) combined with the C3 photosynthesis model of Farquhar et al. (1980) expanded by Collatz et al. (1991) and Collatz et al. (1992) comprise the basis for the photosynthesis-conductance model. Leaf stomata control the rate of CO_2 diffusion into the leaf and water vapor out, regulating the addition of CO_2 with the loss of water. Leaf resistance (r_c) is the canopy integral of stomatal resistance (rst), which is the inverse of stomatal conductance ($rst = 1/g_s$). Canopy resistance (r_b) is the canopy integral of the inverse of the conductance from the leaf to the CAS ($1/g_b$), and it regulates the fluxes from the leaf to the CAS. Sensible heat is assumed to be lost from both sides of the leaf, whereas water and CO_2 are assumed to be lost from one side only.

4.2.1 Assimilation

The Collatz et al. (1991, 1992) version of the photosynthesis model defines the leaf assimilation ($assim$, gross photosynthetic rate) as the minimum of three limiting rates: a leaf enzyme limited rate ($assim_{OMC}$), a light-limited rate ($assim_{OME}$), and a carbon compound export limited rate ($assim_{OMS}$). The physiological limit on assimilation ($assim_{OMC}$) is limited by the maximum catalytic capacity of the photosynthetic enzyme (V_{Max}) and is scaled by temperature, moisture, interior CO_2 ($pco2_i$), reference CO_2 ($pco2_m$), and CO_2 and O_2 temperature

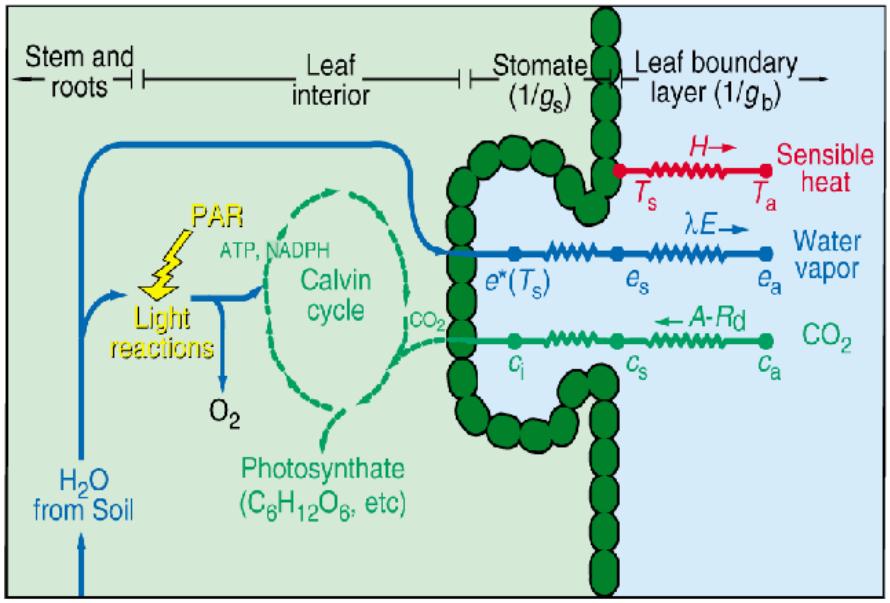

Figure 4.2: SiB Photosynthesis-Conductance Model (Sellers et al., 1996a).

responses (zkc,zko). The light limited rate ($assim_{OME}$) is dependent on the absorbed photosynthetically active radiation ($APAR$) and the CO_2 photocompensation point ($gamma$). The storage-export limiting rate ($assim_{OMS}$) is dependent on V_{Max}, temperature, and soil moisture. These relationships are expressed as:

$$assim \leq \text{Min}(assim_{OMC},\ assim_{OME},\ assim_{OMS}) \tag{104}$$

$$assim_{OMC} = V_{Max,SS}\frac{pco2_i - gamma}{pco2_i + rrkk} * C3 + V_{Max,SS} * C4 \tag{105}$$

$$assim_{OME} = APAR\frac{pco2_i - gamma}{pco2_i + 2gamma} * C3 + APAR * C4 \tag{106}$$

$$assim_{OMS} = omss * C3 + omss * pco2_i * C4 \tag{107}$$

$$rrkk = zkc * (1. + pco2_m/zko) * C3 + \frac{V_{Max}}{5.}(1.8^{0.1(T_C - 298.)}) * C4 \tag{108}$$

$$zkc = 30. * 2.1^{0.1(T_C - 298.)} \tag{109}$$

$$zko = 30000. * 1.2^{0.1(T_C - 298.)} \tag{110}$$

$$omss = \frac{0.5V_{Max} * 1.8^{0.1(T_C - 298.)}}{rstfac_2 * C3 + rrkk * rstfac_2} * C4 \tag{111}$$

$$rstfac_2 = \frac{(1 + wssp) * AW}{wssp + AW} \tag{112}$$

where $V_{Max,SS}$ is a stressed-scaled rubisco velocity, $rstfac_2$ is a rootzone water potential, AW is a vertically-weighted available water potential, and $C3/C4$ are mutually exclusive flags set to 1/0 for PFTs with C3 photosynthesis and set to 0/1 for PFTs with C4 photosynthesis. The leaf net assimilation rate ($assimn$) is given by subtracting the leaf maintenance respiration rate from the gross assimilation.

SiB4 also calculates potential assimilation rates ($assimpot$) that represent the maximum assimilation rate under ideal conditions. For $assimpot_{OMC}$, V_{Max} is used, rather then the stress-scaled, reduced $V_{Max,SS}$. For $assimpot_{OME}$, the top-of-the atmosphere photosynthetically active radiation is used, rather than the surface $APAR$ that is reduced by weather conditions and leaf angle. Finally for $assimpot_{OMS}$, the rootzone water potential is set to the maximum value of one. All of these are combined to produce a single assimilation potential ($assimpot$) that is used to calculate photon pathways and solar-induced fluorescence (SIF).

4.2.2 Stomatal Conductance

Using photosynthesis to link CO_2 gain and water vapor loss, SiB4 calculates the leaf stomatal conductance using the Ball-Berry relationship:

$$g_s = m\frac{assimn}{pco2_s}h_s p + b \tag{113}$$

where $assimn$ is the leaf net assimilation rate, $pco2_s$ is the CO_2 partial pressure at the leaf surface, h_s is the relative humidity at leaf surface, p is the atmospheric pressure, and m and b are empirical coefficients derived from observations. An iterative procedure solves for physiology-specific values of the three assimilation rates along with the CO_2 partial pressures at the chloroplast ($pco2_c$), inside the leaf ($pco2_i$), and at the surface of the leaf ($pco2_s$) and the corresponding conductances.

4.2.3 Canopy Scaling

Since this conductance-photosynthesis model is relevant to a single leaf, it is integrated over the depth of the canopy using a procedure described in Sellers et al. (1992). This method hypothesizes that the maximum rate of photosynthesis exponentially decreases through the canopy following the profile of absorbed photosynthecially active radiation (PAR). Following the equations outlined in Sellers et al. (1996a), canopy photosynthesis and conductance can be scaled from their leaf-level calculations via the summarized relationships

Canopy Rate	=	[Leaf Rate]	[Environmental Forcing]	[Canopy PAR-Use Parameter]
$assim$, g_c	=	$[A_n, g_s]$	$[B1 \cdots B6]$	$[\Pi]$

.

In this method, the enrivonmental forcing terms describe the effects of temperature, humidity, CO_2 concentration and soil moisture stress and are defined in the next section. The canopy PAR-use parameter, Π, can be approximated by

$$\Pi \approx FPAR/\bar{k}, \tag{114}$$

where FPAR is the abosrbed fraction of photosynthetically active radiation and $\bar{k}$ is the time-mean extinction coefficient for PAR. Π varies between zero for no vegetation cover to >1 for dense green vegetation. The canopy assimilation represents the gross photosynthetic rate and the canopy conductance is used to determine the canopy transpiration rate.

4.2.4 Environmental Forcing Potentials

Three environmental potentials (F_{LH}, F_{RZ}, and F_T) are used to scale photosynthesis at various points in the solution, and each of these is unity under optimal conditions and zero in adverse conditions (Sellers, 1987). As a diagnostic, the total environmental potential is the multiplicative of these given by

$$F_E = F_{LH} F_{RZ} F_T. \tag{115}$$

F_{LH} (sometimes referred to as *rstfac1*), is a function of water vapor pressure and represents leaf humidity stress (Collatz et al., 1991; Jarvis, 1976; Sellers et al., 1989, 1992). F_{LH} is calculated as the ratio of the leaf internal water vapor mixing ratio (H_2Oi, hPa/Pa) to the leaf surface water vapor mixing ratio (H_2Os, hPa/Pa), which is expressed as

$$F_{LH} = \frac{H_2Os}{H_2Oi}. \tag{116}$$

F_{RZ} represents root-zone water stress, and following Baker et al. (2008) is calculated as

$$F_{RZ} = \frac{(1 + wssp)\frac{w_{column}}{w_{max}}}{wssp + \frac{w_{column}}{w_{max}}} \tag{117}$$

where w_{column} is water in the column in excess of wilt point (kg), w_{max} is the maximum possible excess of water in the column (field capacity less wilt point, kg), and *wssp* is a water stress curvature parameter, currently set to 0.2. F_{RZ} can be summarized as follows: if the total column soil moisture is above the field capacity, then there is maximum potential and no stress; in contrast, if the soil moisture is below the wilting point, then the plant is totally stressed and thus has zero potential.

F_T is a function of temperature and incorporates high and low temperature stress (Baker et al., 2008; Jarvis, 1976), and it is calculated using the following system of equations:

$$F_T = \frac{1}{T_{High} T_{Low} T_{Frost}} \tag{118}$$

$$T_{High} = 0.98 + e^{shti(T_c - hhti)} \tag{119}$$

$$T_{Low} = 0.98 + e^{slti(hlti - T_c)} \tag{120}$$

$$T_{Frost} = 1 + e^{sfti(hfti - T_{cmin})} \tag{121}$$

$$T_{cmin} = \begin{cases} T_c & T_C < T_{cmin} \\ T_{cmin} + \frac{4dt}{86400} & T_C > T_{Ice} \end{cases} \tag{122}$$

where *shti, slti, hfti, hhti, hlti* are parameters, T_C is the canopy temperature (K), and T_{Ice} is the freezing point of water (273.15 K). T_{cmin} includes a frost recovery at 2°C per day.

Example F_T values are shown in Figure 4.3. The solid black line shows the combined F_T values per corresponding T_c using the parameter values indicated in the caption. The figure shows how the potential decreases rapidly for temperatures near freezing and above a high temperature threshold.

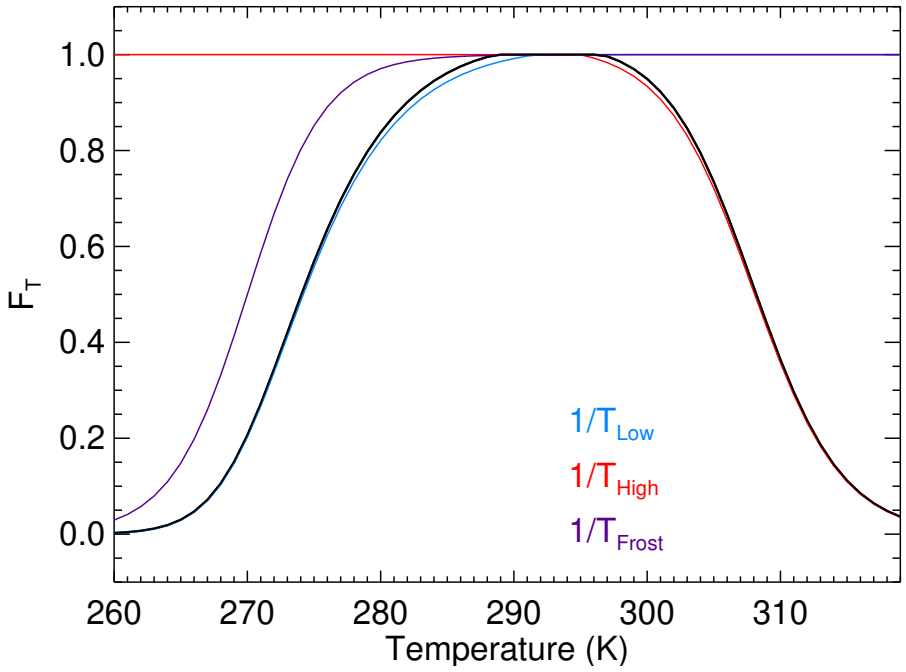

Figure 4.3: Example Environmental Potentials.
The solid black line shows the combined F_T, and the colors show the three components. Parameter values are $slti$=0.2, $shti$=0.3, $hlti$=272, $hhti$=308, $sfti$=0.35, and $hfti$=270.

4.3 Fluxes

As shown in Equation (97), SiB4 calculates fluxes using potential differences and the resistances calculated in the previous sections. Fluxes of sensible heat (H) and latent heat (E) use potential differences represented by temperatures and vapor pressures; and these are summarized in Table 4.1.

Flux	Potential Difference	Resistance
fss	$(T_a$ - $T_m)\ \rho\ c_p$	r_a
H_c	$(T_c$ - $T_a)\ \rho\ c_p$	r_b
H_g	$(T_g$ - $T_a)\ \rho\ c_p$	r_d
fws	$(e_a - e_m)\ \rho c_p/\gamma$	r_a
E_{ct}	$(e^* T_c - e_a)\ \rho c_p/\gamma$	$(r_c + 2r_b)/(1$ - $W_c)$
E_{ci}	$(e^* T_c - e_a)\ \rho c_p/\gamma$	$(2r_b/W_g)$
E_{gs}	$(h_{soil} e^* T_g - e_a)\ \rho c_p/\gamma$	$(r_{soil} + r_d)/(1$ - $W_g)$
E_{gi}	$(e^* T_g - e_a)\ \rho c_p/\gamma$	(r_d/W_g)

Table 4.1: Fluxes, Potential Differences, and Resistances.

where T_a, T_c, T_g, T_m = CAS, canopy, ground, and reference air temperatures (K)
e_a, e_m = CAS and reference vapor pressures (Pa)
e^* = saturation vapor pressure at temperature T (Pa)
ρ, c_p = density, specific heat of air (kg/m^3, J/kg/K)
γ = psychrometric constant (Pa/K)
W_c = canopy wetness fraction (-)
W_g = soil wetness or snow cover fraction (-)
H_c, H_g = canopy and ground sensible heat flux (J/m^2)
E_{ct}, E_{ci} = Canopy interception and transpiration latent heat flux (J/m^2)
E_{gs}, E_{gi} = Ground interception and evaporation latent heat flux (J/m^2)
fss, fws = CAS sensible and latent heat flux (W/m^2)

The full computational procedure that calculates the fluxes, as well as the updates to temperature, hydrology, and radiation, is elaborate; thus, only the simplified predominant equations are shown here. For all of these updates, the partial derivatives are calculated using an implicit solution system, and the system of equations is solved simultaneously by Gaussian elimination at each timestep. Including ten soil layers and five snow layers, the number of equations to be solved simultaneously is 21x21.

4.4 Energy Balance

Energy balance calculations for the CAS, canopy, ground, and total are performed every timestep. All energy balance checks use the formulation:

$$0 = E_{In} - E_{Stor} - E_{Out} \tag{123}$$

where E_{In} is the incoming energy, E_{Stor} is the change in stored energy, and E_{Out} is the outgoing energy. These must sum to 0, or in reality a value near-zero (i.e. 1.E-6), or SiB4 prints the values and stops the simulation.

For the CAS, the energy balance is:

$$E_{In} = (H_g + H_c + E_{ct} + E_{ci} + E_{gs} + E_{gi})/dt \tag{124}$$
$$E_{Stor} = Stor_{HCAS} + Stor_{WCAS} \tag{125}$$
$$E_{Out} = fss + fws \tag{126}$$

where $Stor_{HCAS}$ and $Stor_{WCAS}$ are the changes in CAS heat and water storage (W/m^2) and dt is the timestep length (s). The input fluxes are all saved in units of J/m^2 and are converted to W/m^2 by dividing by the length of the timestep.

For the canopy, the energy balance is:

$$E_{In} = radtc \quad (127)$$
$$E_{Stor} = Stor_{HC} \quad (128)$$
$$E_{Out} = (E_{ct} + E_{ci} + H_c)/dt \quad (129)$$

where $Stor_{HC}$ is the canopy heat storage flux (W/m^2).

For the ground, the energy balance is:

$$E_{In} = radtg \quad (130)$$
$$E_{Stor} = Stor_{HG} \quad (131)$$
$$E_{Out} = (H_g + E_{gi} + E_{gs})/dt \quad (132)$$

where $Stor_{HG}$ is the ground heat storage flux (W/m^2). Using all components, the total energy balance is given by:

$$E_{In} = radtc + radtg \quad (133)$$
$$E_{Stor} = Stor_{HCAS} + Stor_{WCAS} + Stor_{HC} + Stor_{HG} \quad (134)$$
$$E_{Out} = fss + fws \quad (135)$$

These energy balance tests are not necessary in SiB4, and their inclusion is strictly for safety checks. The SiB4 namelist has settings where the user can change the threshold of the error allowed (energyb_thresh), print the energy balance results (energyb_print=True), and not stop when an energy balance error occurs (energyb_stop=False). With small thresholds, occasional errors may occur due to the assumptions and machine precision, particularly during shoulder seasons with rapid changes between liquid water and ice; and the namelist also includes a flag (bnum_allow=10) that allows for a certain number of timesteps to occur before stopping the model (if desired).

5 Hydrology

To simulate the hydrological cycle, SiB4 parameterizes the distribution of precipitation; canopy interception, throughfall, and storage; snow accumulation, compaction, melting, and water transfer between layers; soil liquid and ice water content and redistribution through the soil column; surface runoff; evaporation; and sub-surface drainage and groundwater discharge. The processes are all described in detail in published literature, and this section provides a brief outline of the methods and the associated references. The hydrological variables are listed in Tables B8 and B9.

5.1 Precipitation

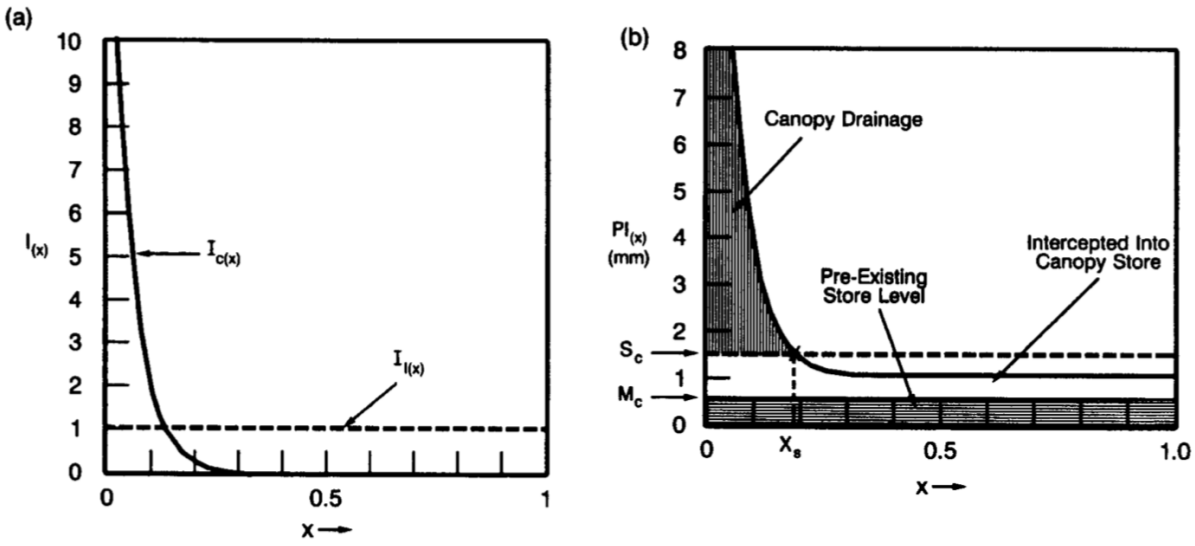

Figure 5.1: SiB Precipitation Relationships (Sellers et al., 1996a).
a) Precipitation area-amount relationships, where x refers to the fraction of the grid area, I_x is the relative amount of precipitation, I_l is the large-scale precipitation (nearly invariant), and I_c is the convective precipitation (nonuniformly distributed). **b)** Precipitation interception dynamics, where the integral of the water amount above $M_{cs} + M_{cw}$ represents the total amount of water intercepted by the canopy. All water above the canopy storage limit S_c drains off the canopy to the ground, and all below is added to the canopy interception store (*capacc*).

Precipitation is provided to SiB4 in two contributions: convective (Pr_{cu}) and large-scale (Pr_{ls}); and the surface precipitation ($p0$) is the sum of these contributions, given by

$$p0 = Pr_{cu} + Pr_{ls}. \tag{136}$$

Hydrological effects resulting from the spatial nonuniformity of convective precipitation are explicitly addressed following Sato et al. (1989b) and Sellers et al. (1996a). For simplicity,

only liquid convective precipitation falling on surfaces above freezing is permitted, and the convective rainfall is spatially distributed according to a simple exponential function (Figure 5.1a).

5.2 Canopy

Canopy throughfall, interception, and storage of precipitation is described in Sato et al. (1989a), Sato et al. (1989b), and Sellers et al. (1996a). Rainfall that falls through gaps in the canopy comprises the direct throughfall component of precipitation and is calculated by a modification of the radiative transfer model. SiB4 has three prognostic interception water stores (canopy surface water, $capcc_{liq}$; canopy surface snow, $capcc_{snow}$; and ground surface liquid, *capcg*). Using the rainfall that is intercepted but not necessarily retained by the canopy, the proportion of the grid area for which the canopy has intercepted enough rainfall to equal or exceed its saturation limit is calculated as

$$PI_{xs} = S_c - M_{cs} - M_{cw} \tag{137}$$

where S_c is the canopy storage limit ($0.0001 L_T$), M_{cs} is the snow already stored on the canopy ($capacc_{snow}$) and M_{cw} is the water already stored on the canopy ($capacc_{liq}$). Figure 5.1b shows how the precipitation area-amount fraction is added to the canopy stores. Integrating the equations provides an estimate of the canopy drainage loss (vertically hatched area), and a canopy wetness fraction (*wetfracc*) is calculated by dividing the current canopy stores by the canopy storage limit. Similarly, the ground surface liquid (*capacg*) is updated, the ground wetness fraction is calculated (*wetfracg*), and the proportion of the grid area for which the ground has intercepted enough rainfall to exceed its surface (puddle) storage limit (S_g=0.2 mm) is also determined. The water in excess of the canopy and ground storage limits is added to the throughfall to provide an effective precipitation rate for the ground surface. If this effective amount is greater than the local infiltration capacity of the soil, overland flow (*roffo*) is generated. Once the overall amounts of precipitation are determined, water on the canopy and ground surface must be determined to be either liquid or snow, and a series of calculations are made to calculate any phase changes, update the necessary variables, and follow through all of the implications.

5.3 Snow

SiB adopted the snow model from the Community Land Model (CLM) Version 3.0 (Dai et al., 2003; Oleson et al., 2000; Schaefer et al., 2009). Snow can occupy up to five layers (*nsl*), and these layers have varying mass and depth. An example of the three snow layers is shown in Figure 5.2. All snow layers have explicit treatment of liquid and ice fraction ($WWW_{Liq,\text{-}nsl:0}$ and $WWW_{Ice,\ \text{-}nsl:0}$), and these prognostic wetness stores are co-located with prognostic snow layer temperatures ($TD_{\text{-}nsl:0}$). Included with the snow hydrology are calculations of the total depth ($snow_{gdepth}$, m) and mass ($snow_{gmass}$, kg/m^2) of snow on the ground, the snow vertical cover fraction ($snow_{cvfc}$), and the snow ground cover fraction ($snow_{gvfc}$). Snow accumulation and the addition of snow layers, along with snow compaction over time, melting, and the remove of snow layers is all described in detail in the CLM technical document (Lawrence et al., 2018).

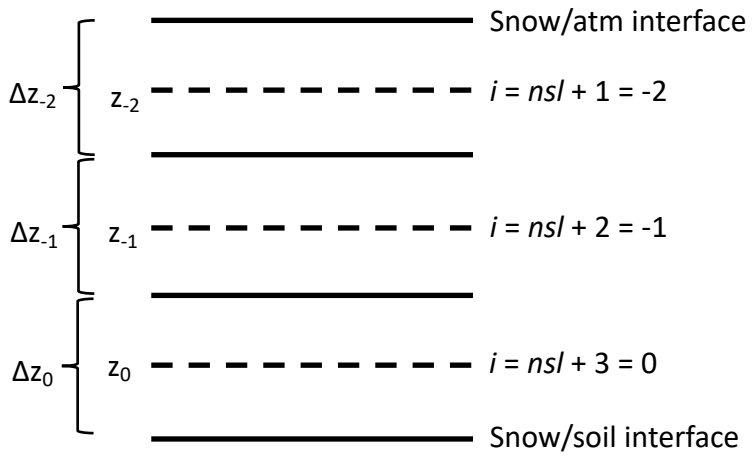

Figure 5.2: Example 3-Layer Snow Pack (Lawrence et al., 2018).

5.4 Soil

SiB adopted the soil model from the Community Land Model Version 2.0 (Bonan, 1996; Oleson et al., 2000). Soil hydrology includes an explicit treatment of frozen and liquid soil water for ten soil layers ($nsoil = 10$, $WWW_{Liq,1:nsoil}$, and $WWW_{Ice,1:nsoil}$). As in the snow model, these prognostic wetness stores are co-located with prognostic soil temperatures ($TD_{1:nsoil}$). Sub-surface runoff (*roff*) occurs when saturated soil moisture conditions exist within the soil column. The soil water predicted in these ten layers is governed by the vertical soil moisture transport dependent on infiltration, surface and sub-surface runoff, gradient diffusion, gravity, and canopy transpiration through root extraction, all of which is described in detail in Lawrence et al. (2018).

5.5 Water Balance

Although not necessary, for safety SiB4 calculates the water balance every timestep:

$$
\begin{aligned}
0 &= p0 - \Delta CAS - Runoff - \Delta Stor - \Delta CAS_{Stor} && (138)\\
\Delta CAS &= fws/(dt * l_{vap}) = (E_{ci} + E_{ct} + E_{gi} + E_{gs})/l_{vap} && (139)\\
Runoff &= roff + roffo && (140)\\
\Delta Stor &= \Delta Int + \Delta Soil + \Delta Snow && (141)\\
\Delta Int &= \Delta capacc_{liq} + \Delta capacc_{snow} + \Delta capacg && (142)\\
\Delta Soil &= \Delta WWW_{liq} + \Delta WWW_{Ice} && (143)\\
\Delta Snow &= \Delta snow_{gmass} && (144)\\
\Delta CAS_{Stor} &= \Delta Stor_{WCAS}/(dt * l_{vap}) && (145)
\end{aligned}
$$

where $\Delta Stor$ is the net change in storage, ΔInt is the change in canopy and ground surface storage, $\Delta Soil$ is the change in the soil moisture stores, $\Delta Snow$ is the change in the snow mass, ΔCAS_{Stor} is the change in CAS water storage from the latent heat flux, and l_{vap}

is the latent heat of vaporization. These all must sum to 0, or in reality a value near-zero (i.e. 1. E-6), or SiB4 prints the values and stops the simulation. As in the energy balance, the SiB4 namelist has settings where the user can change the threshold of the error allowed (waterb_thresh), print the water balance results (waterb_print=True), and not stop when a water balance error occurs (waterb_stop=False). With small thresholds, occasional errors may occur due to the assumptions and machine precision, particularly during shoulder seasons with rapid changes between liquid water and ice; and the namelist also includes a flag (bnum_allow=10) that allows for a certain number of timesteps to occur before stopping the model (if desired).

5.6 Water Availability

SiB includes a number of soil moisture diagnostics in order to predict the moisture availability to plants and the resulting stress on vegetation. Baker et al. (2008, 2013) describe the soil water stress calculations. Here we briefly provide equations of diagnostics that will be used to predict plant phenology and the carbon cycle.

Plant available water (PAW) quantitatively defines how much water in the soil plants have access to. The PAW per soil layer i is defined as:

$$PAW_i = vol_{liq,i} - WP \tag{146}$$

where $vol_{liq,i}$ is the volume of liquid water in soil layer i and WP is the wilting point. To have a metric that quantifies the water available to plants throughout the entire soil column, PAW_{FRW} is defined as:

$$PAW_{FRW} = \frac{\sum_{i=1}^{nsoil} RootF_i \left(vol_{liq,i} - WP\right)}{FC - WP}, \tag{147}$$

where $RootF_i$ is the root fraction in soil layer i, and FC is the field capacity.

Since for many plants the majority of the roots are in the top three soil layers, SiB4 also uses a metric that quantifies the water available to plants in the top three soil layers (PAW_{FTop}), which is calculated as:

$$PAW_{FTop} = \frac{\sum_{i=1}^{3} RootF_i \left(vol_{liq,i} - WP\right)}{FC - WP}, \tag{148}$$

The diagnostics PAW_i, PAW_{FRW}, and PAW_{FTop} are all calculated every timestep.

To quantitatively define the total water available in the soil column, the variable (TAW_{FRW}) can be calculated as:

$$TAW_{FRW} = \frac{\sum_{i=1}^{nsoil} RootF_i \left(\left(vol_{liq,i} + vol_{ice,i}\right) - WP\right)}{FC - WP}, \tag{149}$$

where $vol_{ice,i}$ is the volume of ice in soil layer i. Analogous to PAW, SiB4 also calculates the total water available only in the top three soil layers (TAW_{FTop}),

$$TAW_{FTop} = \frac{\sum_{i=1}^{3} RootF_i \left((vol_{liq,i} + vol_{ice,i}) - WP \right)}{FC - WP}, \tag{150}$$

as well as the daily mean total water available in the top three soil layers (TAW_{FTopD}).

Long-term water availability is used by the prognostic phenology methodology to determine the maximum vegetation coverage suitable for a given climate. SiB4 calculates two climatological water availability values, one for the plant available water ($Clim_{PAWFRW}$) and one for the total available water ($Clim_{TAWFRW}$). In SiB4, these are calculated as long-term running means of their timestep counterparts:

$$Clim_{PAWFRW} = (1 - Clim_{wt}) Clim_{PAWFRW} + Clim_{wt} PAW_{FRW} \tag{151}$$

$$Clim_{TAWFRW} = (1 - Clim_{wt}) Clim_{TAWFRW} + Clim_{wt} TAW_{FRW} \tag{152}$$

$$Clim_{wt} = \frac{1}{Clim_{Len} * steps\_per\_day} \tag{153}$$

where $Clim_{wt}$ is the long-term running mean weighting factor calculated from the parameter $Clim_{Len}$, which is typically set to 10 years.

6 Solar-Induced Fluorescence (SIF)

Plants are able to use sunlight to produce glucose from carbon dioxide and water. During this process, the absorbed photosynthetically active radiation (APAR) has four fates: 1) Photochemistry (P), 2) Thermal Dissipation (D), 3) Energy-Dependent Heat Dissipation (N), and 4) Fluoresence (F) (Kitajima & Butler, 1975; Gentry et al., 1989). While photosynthesis is generally an efficient process, a relatively small ($\sim$1%) fraction of the absorbed energy is re-emitted at longer wavelengths (Jeong et al., 2017). This reemission of natural sunlight is called solar-induced fluorescence (SIF), and it is regulated by the biology of living cells by way of complex mechanisms of energy dissipation (Krause & Weis, 1991; Zhang et al., 2014).

Recently, global satellite measurements of SIF have become available, and these have been used to study plant productivity and phenology (Meroni et al., 2009; Frankenberg et al., 2011; Joiner et al., 2011). Due to phenology, several studies have shown a near linear relationship between remotely-sensed SIF and GPP in seasonal ecosystems (van der Tol et al., 2009; Zarco-Tejada et al., 2013); and ground-based SIF measurements also have been shown to correlate well with GPP from flux towers over seasonal temperate and boreal forests (Joiner et al., 2014; Yang et al., 2015). Since SIF is a physiological process, satellite-based SIF observations offer an alternative view of vegetation function compared to the information on structure and greenness offered by traditional reflectance indices (Jeong et al., 2017).

In order to study and simulate SIF, photosynthesis models have been extended to include SIF predictions (Lee et al., 2015; van der Tol et al., 2014). SiB4 calculates SIF following van der Tol et al. (2014), using leaf-level to canopy-level scaling based on Lee et al. (2015). This section outlines the equations included in the model, and the variables used to calculate SIF are listed in Table B10. For a complete description and derivation of these equations, the readers are referred to the two references listed above.

To calculate SIF, SiB4 uses equations derived by van der Tol et al. (2014) to calculate probabilities for the fate of absorbed photons. First, potential and actual electron transport rates are set from the assimilation rates calculated in the photosynthesis module:

$$sif_{je} = assim \tag{154}$$

$$sif_{jo} = assim_{pot} \tag{155}$$

$$sif_{jejo} = sif_{je}/sif_{jo} \tag{156}$$

where $assim$ is the CO_2 assimilation rate, $assim_{pot}$ is the potential assimilation rate, and sif_{jejo} is their ratio. Using relationships determined from empirical experiments, SiB4 calculates the probabilities of absorbed photons to follow each of the four different pathways:

$$\begin{aligned} sif_{Kd} &= 0.95 \text{ if } T_c < 300 \\ &= 0.95 + 0.0236(T_c - 300) \text{ if } T_c \geq 300 \end{aligned} \tag{157}$$

$$sif_{Kn} = 5.01[(11 {sif_x}^{1.93})/(10.0 + {sif_x}^{1.93})] \tag{158}$$

$$sif_{Kp} = p1(sif_{Kn} + sif_{Kd} + sif_{Kf0})/(1.0 - p1) \tag{159}$$

$$sif_x = 1.0 - sif_{jejo} \tag{160}$$

$$p1 = p2 sif_{jejo} \quad (161)$$
$$p2 = 4.0/(0.05 + sif_{Kd} + 4.0) \quad (162)$$

where sif_{Kd} is the heat dissipation probability, sif_{Kf0} is an initial probability for SIF set to 0.05, sif_{Kn} is the non-photochemical quenching (NPQ) probability, sif_{Kp} is the photosynthesis probability, and sif_x is a GPP scaling factor that is one if there is no GPP and zero is GPP is at its potential. From these constraints, the SIF probability (sif_{Kf}) can be back-calculated:

$$sif_{Kf} = sif_{Kf0}/K_{Tot} \quad (163)$$
$$K_{Tot} = sif_{Kd} + sif_{Kf0} + sif_{Kn} + sif_{Kp} \quad (164)$$

where K_{Tot} is the total probability used to convert these values to yields.

Using these probabilities, yields for each of the four possible actions of an absorbed photon can be calculated:

$$\phi_D = sif_{Kd}/K_{Tot} \quad (165)$$
$$\phi_F = m_f * (1.0 - p1) \quad (166)$$
$$\phi_N = sif_{Kn}/K_{Tot} \quad (167)$$
$$\phi_P = sif_{Kp}/K_{Tot} \quad (168)$$
$$m_f = sif_{Kf0}/(sif_{Kd} + sif_{Kf} + sif_{Kn}) \quad (169)$$

where ϕ_D is the heat dissipation yield, ϕ_F is the SIF yield, ϕ_N is the NPQ yield, and ϕ_P is the photosynthetic yield. The yields sum to one because these processes are mutually exclusive.

Using leaf-to-canopy scaling as described in Lee et al. (2015), SIF is calculated as

$$\text{SIF} = PAR_{NS} * FPAR * 1.\text{E}6 * \phi_F/\kappa \quad (170)$$
$$\kappa = 0.04 * V_{Max} * 1.\text{E}6 + 8.1 \quad (171)$$

where PAR_{NS} is the non-scattered PAR, $FPAR$ is the absorbed fraction of PAR, V_{Max} is the maximum rubisco velocity, and 1.E6 is a units conversion factor.

7 Carbonyl Sulfide (COS)

Carbonyl Sulfide (COS) is an atmospheric trace gas that is an analog of carbon dioxide (CO_2). The main source of COS is biogenic activity in the ocean, and the main sinks of COS are vegetation leaves and soil (Cutter et al., 2004). Because it is taken up by plants during photosynthesis and soils during microbial activity, it can provide information on carbon cycle processes. Berry et al. (2013) implemented mechanistic and empirical descriptions of leaf and soil COS uptake into SiB in order to predict estimates of the COS land flux. The equations included in SiB4 are summarized here, and the SiB4 COS variables are listed in Table B11.

7.1 Leaf Uptake

Atmospheric COS is taken up by vegetation as it is travels from the atmosphere into the leaves, where it is consumed inside chloroplasts in the leaf cells by the carbonic anhydrase (CA) enzyme. Once COS has diffused into leaf cells, it is hydrolyzed in a reaction that is catalyzed by CA at a rate proportional to the partial pressure of COS in the chloroplast. This process is described in detail by Berry et al. (2013), who developed and evaluated a model for predicting COS leaf uptake in SiB.

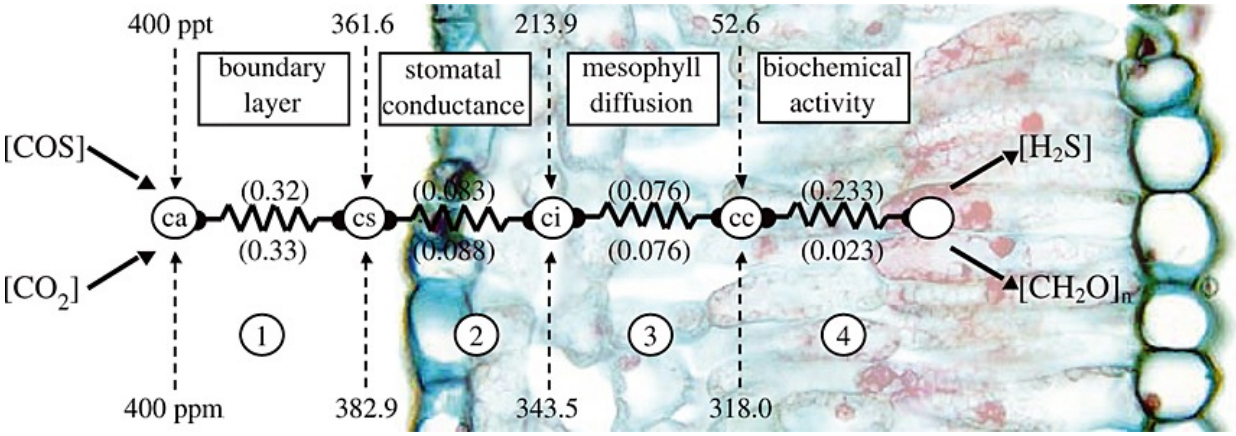

Figure 7.1: COS Uptake-Resistance Model (Berry et al., 2013).
Numbers in parentheses are conductance values corresponding to the process stated in the square boxes: 1) Boundary layer conductance, g_b; 2) Stomatal conductance, g_s, 3) Mesophyll conductance; and 4) Biochemical rate constant. Together steps 3 and 4 comprise the apparent COS conductance, g_{COS}.

Since COS takes the same pathway as CO_2 through a leaf to the location of consumption inside the chloroplasts, the assimilation of COS can be modelled by the same series of resistances as CO_2, as shown in Figure 7.1. Relative to H_2O, which also traverses through the same pathway from the atmosphere to the leaf cells, the greater mass and larger cross section of COS restricts its diffusion by a factor of 1.94 in the stomatal pore and 1.56 in the laminar boundary layer (Seibt et al., 2010; Stimler et al., 2010). Analogous values for CO_2

are 1.6 and 1.4, respectively; leading to ∼20% slower gas phase diffusion of COS than CO_2. Once COS has diffused into the leaf cell, it is hydrolyzed in a reaction that is catalyzed by the CA enzyme. While the rate at which this occurs remains uncertain globally, studies indicate that the mesophyll conductance and biochemical CA activity scale with the photosynthetic capacity (V_{Max}, maximum rubisco velocity in the leaf) (Badger & Price, 1994; Evans et al., 1994). Using this assumption, these two processes can be combined into a single conductance for COS uptake (g_{COS}) that is proportional to V_{Max} such that

$$g_{COS} = \alpha * V_{Max} \tag{172}$$

where α is a parameter that is calibrated to observations of simultaneous measurements of COS and CO_2 uptake (Stimler et al., 2012). Anaysis of these measurements yield estimates of α of ∼1400 for C3 and ∼7500 for C4 species.

Using this framework and simplifications, the COS uptake ($assim_{COS}$) is expressed as

$$\begin{aligned} assim_{COS} &= cos_{CAS} * gt_{COS} && (173)\\ gt_{COS} &= [1.56/g_b + 1.94/g_s + 1.0/g_{COS}]^{-1} && (174)\\ g_{COS} &= 1400 * V_{MaxT} * (1.0 + 5.33 * C4) * APAR_{KK} * RSTFAC_2 && (175)\\ &\quad *(P/P0_{Sfc}) * (T_{Can}/T_{Ice}) \end{aligned}$$

where cos_{CAS} is the COS mole fraction in the canopy air space (CAS), gt_{COS} represents the series conductance of the leaf system for COS calculated from the respective water vapor conductances predicted by SiB (Figure 7.1), V_{MaxT} is the temperature-adjusted V_{Max} rate, $APAR_{KK}$ is the scaling factor for leaf radiation, $RSTFAC_2$ is the rootzone water potential, P is the pressure, $P0_{Sfc}$ is the reference surface pressure (10,000 Pa), T_{Can} is the canopy temperature, and T_{Ice} is the freezing temperature of water (273.15 K).

As a diagnostic, the leaf relative uptake of COS compared to CO_2 (lru_{COS}) is

$$lru_{COS} = (assim_{COS}/assim) * (CO2_m/COS_m) \tag{176}$$

where $assim$ is the assimilation rate of CO_2, $CO2_m$ is the reference level CO_2 concentration, and COS_m is the reference level COS concentration. COS concentrations at the leaf surface and inside the leaf can also be calculated as diagnostics such that

$$\begin{aligned} cos_s &= cos_{CAS} - assim_{COS} * (1.56/g_b) \text{ and} && (177)\\ cos_i &= cos_s - assim_{COS} * 1.94/g_s), && (178) \end{aligned}$$

where cos_s is the COS concentration at the leaf surface and cos_i is the internal leaf COS concentration.

7.2 Soil Uptake

Because uptake also occurs in soil organisms, COS diffused into the soil is also hydrolized (Seibt et al., 2006; Wingate et al., 2008). While an empirical study by Van Diest & Kesselmeier (2008) indicated that the COS soil diffusion rate is a function of the activity of CA, soil temperature, porosity, and water content, explicit values for these relationships is

currently not available globally. Due to this limitation, SiB uses a soil COS uptake that is proportional to CO_2 production by soil respiration (Yi et al., 2007). Since R_h is modeled separately for each soil layer in SiB4, the soil COS uptake is calculated separately for the top three layers (i=1,2,3), with the total flux being sum from these layers scaled to the total soil respiration. The soil COS uptake ($grnd_{COS}$) can be expressed as a function of the heterotrophic respiration (R_h):

$$
\begin{aligned}
grnd_{COS} &= \sum_{i=1}^{3} k_{soil} * cos_{CAS} * F(\theta)_i * R_{h,i}/R_{h3} * R_h && (179)\\
F(\theta)_i &= F(Freeze)_i * F(Temp)_i * F(Moist)_i && (180)\\
F(Freeze)_i &= WWW_{Liq,i}/(WWW_{Liq,i} + WWW_{Ice,i}) && (181)\\
F(Temp)_i &= MHRT_{Soil,Hot,i} && (182)\\
wfract_i &= (WWW_{Liq,i}/(dz_i * poros * denh2o)) * (RootF_i/RootF_3) && (183)\\
F(Moist)_i &= [1.42 - 1.42 * wfract_i] && (184)\\
&\quad *(0.8 * wsat^{((wfract^{zm} - woptzm)/(1.0-woptzm))^2})
\end{aligned}
$$

where k_{soil} is the COS soil decay rate (12000 s^{-1}) relating the COS flux with R_h; the function $F(\theta)$ represents water and temperature responses; $R_{h,i}$ is the heterotrophic soil respiration per soil layer, R_{h3} is the total heterotrophic soil respiration in the top three layers, and R_h is the total heterotrophic soil respiration (sum of all ten layers). In calculating the temperature and moisture sensitivities, $WWW_{Liq,Ice}$ are the soil liquid and ice content (per soil layer), $MHRT_{Soil,Hot}$ is the respiration high temperature potential (per soil layer), dz is the soil layer thickness, $poros$ is the soil porosity, $denh2o$ is the density of water (1000 kg m^{-3}); $RootF$ is the root fraction (per soil layer), $RootF_3$ is the total root fraction in the top three soil layers; and $wfract$, $woptzm$, $wsat$, and zm are variables calculated during the determination of soil respiration. While the temperature sensitivity of COS uptake is the same as that used in heterotrophic respiration, the moisture sensitivity of COS uptake falls more quickly with soil moisture than R_h, reaching a minimum of 0 in completely saturated soils.

7.3 Prognostic Canopy Air Space (CAS) COS

Similar to the prognostic CAS CO_2 calculation, cos_{CAS} is a prognostic variable calculated as

$$
\begin{aligned}
cos_{CAS} &= [cos_{CAS,prev} + dt_{SiB}/cos_{cap} * ((COS_m * g_a) - grnd_{COS} - assim_{COS})] && (185)\\
&\quad /[1.0 + (dt_{SiB} * g_a)/cos_{cap}]
\end{aligned}
$$

where $cos_{CAS,prev}$ is the cos_{CAS} concentration of the previous timestep, dt_{SiB} is the model timestep, cos_{cap} is the air capacity for the COS exchange, and g_a is the mixed-layer to CAS conductance. Using the prognostic cos_{CAS} concentration, the net COS flux is given by

$$flux_{COS} = g_a * (cos_{CAS} - COS_m). \quad (186)$$

8 Dynamic Prognostic Phenology

SiB4 models plant phenology by taking advantage of the growth stage concept without relying on empirical values or satellite vegetation data. To predict plant phenology, SiB4 uses dynamic stages that respond to the leaf state and environmental conditions. The overarching idea is that vegetation progresses through phenology stages during a growing season; however, the phenology stage can change daily. This dynamic behavior means that plants can progress through the stages at different rates, returning to growth stages at any time or never existing in specific stages. For example, desert environments with short rainy seasons rapidly progress through the stages, while evergreen forests are never dormant.

In this approach, described in detail by Haynes et al. (2019a), the timing and length of each phenology stage is not prescribed, but rather is diagnosed using a combination of potentials that respond to assimilation rate, climate, day length, leaf pool size, and plant stress from the associated weather and environmental conditions. This dynamic strategy allows SiB4 to simulate day-to-day, seasonal, and interannual variability using a mechanistic approach. The phenology stage can change daily and is associated with specified maximum rubisco velocities (V_{Max}), carbon pool allocations ($Alloc$), and carbon transfers from live to dead pools. We performed sensitivity studies, finding that five stages optimally captures the leaf-out and senescence of deciduous-type vegetation, while also providing sufficient options to simulate carbon flux and pool variability in evergreen-type vegetation across a broad range of climates. The parameters and variables for the prognostic phenology are listed in Tables A6 and B12.

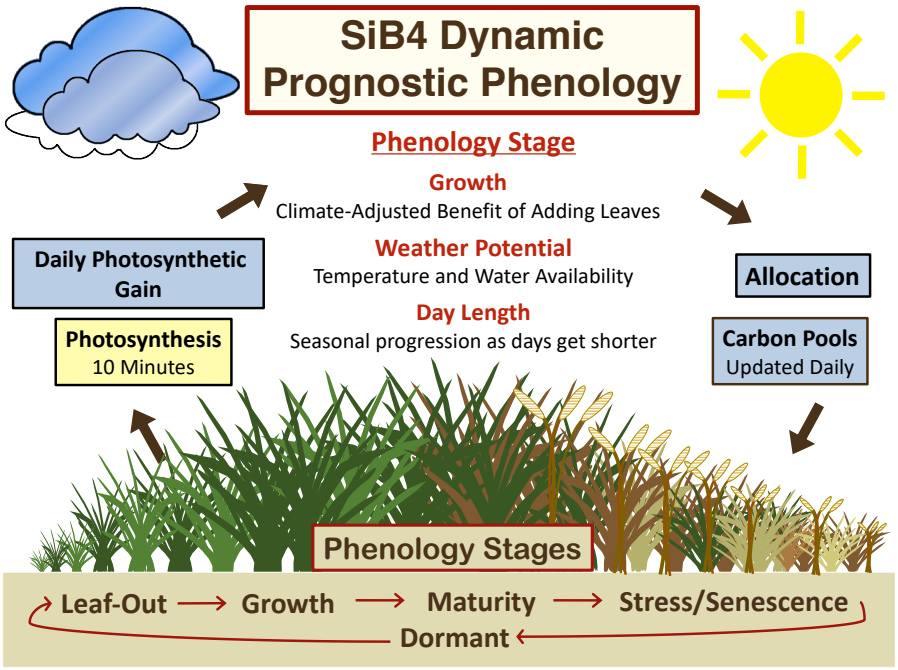

Figure 8.1: SiB4 Dynamic (Non-Crop) Phenology.

An overview of the SiB4 dynamic phenology model is shown in Figure 8.1. Sub-hourly photosynthesized carbon is summed daily and allocated to the live pools depending on the seasonal development, which is represented by the phenology stage (also updated daily). The appropriate aboveground carbon pools are used to determine the LAI, which then is used to calculate photosynthesis. In addition to being used for allocation, the phenology stage also plays a role in determining the maximum rubisco velocity (V_{Max}), which affects the rate of photosynthesis, as well as live pool turnover for senescence (T_P). At the end of the season, a minimal LAI is maintained in order for growth to occur once environmental conditions are suitable, which is analougous to a labile carbon or storage pool used by some models, or the seed carbon used in the crop phenology model.

8.1 Phenology Stages

To represent plants as they develop and mature through the growing season, SiB4 defines five phenology stages ($nstage = 5$), which are listed in Table 8.1.

Num	Stage
1	Leaf-Out
2	Growth
3	Maturity
4	Stress/Senescence
5	Dormant

Table 8.1: Dynamic Phenology Stages.

In leaf-out, growth begins from stored carbon, since the canopy cannot support photosynthesis. This stage begins when the environmental conditions become suitable for photosynthesis, which is determined from day length, soil moisture, and temperature. During the growth stage, leaf growth is still promoted from carbon allocation, since the canopy continues to benefit by growing more leaves to intercept more light. This stage begins when the canopy is large enough to support photosynthesis, and ends when an approximate balance is reached between gains for growing leaves versus costs for maintaining leaves. At maturity, the leaf amount is sustained and allocation is balanced between canopy maintenance, root growth, and product production (seeds, fruit, and flowers). When there is a penalty for growth because of high maintenance costs, plants move to the stress stage, where all carbon is allocated to the roots for storage. During this stage, leaf photosynthetic capacity (V_{Max}) is reduced, and the leaf transfer fraction (T_P) may be increased to help enhance senescence. Once there are no leaves in the canopy or conditions are not suitable for photosynthesis, the vegetation enters the dormancy phase. In this stage, the canopy is inert, there is no photosynthesis, and autotrophic respiration continues at a low rate. This stage continues until phenological triggers initiate a transition to leaf-out.

8.2 Stage Selection

8.2.1 Phenology Index (PI)

The timing and length of each phenology stage are diagnosed from a combination of potentials that depend on climate, day length, leaf pool size, and plant stress from the associated weather and environmental conditions. In order to quantify the shifting between phenology stages, this scheme uses a phenology index (PI) such that:

$$PI = \text{Min}\Big[PS_{DayL},\ PS_{Grw},\ PS_{Wx}\Big] \tag{187}$$

where PS_{DayL} is a day length potential, PS_{Grw} is a growth potential, and PS_{Wx} is a weather potential. When it is beneficial to grow leaves and environmental conditions support photosynthesis, PI will be near 1; however, when there is no benefit to growing leaves or when conditions are not suitable for photosynthesis, then PI will be near 0. To distinguish between the phenology stages, SiB4 applies prescribed threshold values (PI_{Thresh}) to PI. Currently all vegetation uses the same thresholds of 0.8, 0.6, 0.4, and 0.2 between stages 1 to 5, respectively; however, SiB4 has the flexibility for the user to change these for any PFT.

8.2.2 Day Length Potential (PS_{DayL})

Photoperiod is a dominant cue to initiate senescence processes, particularly in the Arctic (Ernakovich et al., 2014; Estiarte & Peñuelas, 2015; Pau et al., 2011). To progress the phenology as days get shorter, as well as to prohibit leaf-out during mild weather events during the winter, this strategy uses a photoperiod potential (PS_{DayL}). The day length potential captures the idea that vegetation responds to shortening days as a trigger for the end of the growing season, allowing a way to model the evolutionary behavior of high-latitude vegetation in preparing for the oncoming winter.

Since sensitivity studies in the Arctic suggest that vegetation in high latitudes may begin to prepare for the end of the growing season even before the equinox, PS_{DayL} has been designed to include expressions that decrease this potential even when day lengths are approaching their longest values. To do this, PS_{DayL} has three parameters: PSD_{Ref}, which is used as a reference value and typically varies between -1 and 2; PSD_{Mul}, which is a multiplier for the rate of the decrease in the day length potential; and PSD_{Min}, the minimum value that PS_{DayL} can drop down to. When PSD_{Ref} is < 0, then PS_{DayL} begins decreasing prior to the equinox. The equations for this circumstance are

$$PS_{DayL} = \begin{cases} 1 - PSD_{Mul}\left(DayL - DayL_O\right) & DayL_{dt} \geq 0 \\ 1 - DayL_A - PSD_{Mul}\left(DayL_{Max} - DayL\right) & DayL_{dt} < 0 \end{cases}, \tag{188}$$

$$DayL_O = \left(DayL_{Max} + PSD_{Ref}\right), \text{ and} \tag{189}$$

$$DayL_A = DayL_{Mul}\left(DayL_{Max} - DayL_O\right). \tag{190}$$

where $DayL$ is the length of day, $DayL_{dt}$ is the change in the length of day, $DayL_{Max}$ is the length of the longest day of the year, and $DayL_O$ is an offset value.

In contrast, when PSD_{Ref} is ge 0, then PS_{DayL} begins decreasing after the equinox. The equations for this circumstance are

$$PS_{DayL} = \begin{cases} 1 & DayL_{dt} \geq 0 \\ 1 - PSD_{Mul}\left(DayL_O - DayL\right) & DayL_{dt} \leq 0 \end{cases} \quad \text{and} \tag{191}$$

$$DayL_O = \left(DayL_{Max} - PSD_{Ref}\right). \tag{192}$$

Regardless of when PSD_{Ref} begins decreasing, it always must satistfy

$$PSD_{Min} \leq PS_{DayL} \leq 1. \tag{193}$$

This set of equations allows the strength of the photoperiod phenological response to vary with vegetation type and with latitude. For PFTs that exist across all latitudes, the length of day can have no impact on the phenology at low latitudes (e.g. tropics), while the length of day can have significant phenological impacts at high latitudes (e.g. arctic). Sample PS_{DayL} values for two different latitudes and four different combinations of parameters are shown in Figure 8.2.

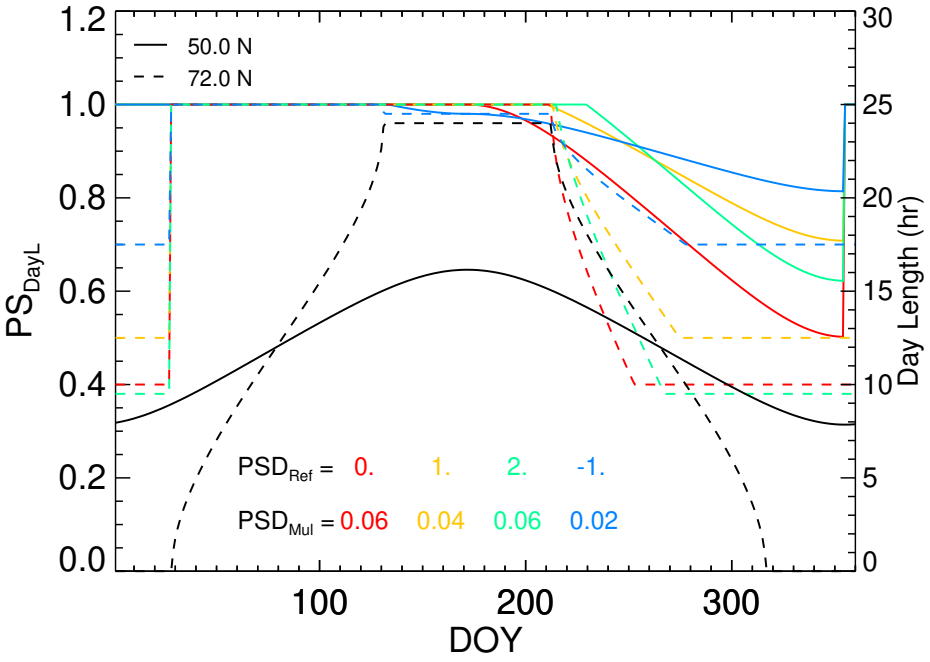

Figure 8.2: Sample Day Length Potentials.
The black lines show the day length, and each of the colors represents a different combination of parameters. The solid lines show the values at 50°N and the dashed lines show the values at 72°N.

8.2.3 Growth Potential (PS_{Grw})

The growth potential evaluates the benefit of adding new leaves as opposed to allocating carbon belowground, capturing the idea that vegetation has evolved to grow to established sizes based on both climate and seasonal conditions. Vegetation grows as large as the environmental conditions will support, be it limited by water, temperature, or nutrients. For example, large, extensive forest canopies exist where both weather and temperatures are optimal for growth; whereas small and sparse vegetation occurs in deserts that are water limited or in tundra environments that are temperature limited. Since climate is likely the dominant determining factor in long-term vegetation growth and sustainability, PS_{Grw} makes use of a climatological LAI and water availability in order to provide a metric to quantitatively evaluate climate suitability. The behavior of the growth potential follows the light-use efficiency curve and radiation saturation effect. When there is minimal vegetation coverage, each additional leaf has a significant impact on the photosynthesis rate. In contrast, as the canopy closes and approaches the maximum aboveground biomass that can be supported by the climate, adding more leaves is no longer beneficial. To mimic this behavior, the growth potential changes as necessary, starting at its maximum value when the vegetation is minimal (highest potential for growth) and decreasing to its minimal value with a full canopy.

The growth potential (PS_{Grw}) linearly decreases with increasing LAI such that:

$$PS_{GI} = \begin{cases} 1 & \text{LAI} \leq ClimLAI_{Min} \\ \dfrac{PSG_{Max} - PSG_{Min}}{ClimLAI_{Min} - ClimLAI_{Max}} & ClimLAI_{Min} \leq \text{LAI} \leq ClimLAI_{Max} \\ PSG_{Min} & \text{LAI} \geq ClimLAI_{Max} \end{cases} \quad (194)$$

where $ClimLAI_{Min}$ and $ClimLAI_{Max}$ are the diagnosed minimum and maximum LAI for a given climate, and PSG_{Min} is a parameter.

Using PFT-specific relationships, minimum and maximum bounds of LAI calculated from long-term water availability are compared to current LAI values, determining PS_{Grw}. Example PS_{Grw} values are shown in Figure 8.3, where each colored line represents different climates with different $ClimP$ values and thus different LAI bounds. At the start of a growing season, the LAI is minimal, so PS_{Grw} is at its maximum potential of 1. As the LAI increases, the benefit of adding more leaves decreases due to increasing respiratory costs or decreasing resources, such as limited light or water. PS_{Grw} linearly decreases with increasing LAI until it reaches its minimum value (PSS_{Min}) when LAI surpasses $ClimLAI_{Max}$. As PS_{Grw} decreases, PI decreases, advancing the phenology stage.

The minimum and maximum canopy fullness values ($ClimLAI_{Min}$, $ClimLAI_{Max}$) supported by climatic conditions is determined from 10-year running means initialized during spin-up using

$$ClimLAI_{Min} = ClimP^{CL_C} + CL_L \text{ and} \quad (195)$$

$$ClimLAI_{Max} = ClimP^{CL_C} + CL_G, \quad (196)$$

where $ClimP$ is a climatological suitability index and CL_C, CL_L, and CL_G are parameters. $ClimP$ can exponentially or linearly scale climatic water availability to cover environmental

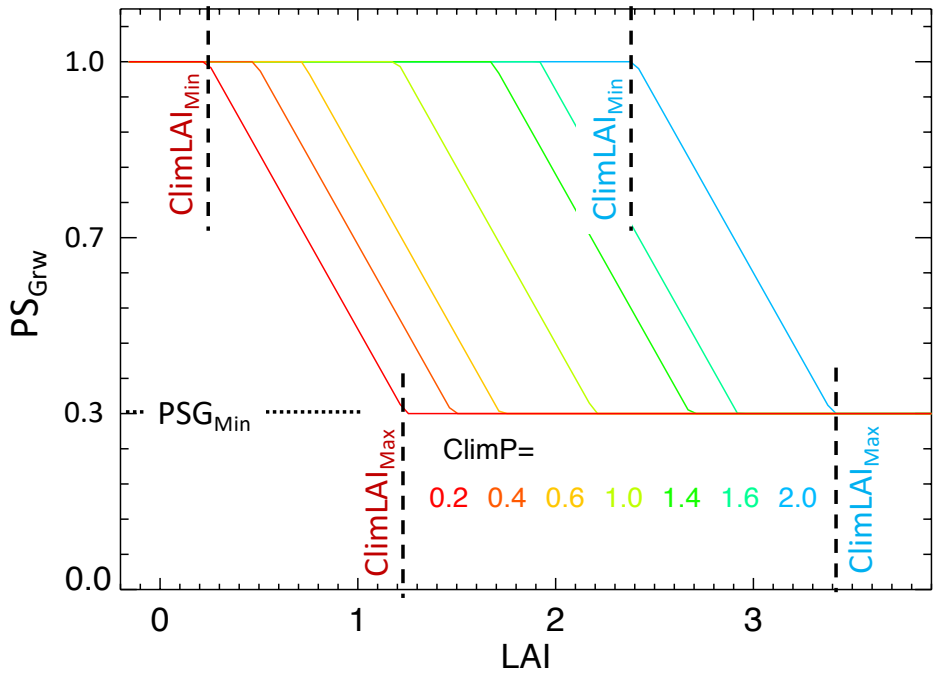

Figure 8.3: Example Growth Potentials.

conditions specific to each vegetation type. Being an index, $ClimP$ is minimal in climates that cannot support vegetation and increases with increasing water availability. $ClimP$ is calculated as

$$ClimP = CP_A(CP_B)^{ClimW} + CP_C(ClimW - CP_D) \tag{197}$$

$$CP_{Min} \leq ClimP \leq CP_{Max} \tag{198}$$

where $ClimW$ is a climatological water availability index and CP_A, CP_B, CP_C, CP_D, CP_{Min}, and CP_{Max} are parameters.

$ClimW$ provides a standardized metric to determine the climatological amount of soil water available to plants, since water availability is a key determinant of plant productivity. Because climates have different responses to various water availability calculations, SiB4 includes the flexibility to change which water availability metric is used for $ClimW$ depending on PFT. Using the parameter CWA_{Type}, the user can specify which of four climatological water availability metrics to use: 1) Convective Precipitation ($Clim_{Cupr}$), 2) Precipitation ($Clim_{Pr}$), 3) Root-Weighted Plant Available Water ($Clim_{PAWFRW}$), or 4) Root-Weighted Total Available Water ($Clim_{TAWFRW}$). All are 10-year running averages of their timestep counterparts, where convective and total precipitation are provided by the driver data and PAW_{FRW} and TAW_{FRW} are calculated as shown in Section 5.6.

The relationships between $ClimP$ and $ClimW$ used for the grassland PFTs are shown in Figure 8.4. Because grasslands grow across a wide climatic range, they demonstrate the different functionalities that can exist between $ClimP$ and $ClimW$, and all three grasslands use $Clim_{PAWFRW}$ as their water availability metric. C4 grasslands use the exponential functionality (using CP_A and CP_B) to rapidly increase $ClimP$ for water availability values in the mid-range of $ClimW$. For these grasslands, small differences in $ClimW$ can produce

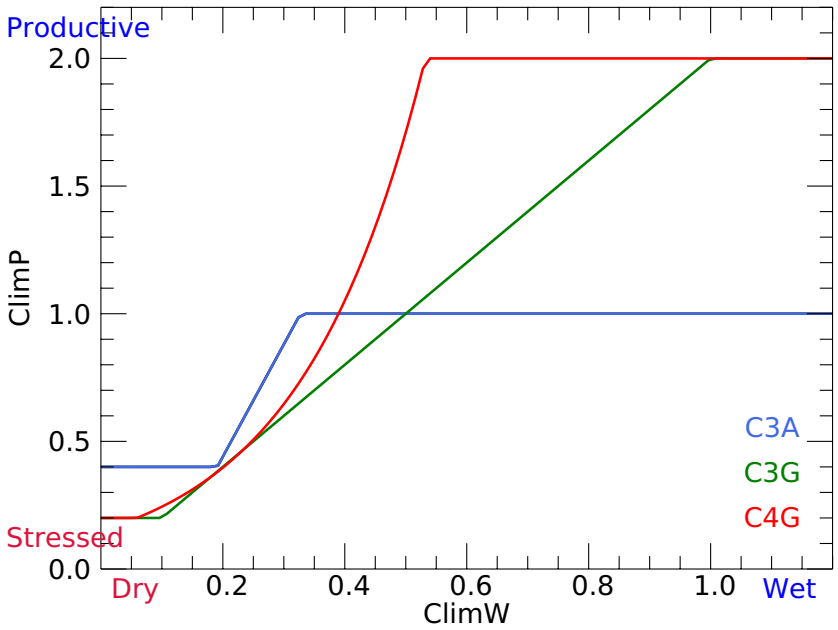

Figure 8.4: Example Climate Suitability and Water Availability Relationships.

large differences in vegetation greenness and productivity, so $ClimP$ values extend from 0.1 to 2. C3 grasslands use the linear relationship between $ClimP$ and $ClimW$. Temperate $C3$ grasslands also cover broader climate conditions, thus $ClimP$ values for this PFT also extend from 0.1 to 2. In contrast, arctic grasslands typically grow in water stressed environments due to either low precipitation amounts or freezing conditions, and because of this the changing $ClimP$ values are focused on low $ClimW$ values.

8.2.4 Weather Potential (PS_{Wx})

The phenology weather potential utilizes real-time weather conditions and soil moisture to represent the potential photosynthesis, capturing how vegetation responds to humidity, temperature, and water stress. This factor allows vegetation to respond to transient conditions. PS_{Wx} is unity at the start of the growing season when environmental conditions are suitable for photosynthesis, ensuring rapid growth immediately at the onset of leaves. As the growing season progresses and the environmental conditions required for photosynthesis deteriorate, PS_{Wx} decreases until it reaches zero under highly stressed conditions when photosynthesis is inhibited.

The equation used to calculate PS_{Wx} is

$$PS_{Wx} = \left(\frac{PF_{Wx}}{PF_{Wx,SM}} \right), \tag{199}$$

where PF_{Wx} is a combined potential that is sensitive to soil moisture, humidity, and temperature, and $PF_{Wx,SM}$ is the seasonal maximum of PF_{Wx}. The combined potential PF_{Wx} is calculated as

$$PF_{Wx} = \frac{1}{2} \left(PF_E + PF_{WA} \right), \tag{200}$$

where PF_E and PF_{WA} are 10-day running mean potentials that represent environmental conditions and water availability. Since the phenology scheme aims to follow seasonal plant progression, 10-day running means provide an optimum length to avoid spontaneous reactions in plant growth due to short-lived weather systems, while still responding to synoptic and seasonal-scale anomalies. All PFTs and running-mean phenology variables use this length; however, each variable has its own input parameter in SiB4 and can be changed as the user sees appropriate.

PF_E is a combined potential from three envoronmental conditions and is the 10-day running mean of the environmental potential used to scale photosynthesis (F_E, Section 4.2). PF_E is the multiplicative of three potentials, F_{LH}, F_{RZ}, and F_T. To summarize, the F_{LH} potential represents leaf humidity stress (Sellers et al., 1992), the F_{RZ} potential represents root-zone water stress (Baker et al., 2008), and the F_T potential incorporates high and low temperature stresses (Baker et al., 2008; Jarvis, 1976).

To intensify the effects of drought, F_{WA} is the 10-day running mean of a water availability metric. The parameter $PSWX_{Type}$ allows the user to select a water availability metric per PFT from eight options:

1. PAW_{FTop}
2. PAW_{FZW}
3. $PAW_{FZW} \cdot 2$
4. No stress for $PAW_{FZW} > 0$
5. TAW_{FTop}
6. TAW_{FZW}
7. F_{RZ}
8. F_E

All of the PAW and TAW options are defined in Section 5.6.

8.3 Growing Season Start

The beginning of the growing season depends on climate and is not always straight-forward. For example, temperate grasslands may have strong seasonality with a dormancy period during the winter, while tropical vegetation continues growing all year. Adding even more complexity, grasslands may have two growing periods within a single year, with a brief period of browning in-between when the environmental conditions are too hot and dry to support growth; while in contrast, deciduous forests typically only have one leaf-out period for the entire growing season. To mimic natural behavior, the phenology scheme needs to be dynamic, with the ability to return to the leaf-out or growing stages when necessary, while not triggering leaf-out mid-season for vegetation experiencing mid-season stress that should only have a single seasonal cycle.

To accomplish this, one of the phenological potentials, PS_{Wx} can be reset in order to help obtain the leaf-out stage when warranted. With PS_{Wx} being a ratio, it is reset to unity by

setting the seasonal maximum value $PF_{Wx,SM}$ equal to the current value PF_{Wx}. For seasonal vegetation, this ensures rapid growth from a minimal leaf pool when day lengths are not substantially decreasing. However, for non-seasonal vegetation that may not ever obtain the conditions required for resetting the stress factor, leaf-out or growth can still be obtained if the conditions support rapid growth.

To determine when $PF_{Wx,SM}$ is reset, SiB4 uses two flags. The first is the growing season suitability flag ($FlagG$), which is true when conditions are suitable for photosynthesis. Following the growing season start drivers used by Jolly et al. (2005), SiB4 uses temperature, soil moisture, and day length requirements to begin a growing season. For temperature, the daily mean temperature (TM_D) must be between a specified minimum temperature (GT_{Min}) and maximum temperature (GT_{Max}) for a specific number of days (GT_{Len}). For soil moisture, SiB4 uses the root-weighted total available fraction of water in the top three layers (TAW_{FTop}). The top three soil layers contain ∼75% of simulated roots, thus these layers can be used to indicate water availability while responding quickly to precipitation events given their shallow depth. To start the growing season, TAW_{FTop} must be above a specified value (GW_{Min}) for a specific number of days (GW_{Len}). For light, the day length must be longer than a specified minimum length. When the days are getting longer, the required day length is given by GL_{MinI}. When the days are getting shorter, SiB4 has two choices to determine if the day length is suitable to start a growing season. If GL_{OffD} is negative, then the day length must be greater than the absolute value of GL_{OffD}. Otherwise, the day length subtracted from the maximum day length must be less than GL_{OffD} to start a growing season, indicating that only a minimal amount of day has passed since the occurrence of the maximum day length. If all three of these conditions are met, then $FlagG$ is true, otherwise $FlagG$ is false.

The second flag used to determine the start of the growing season is an assimilation flag ($FlagA$), which is set to true when the assimilation rate becomes minimal at the end of the growing season. $FlagA$ makes use of an assimilation potential (PF_A) and is true when

$$PF_A < AL_{RV} \text{ and} \tag{201}$$

$$PF_A = \frac{AssimRM}{AssimSM}, \tag{202}$$

where AL_{RV} is a parameter that is currently set to 0.1 for all PFTs. In calculating PF_A, $AssimRM$ is a 10-day running-mean of the assimilation rate, and $AssimSM$ is the seasonal maximum of $AssimRM$. As with the other running-mean lengths used in this phenology approach, SiB4 has a PFT-specific parameter AL_{RL} to change the running-mean length if desired. The occurrence of both $FlagA$ and $FlagG$ indicates a new growing season can begin and the vegetation can commence leaf-out.

8.4 Phenology and Physiology Interactions

SiB4 uses the hypothesis that three physiological processes are directly dependent on phenology: carbon allocation, leaf photosynthetic capacity, and senescence. Carbon allocation determines the fate of assimilated carbon and affects plant growth, and studies have shown that allocation shifts from aboveground to belowground through the growing season (e.g. Aguado et al. (2016); De Kauwe et al. (2014); Guillemot et al. (2017)). This progression

falls in-line with the philosophy that plants adjust their allocation to improve their most limiting resource. At the beginning of the growing season when the leaf pool is small, plants are limited by light and thus allocate resources to growing leaves; however, at the end of the season plants allocate more resources belowground to the roots in order to capture more water and to store carbon for growth the following season.

To capture this behavior, SiB4 includes seasonally-varying allocation by including stage-specific allocation fractions (parameter $AllocP$) that specify the fraction of photosynthesized carbon allocated to each live pool for each phenology stage. In the case of light limitation, if the environmental conditions support growth and if adding leaves would provide an improvement to photosynthesis at a reasonable cost, then the phenology stage shifts to the leaf-out or growth stages with high leaf allocation fractions. Moisture sensitivity is also included in the phenology stage determination: if the vegetation is moisture stressed, then the phenology stage shifts towards the stress stage that has more allocation to the roots.

Second, plants can change their leaf photosynthetic capacity (maximum carboxylation rate of rubisco, V_{Max}) throughout the season. V_{Max} is an important control on the photosynthetic rate that has large seasonal variations, changing the amount of carbon being available for growth and maintenance and having significant impacts on the carbon cycle, energy exchanges, and hydrology (Bauerle et al., 2012; Groenendijk et al., 2011; Houborg et al., 2013; Zhou et al., 2014). Specifying V_{Max} by phenophase ties it to seasonal development, providing a mechanistic way to change it throughout the growing season. SiB4 includes V_{Max} as a parameter that changes with phenology stage and with PFT, and current values use the strategy that it increases through the growth stage and then decreases as the leaves age (Restrepo-Coupe et al., 2013; Saleska et al., 2014; Wu et al., 2016; Xu et al., 2017).

Third, timing of plant senescence occurs seasonally; thus, SiB4 has a parameter, LP_{Tran}, that changes the turnover rate of leaves with phenology stage. This allows litterfall to be tied to senesence for highly seasonal vegetation types, aiding the rapid drop of leaves at the end of the season. Implementing prognostic phenology using dynamic stages provides a powerful mechanism to integrate ecosystem processes, linking carbon pools (storage), land-atmosphere (energy) fluxes, and biosphere-atmosphere (carbon) exchanges.

9 Defined Prognostic Phenology (Crops)

A crop phenology model was incorporated in SiB by Lokupitiya et al. (2009) to improve land-atmosphere carbon exchanges from croplands. This work focused on specific sites for three crops: maize, soybeans, and winter wheat. SiB4 includes all three of these crops. In addition, since there are numerous species of crops that are not specifically simulated, SiB4 has two generic crop PFTs, one for C3 crops and one for C4 crops. These PFTs capture the short and intense growing season that generally occurs for crops, and they follow the soybean and maize phenology strategies, respectively. The crop phenology model was extended to regional applications by Corbin et al. (2010b). We have made further modifications to the crop phenology approach in order to simulate crops globally in a consistent framework with the non-crop vegetation types.

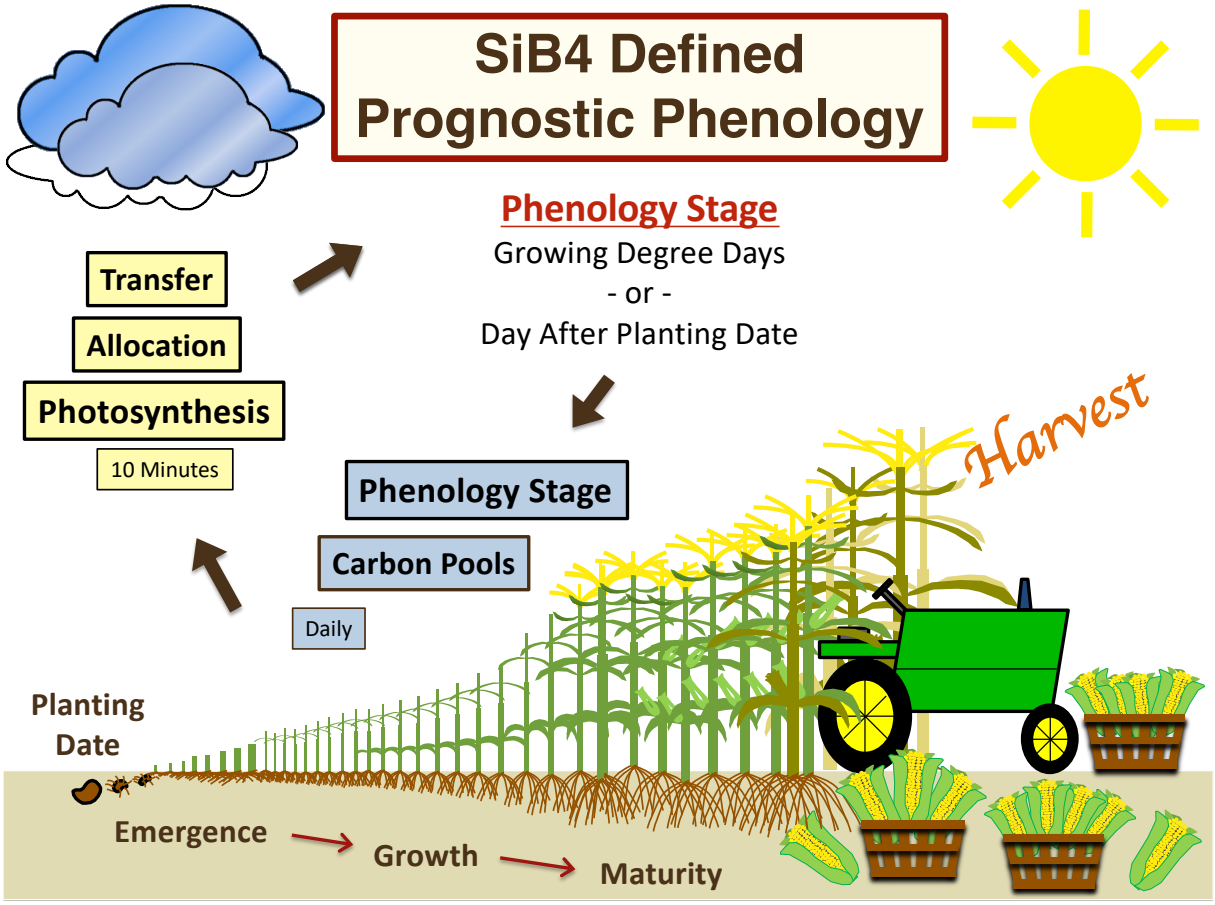

Figure 9.1: SiB4 Defined (Crop) Phenology.

An overview of the SiB4 defined crop phenology model is shown in Figure 9.1. The crop phenology model in SiB4 determines the phenology stage using either growing degree days (GDD) or the number of days since planting ($DAPD$). To start the season, planting dates are estimated based on temperature, soil moisture, and day length. Initial growth occurs

from seed carbon, which quickly transfers to self-sustaining growth from carbon taken up via photosynthesis. Sub-hourly photosynthesized carbon is summed daily and allocated to the live carbon pools depending on seasonal development. In return, the updated carbon pools are used to calculate the LAI, which then closes the cycle and is used to determine carbon uptake. At the end of the season, the crops are harvested, with carbon either being removed or transferred to the dead carbon pools. The parameters and variables needed to model crops are listed in Tables A7 and B13.

SiB4 assumes that crops are not limited by nutrients nor water. Although SiB4 assumes that the crops are well fertilized, it does have an indirect representation of nitrogen limitation through rubisco dynamics within the photosynthetic mechanism. Rather than including irrigation explicitly, SiB4 assumes a basic irrigation strategy such that if water is available in any soil layer, the crops can obtain this water and are not stressed. This approach allows SiB4 to obtain high yields over productive croplands, while still responding to significant droughts when the soil moisture is depleted throughout the entire soil column.

9.1 Phenology Stages

Crops have well-defined growth and development stages that can be modelled using the same basic approach as the dynamic phenology framework. Because crops step through their development sequentially, they are more straight-forward to model than natural vegetation. For each crop, the number of phenology stages is an adjustable parameter ($nstage$). Three options currently exist for predicting the current phenology stage (PI_{Stage}). For each crop, the method can be specified by setting the parameter GPD to one of the following:

1. Growing degree days (GDD). If this option is selected, then additional parameters need to be set to establish the temperature base (GDD_{TBase}) and the temperature maximum (GDD_{TMax}), where the GDD is calculated daily as

$$GDD = \begin{cases} GDD + (TM_{DF} - T_{Base}) & GDD_{TBase} \leq TM_{DF} \leq GDD_{TMax} \\ GDD + (GDD_{TMAX} - T_{Base}) & TM_{DF} > GDD_{TMax} \end{cases} \quad (203)$$

   with TM_{DF} being the daily mean temperature in Farenheit.

2. Days after planting $DAPD$, accumulated daily.

3. Days after planting above freezing $DAPDNF$, accumulated daily if the daily mean temperature is above freezing.

No matter which method is selected, the appropriate values are saved in the phenology index (PI), and thresholds PI_{Thresh} separate PI into different phenology stages PI_{Stage}.

Just as with the dynamic phenology approach, the defined phenology stage controls three physiological properties:

1. Carbon allocation to the live pools, determined by the parameter $AllocP$.

2. Leaf photosynthetic capacity, determined by the parameter V_{Max}.

3. Litterfall (leaf transfer), determined by the parameter LP_{Tran}.

Using this setup allows SiB4 to step through the growing season following the specific crop development stages.

9.2 Growing Season Start

The original crop phenology model by Lokupitiya et al. (2009) only used temperature to predict the planting date; however, to run globally, the growing season initiation has to be altered since the temperatures are always suitable for planting in the tropics. Following the dynamic phenology requirements to begin a growing season, SiB4 uses the growing season suitability flag $FlagG$ as described in Section 8.3, where the flag is set to true if day length, temperature, and water availability conditons are all satisfied.

Additionally, SiB4 uses a precipitation flag $FlagP$ to establish a planting window centered around the seasonal peak precipitation. This flag aids the starting dates in tropical ecosystems, where the crop growing season should be centered on the time period with the maximum rainfall. To do this, SiB4 saves four variables associated with precipitation: the running-mean precipitation PF_{Pr}, the seasonal maximum precipitation $PF_{Pr,SM}$, the day of year the seasonal maximum precipitation occurred $PF_{Pr,SDOY}$, and the climatological mean day of seasonal maximum precipitation ($PF_{Pr,CDOY}$). A planting window can then be created, setting $FlagP$ to True if the following condition is satisfied:

$$PF_{Pr,CDOY} - GP_{Bef} \leq DOY \leq PF_{Pr,CDOY} + GP_{Aft} \tag{204}$$

where DOY is the current day of the year and GP_{Bef} and GP_{Aft} are parameters. If the DOY is outside of this window, then $FlagP$ is set to False. Both $FlagA$ and $FlagP$ must be true to start a growing season.

9.3 Seasonal Progression

Once the growing season start flags are set to true, if not already set then the planting day (PD) is set to the current day of the year and the seed pool ($Seed_{Pool}$) is set to the crop-specific seed carbon (parameter $Seed_C$). The initial growth comes from the seed pool, which releases carbon to the live carbon pools (lp) in daily increments ($Gain_{Seed,lp}$) such that

$$Gain_{Seed,lp} = Seed_R \cdot AllocP_{lp,1} \tag{205}$$

$$Seed_{Pool} = Seed_{Pool} - Seed_R \tag{206}$$

where $AllocP_{lp,ips}$ is the parameter prescribing the pool allocations per phenology stage, $Seed_R$ is the daily carbon released from the seed pool, and the seed pool depletes daily. Once the seed carbon pool has been spent, the crop must be self-sustaining, and the biomass increments come from the daily photosynthetic assimilate. As the crop progresses through the growth cycle, the specific stages are set based on the defined thresholds (PF_{Thresh}). The rate of photosynthesis varies based on the growth stage via stage-specific V_{Max} values, and the photosynthesized carbon is allocated to the different live carbon pools depending on phase of the growth cycle (Section 11.1). Additionally, biomass transfer rates vary with the

growth stage to further control development and senescence (Section 11.3.2). The crop is harvested once it reaches the last specified PF_{Thresh} or once it reaches the maximum growing season length (GSL_{Max}), whichever occurs first.

9.4 Harvest

At the end of the growing season, crops are harvested and all live biomass is removed. To update the carbon pools, the live pool (lp) biomass is transferred into the $Loss_{Hrv,lp}$ variable and added to the daily net live pool loss ($Loss_{lp}$). The carbon lost from all pools is summed (Hrv_C) and moved to the locations specified by the parameter Hrv_{Tran}. This parameter includes indices for all dead pools, as well as for respiration and removal of the carbon harvested from crops. Hrv_{Tran} must sum to 1, ensuring that all the harvested carbon is removed or transferred. The transfer of harvested carbon is expressed as

$$Resp_{Hrv} = Hrv_{Tran,1} \cdot Hrv_C/dt \quad (207)$$

$$Rmvd_{Hrv} = Hrv_{Tran,2} \cdot Hrv_C \quad (208)$$

$$Gain_{Hrv,dp} = Hrv_{Tran,2+dp} \cdot Hrv_C \quad (209)$$

where $Resp_{Hrv}$ is the respired carbon from harvest, $Rmvd_{Hrv}$ is the carbon removed, and $Gain_{Hrv,dp}$ is the carbon gained to dead pool dp. The carbon gained in each of the dead pools is added to the daily net dead pool gain ($Gain_{dp}$). For the dead soil carbon pools, the carbon is distributed throughout the soil column using the fraction of carbon per soil layer ($Pool_{FLay}$). At the beginning of the simulation, this fraction is set to the rooting fraction ($RootF$).

9.5 Redistribution

If harvested carbon is removed, SiB4 includes a post processing routine to redistribute this carbon in a constant respiration flux. The routine sums the global harvested carbon that is removed and redistributes it using human and livestock populations. The routine also includes a parameter controlling the amount of removed carbon that is respired regionally (using 11 different regions as defined by TransCom in Gurney et al. (2002)) or respired internationally (i.e. export). Once the removed carbon is redistributed, it is respired at a constant rate.

9.6 Switching Corn and Soybeans

Since it is common practice for farmers to rotate fields between corn and soybeans, SiB4 includes an option to alternate the crop type between corn and soybeans every other year. To do this, in the model namelist the user can set the flag *cornsoy_switch* to true. This option is useful for agricultural sites, as it simplifies comparisons to observations.

10 Disturbance

10.1 Fire

SiB4 includes the capability to read in fire emissions and remove the burned carbon from the carbon pools. SiB4 expects both the carbon loss from fire ($Fire_C$) and the carbon dioxide emissions ($Fire_{CO2}$) to be provided in fire dataset. Fire emissions are read in from a file following the procedure for the meteorological data. During this process, both $Fire_C$ and $Fire_{CO2}$ are interpolated to fluxes that specify the loss and respiration per second.

Fire emissions are removed from the carbon pools using the parameters and variables listed in Tables A8 and B14 and following the procedure outlined below.

1. Calculate the aboveground and total biomass.
2. Rank the PFTs by the aboveground biomass.
3. Remove carbon from the top PFTs, using up to three PFTs where the amount of carbon removed from each corresponds to their normalized areal coverage. The amount of carbon removed from each pool is specified by parameters corresponding to the aboveground carbon pools. Currently, the fractions of carbon burned from the surface pools are:
   - Leaf Pool ($FireF_L$) = 0.3
   - Coarse Dead Biomass ($FireF_C$) = 0.2
   - Metabolic Litter ($FireF_{ML}$) = 0.2
   - Structural Litter ($FireF_{SL}$) = 0.2
   - Wood Pool ($FireF_W$) = 0.1
4. Check the carbon removed. If all of the fire emissions have not been burned, attempt to remove the carbon from the soil litter, soil slow, and soil armored pools, respectively.
5. If fire emissions still have not been burned, add them to the variable $Rmvd_{Fire}$.
6. Set the carbon loss ($Loss_{Fire}$) to the calculated fire loss per pool, and the fire respiration ($Resp_{Fire}$) to the total carbon loss from the fire ($Fire_C$).
7. Check the fire carbon balance, ensuring the carbon emissions equal the carbon burned and removed.

10.2 Grazing

Grasslands have a long history of grazing, and grazing is an important disturbance that has direct impacts on the carbon cycle from the local-scale vegetation dynamics, to regional productivity, to global sources and sinks (Kang eq al., 2007; Knapp et al., 2012; Koerner et al., 2014; Yan et al., 2013). Grazing removes aboveground plant material, which has considerable effects on the land-atmosphere interactions by changing the aboveground vegetation cover, and hence altering the LAI, litter, albedo, roughness length and resulting energy and momentum exchanges. Changing the aboveground carbon pools also alters the carbon fluxes and plant productivity, which feeds back to impact not only the root biomass, but also the resulting carbon stored in the soil. Extensive grazing occurs globally, and these local impacts scale up to have global implications.

Since grazing has widespread impacts, SiB4 includes a rudimentary grazing scheme that is called every timestep. A flag ($Flag_{PFT}$) controls whether each PFT uses grazing or not; thus, all PFTs have the option to use grazing with the idea that grazing may extend beyond grasslands to provide a first effort at representing insect infestation for shrubs and forests. The parameters and variables used by this grazing approach are listed in Tables A9 and B15. The amount of removed carbon from grazing is a constant fraction of the aboveground biomass. SiB4 uses two different grazing intensities (Grz_F) depending on climatological LAI $Clim_{LAI}$ such that

$$Grz_F = \begin{cases} Grz_{CFracP}/86400. & Clim_{LAI} > Grz_{SLAI} \\ Grz_{CFracD}/86400. & Clim_{LAI} \leq Grz_{SLAI} \end{cases} \tag{210}$$

where Grz_{CFracP} and Grz_{CFracD} are parameters specifying the daily fraction of carbon grazed in productive and sparse ecosystems, respectively. Grazing occurs on days when the LAI greater than the minimum LAI required by the parameter Grz_{MLAI}. A counter variable, nd_{Grz}, keeps a running total of the number of days grazed for the entire simulation.

The daily carbon loss in canopy pool cp due to grazing ($Loss_{Grz,cp}$) is

$$Loss_{Grz,cp} = C_{cp} \cdot Grz_F \cdot dt. \tag{211}$$

where C_{cp} is the carbon in the canopy pools. The total loss of carbon from the canopy pools due to grazing (Grz_C) is

$$Grz_C = \sum Loss_{Grz,cp}. \tag{212}$$

Grazed carbon can be removed, respired (R_{Grz}) or transferred to the dead carbon pools ($Gain_{Grz,dp}$) as dictated by the parameter Grz_{Tran} following

$$Resp_{Grz} = Grz_{Tran,1} \cdot Grz_C \tag{213}$$

$$Rmvd_{Grz} = Grz_{Tran,2} \cdot Grz_C \cdot dt \tag{214}$$

$$Gain_{Grz,dp} = Grz_{Tran,2+dp} \cdot Grz_C \cdot dt \tag{215}$$

where the fractions of carbon being distributed to each fate (Grz_{Tran}) must sum to 1. For the portion of carbon that is respired, it is released at a constant rate the day the grazing occurs.

11 Carbon Pool Exchanges

11.1 Allocation

Every day the carbon taken up via photosynthesisis is allocated back out to the live carbon pools at midnight LST. Assimilated carbon is allocated to the live carbon pools using both phenology and weather-based adjustments. All of the parameters and variables used to do this are listed in Tables A10 and B16.

The daily carbon gain from assimilation ($Gain_A$) can be assigned to each live pool (lp) such that:

$$Gain_{A,lp} = \sum_{i=1}^{nsoil} Distrib_{lp,i} \cdot Alloc_{lp} \cdot Assim_{Day}, \tag{216}$$

where *Distrib* is the vertical distribution fraction of carbon through the soil, *Alloc* is the carbon allocation fraction, and $Assim_{Day}$ is the daily carbon assimilation. For live pool lp and soil layer i, *Distrib* is defined as

$$Distrib_{lp,i} = \begin{cases} 1 \quad i{=}1 \\ 0 \quad i{=}2 \text{ to } nsoil & lp = \text{leaf, stwd, prod} \\ RootF_i & lp = \text{roots} \end{cases} . \tag{217}$$

Using this formulation, the carbon gain for the root pools is distributed vertically in the soil layers using the rooting depth profile (*RootF*). The capability of SiB4 to simulate the vertical movement of carbon in the soil and thus varying vertical profiles is one of the next goals for future development; however, currently the carbon fraction per layer for all soil pools is the same as the root fraction.

Carbon allocation (*Alloc*) depends on phenology stage and ambient conditions such that for live pool lp and phenology stage s

$$Alloc_{lp,s} = AllocP_{lp,s} + AllocA_{lp,s}, \tag{218}$$

where *AllocP* are the phenology-based allocation fractions and *AllocA* are weather-based allocation fraction adjustments. The values of *AllocP* are parameters that are specified per pool and per phenology stage and have the requirement that for every stage the pool allocation fractions must sum to one. Utilizing phenology stages with unique allocation fractions provides a method to shift carbon allocation from canopy pools during leaf-out to root pools during maturity and stress if desired (by PFT).

The adjustments in *AllocA* are calculated from weather and environmental functions and vary depending on phenology stage, such that for stage s

$$AllocA_{lp,s} = \begin{cases} 0 & s = 1, nstage \\ AllocAM_{lp} + AllocAT_{lp} & s = 2 \text{ to } (nstage - 1) \end{cases} , \tag{219}$$

where $AllocAM$ is a soil moisture adjustment and $AllocAT$ is a temperature adjustment. If the flag Adj_{Moist} is set to true, then the moisture adjustments are used; and if the flag Adj_{Temp} is set to true, then the temperature adjustments are used. Both allocation adjustments are based on the philosophy that plants adjust their allocation to improve the most limiting resource. Friedlingstein et al. (1999) presented the original implementation of this idea in land surface models, and SiB3-CASA utilizes this concept to modify pool allocations based on light, water, and temperature adjustments (Schaefer et al., 2008). In SiB4, allocation to the leaf pool in the case of light limitation is captured in the phenology stage selection: if the environmental conditions support growth and if adding leaves would provide an improvement to photosynthesis at a reasonable cost, both PS_{Grw} and PS_{Wx} are high and the phenology stage shifts to the leaf-out or growth stages with high leaf allocation fractions. Moisture sensitivity is also included in the phenology stage determination via the PS_{Wx} potential: if the plant is moisture-stressed, then the phenology will shift towards later stages that have more allocation to the roots in an attempt to acquire more water. The phenology stage is meant to represent the plant progression through the season, and the phenology-based allocation and adjustments are complimentary, providing a way to capture basic seasonality and day-to-day ambient condition impacts.

To calculate the $AllocAM$ adjustment, a root allocation adjustment potential (AF_{Root}) is created based on the daily mean of the root zone water potential (F_{RZ}), where

$$AF_{Root} = 1 - 2.8AF_{RZ}. \tag{220}$$

Since moisture stress increases allocation to the fine root pool in an attempt to attain more water, the moisture allocation adjustment removes carbon allocation from the canopy pools and adds carbon allocation to the fine root pool where the soil water is extracted. This is expressed as

$$AllocAM_{lp} = \left\{ \begin{array}{ll} -AF_{Root} \cdot AllocP_{lp} & lp = \text{leaf, stwd, prod} \\ AllocAM_{Tot} & lp = \text{croot, froot} \end{array} \right\}, \text{ where} \tag{221}$$

$$AllocAM_{Tot} = AF_{Root}(AllocP_{leaf} + AllocP_{stwd} + AllocP_{prod}). \tag{222}$$

Using $AllocAM$ allows the allocation fractions to be modified within the phenology stages as an additional and direct response to soil moisture and drought stress.

The $AllocAT$ adjustment uses the temperature stresses from SiB3-CASA (Schaefer et al., 2008), and it is based on the premise that leaf and wood growth decline in response to seasonally cold temperatures. The leaf growth declines when daily minimum temperatures ($TMin_D$) drop below freezing (< 273 K), and the wood growth declines under cool temperatures (< 278 K). Allocation potentials for leaf freeze (AF_{LeafF}) and wood freeze (AF_{WoodF}) are defined as

$$AF_{LeafF} = Max\left(0.6, \frac{1}{(1 + e^{1.3(273 - TMin_D))}}\right) \tag{223}$$

$$AF_{WoodF} = \frac{1}{(1+e^{1.3(278-TMin_D)})}. \quad (224)$$

Since wood growth is more sensitive to cool temperatures for specific types of vegetation, SiB4 includes a second PFT-specific wood temperature potential (F_{WoodT}):

$$AF_{WoodT} = \frac{1+e^{shti(TMin_D-hhti)}}{1+e^{slti(hlti-TMin_D)}}, \quad (225)$$

where *shti*, *hhti*, *slti*, *hlti* are originally defined in Sellers et al (1996b) and are now PFT-specific physiological parameters. Both wood potentials are combined into a total wood temperature potential (F_{Wood}):

$$AF_{Wood} = AF_{WoodF} \cdot AF_{WoodT}. \quad (226)$$

The temperature stress adjustment decreases the allocation to the leaf and wood pools, and therefore must increase the allocation to the remaining live carbon pools, such that

$$AllocAT_{lp} = \left\{ \begin{array}{ll} -AllocP_{lp}(1-AF_{LeafF}) & lp = \text{leaf} \\ -AllocP_{lp}(1-AF_{Wood}) & lp = \text{croot, wood} \\ AllocAT_{Tot} & lp = \text{froot, stem, prod} \end{array} \right\}, \text{ where } (227)$$

$$AllocAT_{Tot} = (1-AF_{LeafF})AllocP_{leaf} + (1-AF_{Wood})(AllocP_{croot} + AllocP_{wood}) \quad (228)$$

The *AllocAT* factor allows the leaf and wood pools to be reduced under low temperatures in response to cold spells during the growing season.

11.2 Autotrophic Respiration

Autotrophic respiration is the carbon plants release to the atmosphere from the metabolic energy expended to grow and maintain living tissue. To simulate this process, SiB4 is based on the growth-and-maintenance-respiration paradigm (GMRP) (Amthor, 2000)), which divides autotrophic respiration into growth and maintenance contributions. The total respiration is the sum of these components, which are defined in this section. All of the parameters and variables used to calculate autotrophic respiration are defined in Tables A11 and B17.

All live pools have growth (R_G) and maintenance (R_M) requirements, and the total autotrophic respiration rate (R_A) is the sum of these costs:

$$R_A = R_G + R_M. \quad (229)$$

11.2.1 Growth Respiration

The carbon loss per live pool ($Loss_{GResp,lp}$) and the growth respiration (R_G) are defined as

$$Loss_{GResp,lp} = GR_{Frac,lp} \cdot Gain_{A,lp} \tag{230}$$

$$R_G = \frac{1}{dt} \sum_{lp=1}^{nlpool} Loss_{GResp,lp} \tag{231}$$

where GR_{Frac} is the growth respiration fraction, $Gain_A$ is the daily carbon allocated to the pool, and dt is the model timestep in seconds. Moving and storing the carbon in specific pools requires energy, and this cost is proportional to the amount of allocated carbon ($Gain_A$). Although the carbon pools are only updated daily, the growth respiration is released every timestep as the carbon is assimilated.

Using different values for GR_{Frac} allows SiB4 to model different strategies regarding the costs of growth respiration. Currently, the model uses the strategy that the growth costs for the product pool are the highest, since seeds and flowers have more complicated structures that are carbon and energy intensive to build. In contrast, the cost for new leaves is lower, under the premise that the energy required to build the leaf structure is less to counter higher maintenance costs. Parameterizing R_G in this way allows the user to easily change the growth respiration as more PFT and pool-specific data become available.

11.2.2 Maintenance Respiration

Maintenance respiration is associated with any costs necessary to retain the living tissue, thus it has pool-specific requirements. The maintenance loss per live pool $Loss_{MResp,lp}$ and associated respiration are proportional to the amount of carbon in the pool, and these are calculated using the following system of equations:

$$Loss_{MResp,lp} = E_{lp}\, C_{lp}\, krate_{r,lp}\, dt \tag{232}$$

$$krate_{r,lp} = \begin{cases} \frac{1}{\tau_{cp}} MCR_{Scale} & cp = \text{leaf, stwd, prod} \\ \frac{1}{\tau_{rp}} MRR_{Scale} & rp = \text{croot, froot} \end{cases} \tag{233}$$

$$R_M = \frac{1}{dt} \sum_{lp=1}^{nlpool} Loss_{MResp,lp} \tag{234}$$

where C is the live pool carbon, dt is the timestep length, E is the respiration efficiency, $krate_r$ is a scaled maintenance loss rate, MCR_{Scale} is the canopy maintenance respiration scaling coefficient, MRR_{Scale} is the root maintenance respiration scaling coefficient, and τ is the pool turnover time. For the root pools, the pool carbon and scaling coefficient vary per soil layer. Both E and τ are parameters that vary with PFT and are used for respiration and live pool transfers to dead carbon pools. The scaling coefficients MCR_{Scale} and MRR_{Scale} are designed to include all non-growth related contributions to autotrophic respiration. While SiB4 includes several different processes in the respiration scaling coefficients, the specific

mechanisms influencing autotrophic respiration are still uncertain, particularly the amount of respiration from plant components as well as the causes of day-to-day variability (Amthor, 2000; Meir et al., 2008; Molchanov, 2009).

11.2.3 Canopy Maintenance Respiration Scaling Coefficient

SiB4 applies the hypothesis that MCR_{Scale} is influenced by the assimilation rate, freezing conditions, and high temperatures and is given by:

$$MCR_{Scale} = MCR_{Assim} \cdot MCR_{Freeze} \cdot MCR_{Hot} \tag{235}$$

where MCR_{Assim} is an assimilation-based canopy scaling coefficient, and MCR_{Freeze} and MCR_{Hot} are temperature-based scaling coefficients.

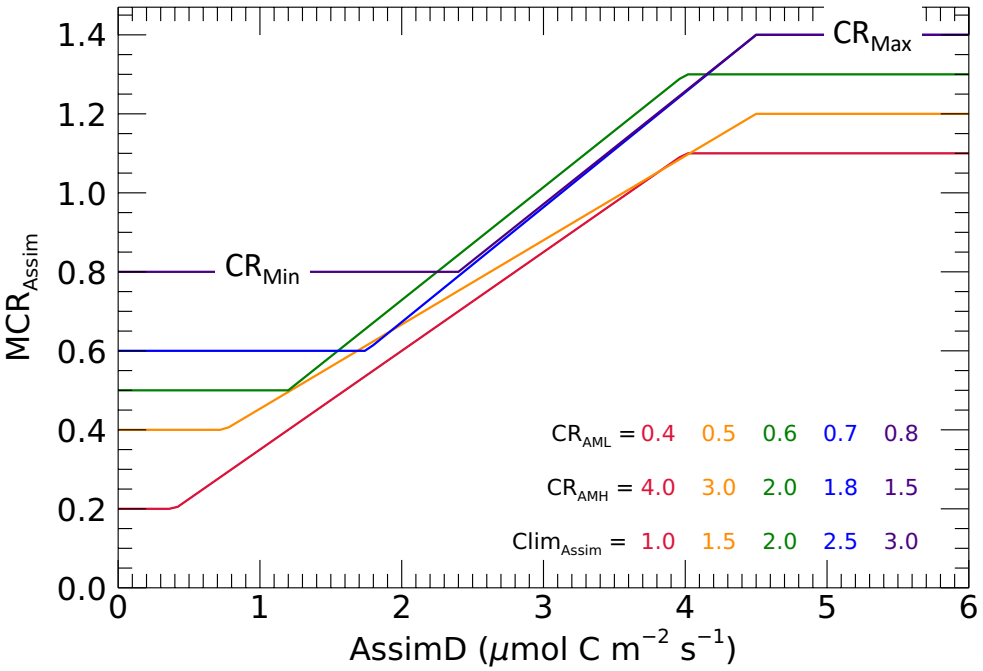

Figure 11.1: Sample Canopy Assimilation Scalars for Autotrophic Respiration. The colors show different parameter values.

The first influence that SiB4 uses to scale maintenance respiration is an assimilation-based scalar, MCR_{Assim}. This factor was developed from studies that have suggested that autotrophic respiration scales predominantly with the assimilation rate (Flexas et al., 2006; Meir et al., 2008; Molchanov, 2009). SiB4 uses a combination of climatological and daily assimilation in calculating MCR_{Assim}.

$$\begin{aligned} \text{If} \quad & Assim_D < CR_{AML}\ Clim_{Assim} \\ \text{Then} \quad & MCR_{Assim} = CR_{AMin} \end{aligned} \tag{236}$$

$$\text{If} \qquad CR_{AML}\ Clim_{Assim} < Assim_D < CR_{AMH}\ Clim_{Assim} \tag{237}$$

$$\text{Then} \qquad MCR_{Assim} = Assim_D \cdot \text{slope} + \text{yint} \tag{238}$$

$$\text{Where} \qquad \text{slope} = \text{S1/S2}$$

$$\text{S1} = CR_{AMax} - CR_{AMin}$$

$$\text{S2} = CR_{AMH} Clim_{Assim} - CR_{AML} Clim_{Assim}$$

$$\text{yint} = CR_{AMin} - \text{slope} \cdot CR_{AML} Clim_{Assim}$$

$$\text{If} \qquad Assim_D > CR_{AMH} Clim_{Assim} \tag{239}$$

$$\text{Then} \qquad MCR_{Assim} = CR_{AMax} \tag{240}$$

In this system of equations, CR_{AMH}, CR_{AML}, CR_{AMin}, and CR_{AMax} are parameters; $Assim_D$ is the daily assimilation rate, and $Clim_{Assim}$ is the climatological assimilation rate (10-year running mean). Using the climatological assimilation rates shifts the maintenance respiration rates in response to different environments, and sample MCR_{Assim} values are shown in Figure 11.1.

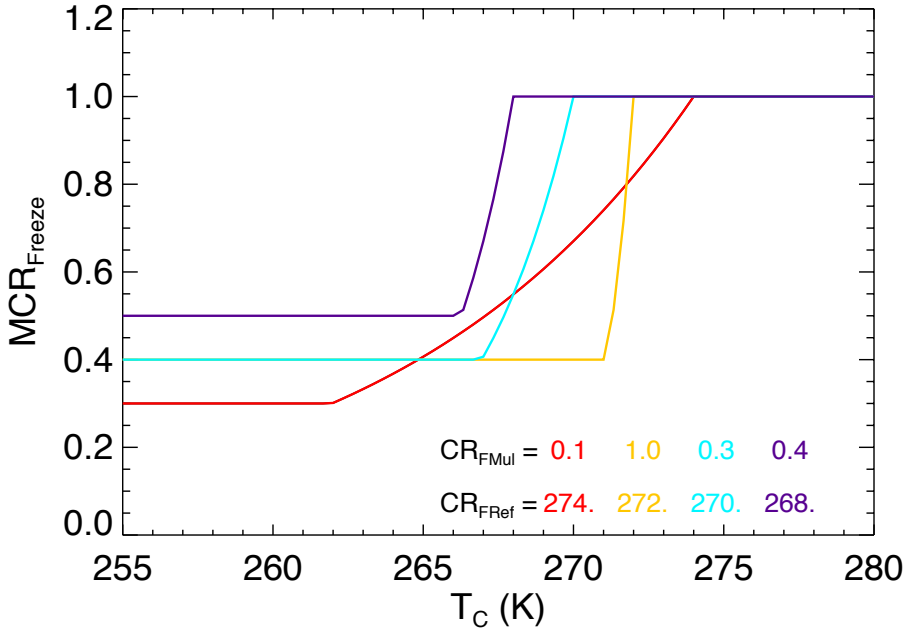

Figure 11.2: Sample Canopy Freeze Inhibition Scalars (MCR_{Freeze}). The colors show different parameter values.

The second influence that SiB4 uses to scale canopy respiration is a freezing inhibition coefficient MCR_{Freeze}, which uses an exponential function that rapidly decreases to a specified minimum value when the temperature drops below a threshold value. This is expressed as

$$MCR_{Freeze} = e^{CR_{FMul}(T_C - CR_{FRef})} \quad \text{and} \tag{241}$$

$$CR_{Fmin} \leq MCR_{Freeze} \leq 1 \tag{242}$$

where CR_{FMin}, CR_{FMul}, and CR_{FRef} are parameters and T_C is the canopy temperature. This equation illustrates that MCR_{Freeze} is unity in non-freezing conditions and decreases below freezing. Example MCR_{Freeze} functions are shown in Figure 11.2.

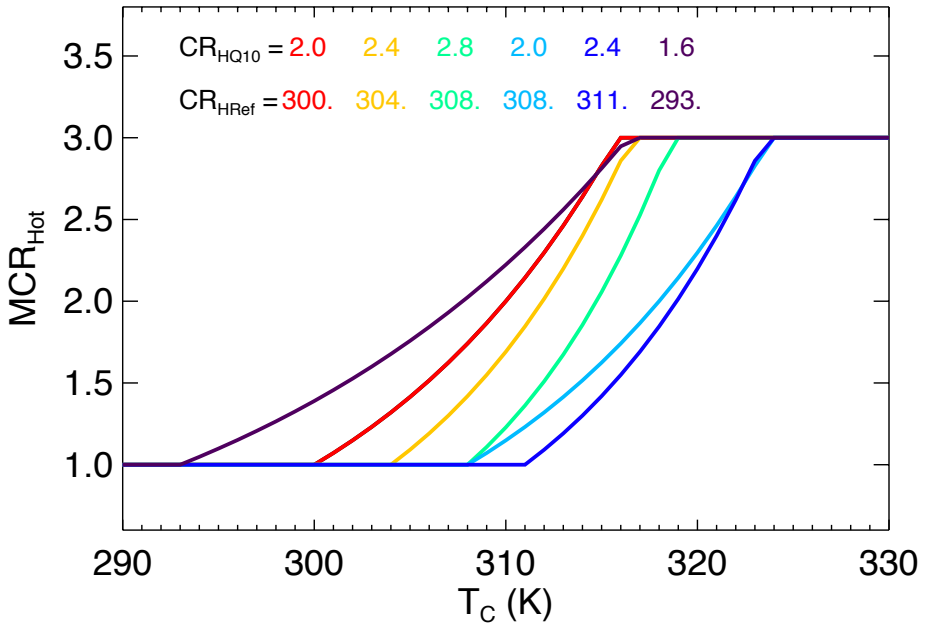

Figure 11.3: Sample Canopy High Temperature Scalars (MCR_{Hot}). The colors show different parameter values.

The third influence on canopy respiration is a high temperature coefficient, MCR_{Hot}. As in SiB3, SiB4 exponentially increases R_M with increasing temperatures using the Q_{10} empirical relationship reported by Ryan (1991). When the temperature is less than the reference temperature, the scaling coefficient is 1. As the temperature increases above the reference, the scalar increases exponentially to a specified maximum value. For any canopy pool, this relationship is expressed as

$$MCR_{Hot} = CR_{HQ10}{}^{0.1(T_C - CR_{HRef})} \text{ and} \tag{243}$$

$$1 \leq MCR_{Hot} \leq CR_{HMax} \tag{244}$$

where CR_{HQ10}, CR_{HMax}, and CR_{HRef} are parameters. Example MCR_{Hot} functions are shown in Figure 11.3.

11.2.4 Root Maintenance Respiration Scaling Coefficient

Belowground, partitioning soil respiration into root, microbial, and mycorrhizal contributions remains difficult; thus, the driving mechanisms remain uncertain despite soil respiration being intensively studied (Hopkins et al., 2013; Ryan & Law, 2005; Wei et al., 2009). Recent evidence suggests that the assimilation rate may be playing an important role in root respiration; therefore, SiB4 incorporates this concept and uses four different mechanisms to scale

root maintenance respiration: assimilation (MRR_{Assim}), LAI (MRR_{LAI}), freezing conditions (MRR_{Freeze}), and high temperatures (MRR_{Hot}). These responses are multiplicative to allow for interaction, and SiB4 combines the four contributions into a total respiration scaling coefficient MRR_{Scale} such that

$$MRR_{Scale} = MRR_{Assim} \cdot MRR_{LAI} \cdot MRR_{Freeze} \cdot MRR_{Hot}. \tag{245}$$

Each of these scalars is the root-weighted column-average of their layer-specific counterpart. The assimilation and temperature factors use the same equations as described for the canopy respiration; however, all of the parameters (CR) are replaced by root parameters (RRT). The LAI scaling coefficient uses vegetation to increase root respiration, with the hypothesis that roots work harder to supply water to larger canopies. This is expressed as

$$MRR_{LAI} = \mathrm{LAI}/Clim_{LAI} \text{ and} \tag{246}$$

$$RRT_{LMin} \leq MRR_{LAI} \leq RRT_{LMax} \tag{247}$$

where LAI is the current LAI, $Clim_{LAI}$ is the climatological mean LAI, and RRT_{LMin} and RRT_{LMax} are parameters.

11.2.5 Diagnostic Respiration Rates

Along with autotrophic, growth, and maintenance respiration rates, SiB4 calculates two additional respiration rates: leaf respiration (R_{Leaf}) and root respiration (R_{Root}). These are calculated as:

$$\begin{aligned} R_{Leaf} &= R_{G,Leaf} + R_{M,Leaf} \text{ and} && (248)\\ R_{Root} &= R_{G,CRoot} + R_{G,FRoot} + R_{M,CRoot} + R_{M,FRoot}. && (249)\\ & && (250) \end{aligned}$$

Finally, SiB4 includes a nonvegetation respiration rate, R_{NVeg}, which respires any assimilation that is taken up when all the pools are at their minimum values. This condition occurs occasionally for bare ground, and including this respiration rate is required for carbon balance.

11.3 Senescence

The parameters and variables used to model senescence are listed in Tables A12 and B18.

11.3.1 Turnover

Pool turnover is tied to respiration, and the loss of carbon from any live pool ($Loss_{T,lp}$) that is transferred to a dead carbon pool (dp) uses the equation

$$Loss_{T,lp} = (1 - E_{lp})\ C_{lp}\ krate_{r,lp}\ dt \tag{251}$$

where $Loss_T$ is the timestep loss due to pool turnover. For seasonal vegetation types, such as grasslands and deciduous forests, the aboveground biomass mortality occurs primarily at the end of the growing season as litterfall (see next section); thus, for those PFTs $E_{cp} = 0.95$. In contrast, because root turnover is still poorly constrained, in SiB4 the root mortality depends solely on turnover. Since root production, respiration, mortality, and turnover all interact, SiB4 uses root respiration efficiencies ranging from 0.45 to 0.6.

11.3.2 Litterfall

At the end of the season, senescence is characterized by a very rapid death in the canopy plant material, and hence rapid transfer and accumulation in the dead surface pools. Using phenology stages updated daily provides a mechanistic approach for modeling the seasonal growth onset and progression; however, changing allocation and photosynthetic rate alone combined with continuous turnover is not enough to capture the rapid browning seen by several vegetation types at the end of the growing season. To predict senescence, SiB4 uses four explicit processes for litterfall: day length, temperature, soil moisture, and phenology stage.

During litterfall, the loss of carbon from the live pools ($Loss_{LF,lp}$) is calculated as

$$Loss_{LF,lp} = (T_D + T_F + T_W + T_P)\ C_{cp}\ dt, \tag{252}$$

where $Loss_{LF}$ is the timestep loss of carbon, T_D is the fraction of the canopy pool that is transferred to the dead carbon pools due to decreasing day length, T_F is the fraction transferred due to freezing temperatures, TF_W is the fraction transferred due to water deprivation, and TF_P is the fraction due to phenology. For litterfall, the live pools are restricted to the canopy pools (cp).

For day length, T_D increases as the days get shorter following

$$T_D = LT_{DC}(DayL_{Max} - DayL)(DayL_{Max} - LT_{DR}) \text{ and} \tag{253}$$

$$0 \leq T_D \leq LT_{DMax} \tag{254}$$

where LT_{DC}, LT_R, and LT_{DMax} are parameters. Sample daylength transfer fractions at 52°N are shown in Figure 11.4A.

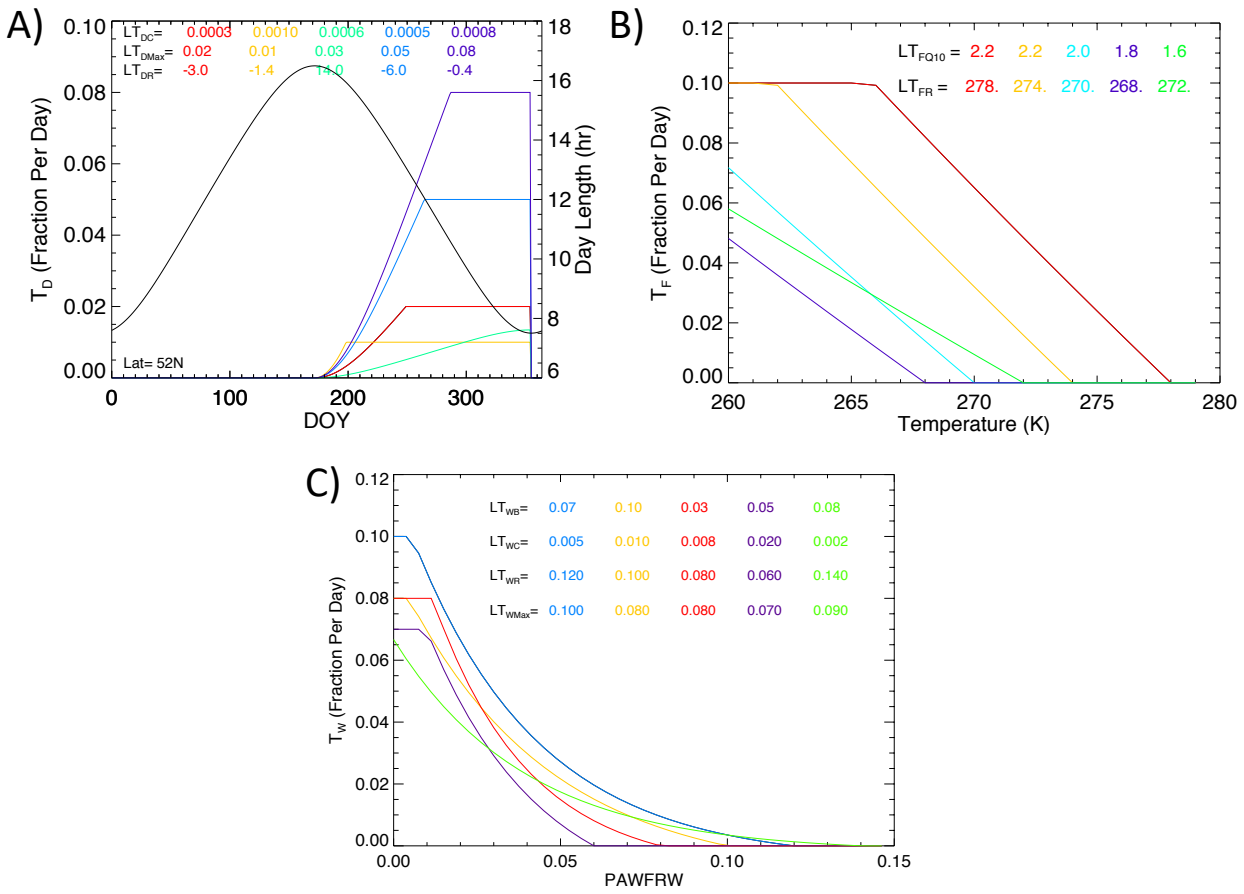

Figure 11.4: Sample Litterfall Transfer Fractions.
A) T_D **B)** T_F **C)** T_W. The black line shows the day length. The parameter values are listed by color.

For freezing temperatures, T_F increases with decreasing temperatures using a Q10 relationship following

$$T_F = LT_{FQ10}{}^{0.01(LT_{FR}-T_C)} - 1 \text{ and} \tag{255}$$

$$0 \le T_F \le LT_{FMax} \tag{256}$$

where LT_{FQ10}, LT_{FR}, and LT_{FMax} are parameters. Sample freezing transfer fractions are shown in Figure 11.4B.

For moisture deprivation, T_W increases with lowering PAW_{FRW} such that

$$T_W = LT_{WC}(LT_{WB}{}^{10(PAW_{FRW}-LT_{WR})} - 1) \text{ and} \tag{257}$$

$$0 \le T_W \le LT_{WMax} \tag{258}$$

where LT_{WB}, LT_{WC}, LT_{WR}, and LT_{WMax} are parameters. Examples of T_W are shown in Figure 11.4C.

Finally, litterfall increases with increasing phenology stage such that

$$T_P = T_P + LP_{Tran}/\text{steps\_per\_day} \tag{259}$$

where LP_{Tran} is a parameter with fractions specified per PFT and per pool and steps_per_day is the daily number of simulated timesteps. LP_{Tran} increases incrementally as long as the same stage is maintained. Once a new stage is predicted, it is reset.

11.3.3 Transfer

The gain of carbon in the dead pools from the loss of live pool carbon due to turnover and litterfall is expressed as

$$Gain_{TL,dp} = \sum_{lp=1}^{nlpool} TF_{lp,dp} \left(Loss_{LF,lp} + Loss_{T,lp} \right) \tag{260}$$

where $TF_{lp,dp}$ is the transfer fraction of carbon from live pool lp to dead pool dp. If the carbon is being transferred from an aboveground pool to a soil pool, the vertical distribution of carbon in the soil is set to the rooting profile.

11.4 Heterotrophic Respiration and Decay

Heterotrophic respiration is the carbon that decomposer organisms release to the atmosphere during the breakdown of organic matter, while decay is the process of transferring the remaining organic matter into subsequent carbon pools (typically with longer lifetimes). These two processes are tied together and depend on the efficiency of the carbon breakdown between dead pool dp and the subsequent dead pool $dp2$, as well as the fraction of carbon that is transferred from dp to $dp2$. Per pool dp, its loss of carbon due to respiration ($Loss_{HR,dp}$) and decay ($Loss_{HT,dp}$) and gain of carbon from the decay of other dead pools ($Gain_{TD,dp}$), along with the total heterotrophic respiration (R_H), are expressed in the following system of equations, and the parameters and variables used in this section are listed in Tables A13 and B19.

$$Loss_{HR,dp} = \sum_{dp2=1}^{ndpool} E_{DP,dp,dp2}\ TR_{DP,dp,dp2}\ C_{dp}\ krate_{r,dp}\ dt \tag{261}$$

$$Loss_{HT,dp} = \sum_{dp2=1}^{ndpool} (1 - E_{DP,dp,dp2})\ TR_{DP,dp,dp2}\ C_{dp}\ krate_{r,dp}\ dt \tag{262}$$

$$krate_{r,dp} = \begin{cases} \frac{1}{\tau_{fp}} MH_{Sfc,Scale} & fp = \text{cdb, metl, strl} \\ \frac{1}{\tau_{sp}} MH_{Soil,Scale} & sp = \text{slit, slow, arm} \end{cases} \tag{263}$$

$$R_H = \frac{1}{dt} \sum_{dp=1}^{ndpool} Loss_{HR,dp} \tag{264}$$

$$Gain_{TD,dp} = \sum_{dp2=1}^{ndpool} Loss_{HT,dp2}\, TR_{DP,dp2,dp}\, dt \tag{265}$$

The parameter E_{DP} is the respiration efficiency between dead pools, the parameter TR_{DP} is the transfer fraction between dead pools, C is the pool carbon, $krate_{r,dp}$ is a scaled decay rate, $MH_{Sfc,Scale}$ is the surface pool heterotrophic respiration scaling coefficient, $MH_{Soil,Scale}$ is the soil pool heterotrophic respiration scaling coefficient, and τ is the pool turnover time.

Microbes control the heterotrophic respiration rate and are sensitive to both moisture and temperature; however, similar to root respiration, the exact relationships controlling their activity are still being investigated. The carbon released from the decomposition of the dead pools depends on the pool as given by:

$$MH_{Sfc,Scale} = MH_{Sfc,Assim} \cdot MH_{Sfc,Freeze} \cdot MH_{Sfc,Hot} \cdot MH_{Sfc,Precip} \quad \text{and} \tag{266}$$

$$MH_{Soil,Scale} = MH_{Soil,Freeze} \cdot MH_{Soil,Hot} \cdot MH_{Soil,Moist} \cdot MH_{Soil,PAW}, \tag{267}$$

where $MH_{Sfc/Soil,Assim}$ is an assimilation rate scaling coefficient, $MH_{Sfc/Soil,Freeze}$ are freeze inhibition scalars, and $MH_{Sfc/Soil,Hot}$ are high temperature exponentials, $MH_{Sfc,Precip}$ is a surface moisture scalar based on precipitation, and $MH_{Soil,Moist/PAW}$ are soil moisture scalars.

The assimilation-rate scaling coefficients, freeze inhibition scalars, and high temperature scaling coefficients use the same calculations as defined for the canopy pools in Section 11.2.3. To apply these equations to heterotrophic respiration, the following modifications are made:

- For assimilation rate, the four parameters are replaced by surface and soil pool specific parameters ($HRT_{Sfc/Soil,AMH}$, $HRT_{Sfc/Soil,AML}$, $HRT_{Sfc/Soil,AMax}$, and $HRT_{Sfc/soil,AMin}$).
- For freeze inhibition, the three parameters are replaced by surface and soil specific parameters ($HRT_{Sfc/Soil,\ FMin}$, $HRT_{Sfc/Soil,FMul}$, and $HRT_{Sfc/Soil,FMax}$). Additionally, the temperatures used in the calculation are the top layer of the soil temperature (TD_1) for the surface pools and the soil temperature per soil layer s (TD_s) for the soil pools.
- For high temperature, the three parameters are replaced by surface and soil specific parameters ($HRT_{Sfc/Soil,HMax}$, $HRT_{Sfc/Soil,HQ10}$, and $HRT_{Sfc/Soil,HRef}$. Additionally, the temperatures used in the calculation are the top layer of the soil temperature (TD_1) for the surface pools and the soil temperature per soil layer s (TD_s) for the soil pools.

Heterotrophic respiration also includes a moisture response. For the surface pools, the moisture scalar is a precipitation inhibition given by

$$MH_{Sfc,Precip} = Pr_{Seas}/(Pr_{Clim} \cdot HRT_{PML}) \quad \text{and} \tag{268}$$

$$HRT_{PMin} \leq MH_{Sfc,Precip} \leq 1, \tag{269}$$

where HRT_{PML} and HRT_{PMin} are parameters, Pr_{Seas} is the seasonal precipitation rate, and Pr_{Clim} is the climatological precipitation rate. Pr_{Seas} is the 18-day running-mean of precipitation (mm/day); however, the time averaging length is a parameter that can be adjusted ($Seas_{Len,Precip}$). Similarly, Pr_{Clim} is the the 10-year running-mean of precipitation (mm/day), and the averaging length is set by the parameter $Clim_{Len}$. In SiB4, this rainfall inhibition

is based on two premises. First is that surface pool respiration is responsive to immediate water limitations as given by precipitation, rather than soil moisture deficiencies that are time-integrals of wetness conditions. Second is that surface pool respiration largely does not saturate as seen in the soil respiration, and instead is primarily water-limited such that a lack of rain will reduce surface pool respiration. In the case of drought, $MH_{Sfc,Precip}$ is highly suppressed down to its minimum value. Example $MH_{Sfc,Precip}$ values are shown in Figure 11.5A.

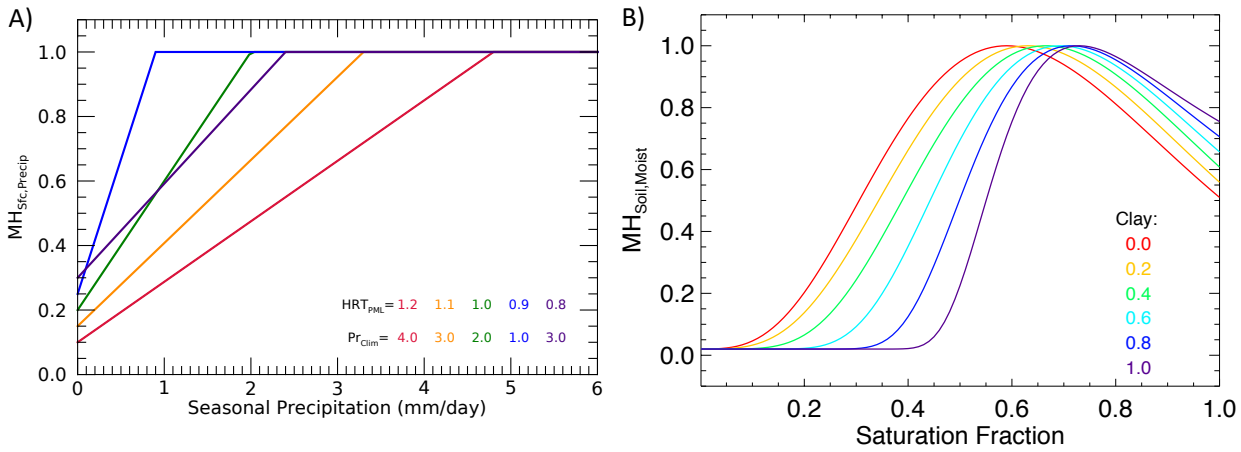

Figure 11.5: Sample Moisture Inhibitions for Heterotrophic Respiration. **A)** Surface precipitation inhibition values, where the colors show different parameter values. **B)** Soil moisture inhibition values, where the colors show different soil clay content.

For the soil pools, SiB4 uses two moisture responses. The first is $MH_{Soil,\ Moist}$, and SiB4 uses the same relationship to moisture that is seen in SiB3, which is based on the premise that mycorrhizal fungi activity are optimal at a given soil moisture content (Flexas et al., 2005, 2006; Li & Arora, 2012). From Denning et al. (1996a), the equations governing this relationship are

$$W_{Exp} = \left(\frac{W^{Zm} - W_{Opt}^{Zm}}{1 - W_{Opt}^{Zm}} \right)^2 \quad \text{and} \tag{270}$$

$$MH_{Soil,Moist} = 0.98 W_{Sat}^{W_{Exp}} + 0.02, \tag{271}$$

$$HRT_{\text{Soil,MMin}} \leq MH_{\text{Soil,Moist}} \leq 1 \tag{272}$$

where W is the water saturation fraction, W_{Sat} is the saturated soil moisture fraction, W_{Opt} is the optimal soil moisture fraction, Zm is a soil constant, and $HRT_{Soil,MMin}$ is a parameter. Sample $MH_{Soil,Moist}$ values are in Figure 11.5B, illustrating that it is unity at optimal conditions and near zero when soil moisture is depleted, severly restricting soil respiration.

The second is $MH_{Soil,PAW}$, which is equal to the plant available water fraction per soil layer PAW_F. Since this represents the fraction of water available plants, it has a maximum value of 1 and is restricted to be above a minimum value given by the parameter $HRT_{Soil,PAWMin}$.

11.5 Pool Updates

The carbon pools are updated daily at midnight LST, when no photosynthesis is occurring. This is done so that the change in pools and vegetation state occurs at night at every location in order to minimally impact the fluxes. For any pool p:

$$\frac{dC_p}{dt} = Gain_p - Loss_p, \tag{273}$$

$$Gain_p = \begin{cases} Gain_{A,p} + Gain_{Seed,p} & p = live\ pools \\ Gain_{Hrv,p} + Gain_{Grz,p} + Gain_{TD,p} + Gain_{TL,p} & p = dead\ pools \end{cases} \tag{274}$$

$$Loss_p = \begin{cases} Loss_{GResp,p} + Loss_{MResp,p} + Loss_{LF,p} + Loss_{T,p} & p = live\ pools \\ \quad + Loss_{Fire,p} + Loss_{Grz,p} + Loss_{Hrv,p} & \\ Loss_{HR,p} + Loss_{HT,p} + Loss_{Fire,p} & p = dead\ pools \end{cases} \tag{275}$$

12 Terrestrial Carbon Cycle

12.1 Overview

SiB4 fully simulates the terrestrial carbon cycle by using prognostic phenology to integrate ecosystem processes, linking carbon pools, land-atmosphere fluxes, and biosphere-atmosphere exchanges. This approach leads to a fully predictive terrestrial carbon cycle, rather than relying on satellite data for the vegetation state (Figure 12.1). Every timestep SiB4 computes albedo, hydrology, radiation, soil moisture, and temperature, as well as the resulting energy exchanges, moisture fluxes, and carbon fluxes. Fire emissions are also released every timestep, as well as the changes in carbon pools from burning and grazing. From sums of carbon pool gains and losses, SiB4 updates the carbon pools daily. Using the updated pools, all related land surface properties are diagnosed and used for sub-hourly photosynthetic assimilation as well as sub-hourly autotrophic and heterotrophic respiration and pool transfer rates. This sequence completes the carbon cycle, providing self-consistent predicted vegetation state, carbon pools, and land-atmosphere exchanges.

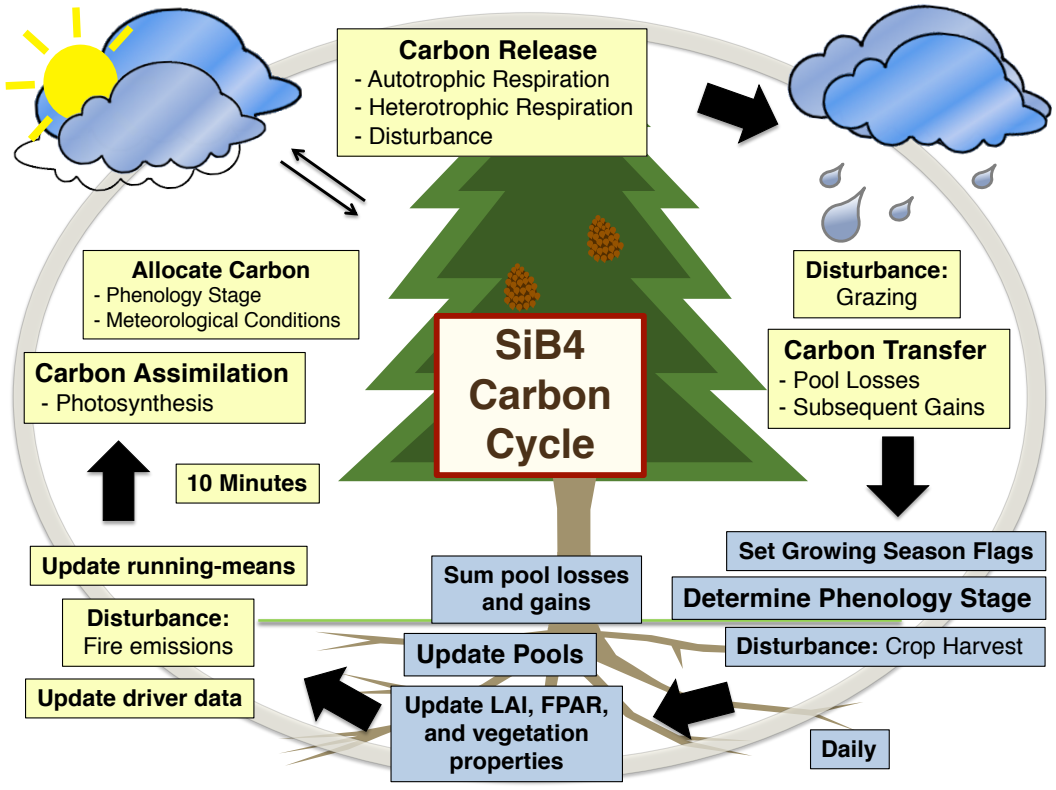

Figure 12.1: SiB4 Carbon Cycle.
Processes calculated every model timestep are in the yellow boxes. Processes calculated daily are in the blue boxes.

12.2 Calculation Sequence

1. Initialize SiB4.
2. Update driver meteorology, including zenith angle.
3. Update fire emissions, including determining the carbon pool reduction from burning.
4. Update the phenology potentials, and determine the phenology stage daily.
5. Update the carbon pools and vegetation state daily.
6. Calculate the radiation budget via a two-stream radiation approximation, updating surface reflectance, transmissivity, albedo, absorbed radiation, and net radiation.
7. Update canopy conductances and resistances.
8. Simulate photosynthesis.
9. Calculate carbonyl sulfide fluxes.
10. Calculate solar induced fluorescence (SIF).
11. Increment the prognostic variables (CAS, ground, and soil temperatures, CAS water vapor mixing ratio and pressure, CAS turbulent kinetic energy, CAS CO_2 partial pressure, and CAS COS partial pressure).
12. Calculate the latent and sensible heat fluxes.
13. Update the model hydrology, including canopy, snow, and soil variables.
14. Calculate autotrophic respiration, live pool turnover, and litterfall.
15. Simulate grazing.
16. Calculate heterotrophic respiration.
17. Write requested output.

References

Aguado, P.L., Curt, M.D., Pereira, H., & Fernández, J. (2016). The influence of season on carbon allocation to suberin and other stem components of cork oak saplings. *Tree Physiol.*, **37**, 165-172, https://doi.org/10.1093/treephys/tpw116.

Amthor, J.S. (2000). The McCree-de Wit-Penning de Vries-Thornley respiration paradigms: 30 years later. *Ann. Bot.*, **86**, 1-20, https://doi.org/10.1006/anbo.2000.1175.

Avissar, R. & Pielke, R. (1989). A parameterization of heterogeneous land surfaces for atmospheric numerical models and its impact on regional meteorology. *Mon. Wea. Rev.*, **117**, 2113-2136.

Badger, M.R. & Price, G.D. (1994). The role of carbonic-anhydrase in photosynthesis. *Annu. Rev. Plant Physiol.*, **45**, 369-392.

Baker, I.T., Prihodko, L., Denning, A.S., Goulden, M., Miller, S., & da Rocha, H.R. (2008). Seasonal drought stress in the Amazon: Reconciling models and observations. *J. Geophys. Res.*, **113**, G00B01, https://doi.org/10.1029/2007JG000644.

Baker, I.T., Denning, A.S., & Stöckli, R. (2010). North American gross primary productivity: regional characterization and interannual variability. *Tellus*, **62B** (5), 533-549, https://doi.org/10.1111/j.1600-0889.2010.00492.x.

Baker, I.T. (2011). Biophysical behavior in tropical South America, Ph.D. Dissertation, Atmospheric Science Department, Colorado State University, Fort Collins, Colorado.

Baker, I.T., Harper, A.B., da Rocha, H.R., Denning, A.S., Araújo, A.C., Borma, L.S., ... Wofsy, S.C. (2013). Surface ecophysiological behavior across vegetation and moisture gradients in tropical South America. *Agric. For. Meteorol.*, **182-183**, 177-188, https://dx.doi.org/10.1016/j.agrformet.2012.11.015.

Baker, I.T., Berry, J.A., Frankenberg, C., Joiner, J., van der Tol, C., Lee, J.-E., & Denning, A.S. (2014). Simulations of Solar-Induced Fluorescence using the Simple Biosphere Model (SiB) evaluated against data form satellites, presented at 5th International Workshop on Remote Sensing of Vegetation Fluorescence, Paris, France.

Baldocchi, D.D. & Wilson, K.B. (2001). Modeling CO_2 and water vapor exchange of a temperate broadleaved forest across hourly to decadal time scales. *Ecol. Model.*, **142**, 155-184.

Baldocchi, D., Falge, E., Gu, L., Olson, R., Hollinger, D., Running, S., ... Wofsy, S. (2001). FLUXNET: A new tool to study the temporal and spatial variability of ecosystem-scale carbon dioxide, water vapor, and energy flux densities. *Bull. Am. Meteorol. Soc.*, **82**, 11 2415-2435.

Ball, J.T. (1988). An analysis of stomatal conductance. Ph.D. Thesis, Standford University, 89 pp.

Ballantyne, A.P., Miller, J.B., Baker, I.T., Tans, P.P., & White, J.W.C. (2011). Novel applications of carbon isotopes in atmospheric CO_2: what can atmospheric measurements teach us about processes in the biosphere? *Biogeosciences*, **8**, 3093-3106, https://doi.org/10.5194/bg-8-3093-2011.

Bauerle, W.IL, Oren, R., Way, D.A., Qian, S.S., Stoy, P.C., Thornton, P.E., Bowden, J.D., Hoffman, F.M., & Reynolds, R.F. (2012). Photoperiodic regulation of the seasonal pattern of photosynthetic capacity and the implications for carbon cycling. *Proc. Natl. Acad. Sci.*, **109**, 22, 8612-8617, https://doi.org/10.1073/pnas.1119131109.

Berry, J., Wolf, A., Campbell, J.E., Baker, I., Blake, N., Blake, D., ... Zhu, Z. (2013). A coupled model of the global cycles of carbonyl sulfide and CO_2: A possible new window on the carbon cycle. *J. Geophys. Res. Biogeosci.*, **118**, 842-852, https://doi.org/10.1002/jgrg.20068.

Bonan, G.B. (1996). A land surface model (LSM Version 1.0) for ecological, hydrological, and atmospheric studies: Technical descxription and users guide. *Technical Note NCAR/TN-417+STR*, Natl. Cent. for Atmos. Res., Boulder, CO, USA.

Bonan, G.B., Levis, S., Kergoat, L., & Oleson, K.W. (2002). Landscapes as patches of plant functional types: An integrating concept for climate and ecosystem models. *Glob. Biogeochem. Cycles*, **16**(2), https://doi.org/10.1029/2000GB001360.

Borchert, R., Robertson, K., Schwartz, M.D., & Williams-Linera, G. (2005). Phenology of temperate trees in tropical climates. *Int. J. Biometeorol.*, **50**, 57-65, https://doi.org/10.1007/s00484-005-0261-7.

Butler, M.P., Davis, K.J., Denning, A.S., & Kawa,S.R. (2010). Using continental observations in global atmospheric inversions of CO_2: North American carbon sources and sinks. *Tellus*, **62B**(5), 550-572, https://doi.org/10.1111/j.1600-0889.2010.00501.x.

Caldararu, S., Purves, D.W., & Palmer, P.I. (2014) Phenology as a strategy for carbon optimality: a global model. *Biogeosciences*, **11**, 763-778, https://doi.org/10.5194/bg-11-763-2014.

Chapin, F.S. III, McFarland, J., McGuire, A.D., Euskirchen, E.S., Ruess, R.W. & Kietland, K. (2009). The changing global carbon cycle linking plant-soil carbon dynamics to global consequences. *J. Ecology*, **97**, 840-850.

Cheeseman, M.J. (2018). Productivity and phenology in a process-driven carbon cycle model. Master's Thesis, available from Colorado State University Theses and Dissertations database, https://hdl.handle.net/10217/193205.

Chen, X. (2003). East Asia. In *Phenology: An Integrative Environmental Science*, edited by M.D. Schwartz, 11-26, Kluwer Academic Publishers, Dordrecht, The Netherlands.

Chen, X., Post, W.M., Norby, R.J., & Classen, A.T. (2011). Modeling soil respiration and variations in source components using a multi-factor global climate change experiment. *Climatic Change*, **107**, 459-480, https://doi.org/10.1007/s10584-010-9942-2.

Chmielewski, F.-M. (2013). Phenology in agriculture and horticulture. In *Phenology: An Integrative Environmental Science, Second Edition*, edited by M.D. Schwartz, pp. 539-561, Springer, Dordrecht.

Chuine, I., Garcia de Cortazar-Atauri, I., Dramer, K., & Hanninen, H. (2013). Plant Development Models. In *Phenology: An Integrative Environmental Science, Second Edition*, edited by M.D. Schwartz, pp. 275-294, Springer, Dordrecht.
Flexas, J., Galmés, J., Ribas-Carbó, M. & Medrano, H. (2005). The effects of drought in plant respiration. In *Advances in photosynthesis and respiration 18. Plant respiration: from cell to ecosystem*, edited by H. Lambers and M. Ribas-Carbó, pp. 85-94, Kluwer Academic Publishers, Dordrecht.

Clapp, R.B. & Hornberger, G.M. (1978). Empirical equations for some soil hydraulic properties. *Water Resourc. Res.*, **14**, 4, 601-604, https://doi.org/10.1029/WR014i004p00601.

Collatz, G.J., Ball, J.T., Grivet, C., & Berry, J.A. (1991). Physiological and environmental regulation of stomatal conductance, photosynthesis and transpiration: a model that includes a laminar boundary layer. *Agric. For. Meteorol.*, **54**, 107-136.

Collatz, G.J., Ribas-Carbo, M., & Berry, J.A. (1992). Coupled photosynthesis-stomatal conductance model for leaves of C4 plants. *Aust. J. Plant Physiol.*, **19**, 519-538.

Corbin, K.D., Denning, A.S., Lu, L., Wang, J.-W., & Baker, I.T. (2008). Possible representation errors in inversions of satellite CO_2 retrievals. *J. Geophys. Res.*, **113**, D02301, https://doi.org/10.1029/2007JD008716.

Corbin, K.D., Denning, A.S., & D.R. Gurney (2010b). The space and time impacts on U.S. regional atmospheric CO_2 concentrations from a high resolution fossil fuel CO_2 emissions inventory. *Tellus*, **62B**, 506-511. https://doi.org/10.1111/j-1600-0889.2010.00480.x.

Corbin, K.D., Denning, A.S., Lokupitiya, E.Y., Schuh, A.E., Miles, N.L., Davis, K.J., Richardson, S., & Baker, I.T. (2010b). Assessing the impact of crops on regional CO_2 fluxes and atmospheric concentrations. *Tellus*, **62B**, 521-532, https://doi.org/10.1111/j.1600-0889.2010.00485.x.

Cosby, B.J., Hornberger, G.M., Clapp, R.B., & Ginn, T.R. (1984). A statistical exploration of the relationships of soil-moisture characteristics to the physical-properties of soils. *Water Resours. Res.*, **20**, 682-690.

Curry, R.A., Denning, A.S., Smith, M., & Peek, L. (2016). Impacts of drought on grassland productivity across the wet-dry gradient in the U.S. Great Plains in 2010-2012. Master's Thesis, available from Colorado State University Theses and Dissertations database, http://hdl.handle.net/10217/178924.

Cutter, G.A., Cutter, L.S., & Filippino, K.C. (2004). Sources and cycling of carbonyl sulfide in the Sargasso Sea. *Limno. Oceanogr.*, **49**(2), 555-565.

Dahlin, K.M., Fisher, R.A., & Lawrence, P.J. (2015). Environmental drivers of drought deciduous phenology in the Community Land Model. *Biogeosciences*, **12**, 5061-5074, https://doi.org/10.5194/bg-12-5061-2015.

Dahlin, K.M., Del Ponte, D., Setlock, E., & Nagelkirk, R. (2017). Global patterns of drought deciduous phenology in semi-arid and savanna-type ecosystems. *Ecography*, **40**, 314-323, https://doi.org/10.1111/ecog.02443.

Dai, Y., Zeng, X., Dickinson, R.E., Baker, I.T., Bonan, G.B., Bosilovich, M.G., Denning, A.S., ... Yang, Z.-L. (2003). The Common Land Model. *Bull. Am. Meteorol. Soc.*, **84**, 1013-1023, https://doi.org/10.1175/BAMS-84-8-1013.

De Kauwe, M.G., Medlyn, B.E., Zaehle, S., Walker, A.P., Dietze, M.C., Wang, Y.-P., ... Norby, R.J. (2014). Where does the carbon go? A model-data intercomparison of vegetation carbon allocation and turnover processes at two temperate forest free-air CO_2 enrichment sites. *New Phytol.*, **203**, 883-899, https://doi.org/10.1111/nph.12847.

Denning, A.S., Collatz, G.J., Zhang, C., Randall, D.A., Berry, J.A., Sellers, P.J., Colello, G.D., & Dazlich, D.A. (1996a). Simulations of terrestrial carbon metabolism and atmospheric CO_2 in a general circulation model. Part 1: Surface carbon fluxes. *Tellus*, **48B**, 521-542.

Denning, A.S., Randall, D.A., Collatz, G.J., & Sellers, P.J. (1996b). Simulations of terrestrial carbon metabolism and atmospheric CO_2 in a general circulation model. Part 2: Simulated CO_2 concentrations. *Tellus*, **48B**, 543-567.

Denning, A.S., Takahashi, T., & Friedlingstein, P. (1999). Can a strong atmospheric CO_2 rectifier effect be reconciled with a reasonable carbon budget? *Tellus*, **51B**, 249-253.

Denning, A.S., Nicholls, M., Prihodko, L., Baker, I., Vidale, P.-L., Davis, K., & Bakwin, P. (2003). Simulated variations in atmospheric CO_2 over a Wisconsin forest using a couple ecosystem-atmosphere model. *Glob. Chang. Biol.*, **9**, 1241-1250.

Dickinson, R.E. (1983). Land surface processes and climate-surface albedos and energy balance. *Advances in Geophysics*, **Academic Press**, 48 pp.

Doney, S.C., Lindsay, K., Fung, I., & John, J. (2006). Natural variability in a stable, 1000-yr global coupled climate-carbon cycle simulation. *J. Clim.*, **19**, 3033-3054.

Eamus, D., Huete, A., & Yu, Q. (2016). *Vegetation Dynamics: A Synthesis of Plant Ecophysiology, Remote Sensing, and Modelling.* Cambridge University Press, New York, NY, 518 pp.

Ernakovich, J.G., Hopping, K.A., Berdanier, A.B., Simpson, R.T., Kachergis, E.J., Steltzer, H. & Wallenstein, M.D. (2014). Predicted responses of arctic and alpine ecosystems to altered seasonality under climate change. *Global Change Biology*, **20**(10), 3256-3269, https://doi.org/10.1111/gcb.12568.

Essery, R.L.H., Best, M.J, Betts, R.A., Cox, P.M. & Taylor, C.M. (2002). Explicit representation of subgrid heterogeneity in a GCM land surface scheme. *J. Hydrometeorol.*, **4**, 530-543.

Estiarte, M. & Peñuelas, J (2015). Alteration of the phenology of leaf senescence and fall in winter deciduous species by climate change: effects on nutrient proficiency. *Global Change Biology*, **21**(3), https://doi.org/10.1111/gcb.12804.

Evans, J.R., Voncaemmerer, S., Setchell, B.A., & Hudson, G.S. (1994). The relationship between CO_2 transfer conductance and leaf anatomy in transgenic tobacco with a reduced content of Rubisco. *Aust. J. Plant Physiol.*, **21**(4), 475-495.

Farquhar, G.D., von Caemmerer, S., & Berry, J.A. (1980). A biochemical model of photosynthetic CO_2 assimilation in leaves of C3 species. *Planta*, **149**, 78-90.

Fetzel, T., Havlik, P., Herrero, M., Kaplan, J.O., Kastner, T., Kroisleitner, C., ... Erb, K.-H. (2017). Quantification of uncertainties in global grazing systems assessment. *Global Biogeochem. Cycles*, **31**, 1089-1102, https://doi.org/10.1002/2016GB005601.

Fisher, J.I., Richardson, A.D., & Mustard, J.F. (2007). Phenoloogy model from surface meteorology does not capture satelitte-based greenup estimations. *Glob. Chang. Biol.*, **13**, 707-721, https://doi.org/10.1111/j.1365-2486.2006.01311.x.

Flexas, J., Galmés, J., Ribas-Carbó, M. & Medrano, H. (2005). The effects of drought in plant respiration. In *Advances in photosynthesis and respiration 18. Plant respiration: from cell to ecosystem*, edited by H. Lambers and M. Ribas-Carbó, pp. 85-94, Kluwer Academic Publishers, Dordrecht.

Flexas, J., Bota, J., Galmés, J., Medrano, H., & Ribas-Carbó, M. (2006). Keeping a positive carbon balance under adverse conditions: responses of photosynthesis and respiration to water stress. *Physiol. Plant.*, **127**, 343-352, https://doi.org/10.1111/j.1399-3054.2005.00621.x

Forkel, M., Carvalhais, N., Schaphoff, S., Bloh, W.v., Migliavacca, M., Thurner, M., & Thonicke, K. (2014). Identifying environmental controls on vegetation greenness phenology through model-data integration. *Biogeosciences*, **11**, 7025-7050, https://doi.org/10.5194/bg-11-7025-2014.

Frankenberg, C. Fisher, J.B., Worden, J., Badgley, G., Saatchi, S.S., Lee, J.-E., ... Yoota, T. (2011). New global observations of the terrestrial carbon cycle from GOSAT: Patterns of plant fluorescence with gross primary productivity. *Geophys. Res. Lett.*, **38**, L17706, https://doi.org/10.1029/2011GL048738.

Friedl, M.A., Gray, J.M., Melaas, E.K., Richardson, A.D., Hufkens, K., Keenan, T.F., Bailey, A., & O'Keefe, J. (2014) A tale of two springs: using recent climate anomalies to characterize the sensitivity of temperate forest phenology to climate change. *Environ. Res. Lett.*, **9**, https://doi.org/10.1088/1748-9326/9/5/054006.

Friedlingstein, P., Joel, G., Field, C.B., & Fung, I.Y. (1999). Toward an allocation scheme for global terrestrial carbon models. *Glob. Chang. Biol.*, **5**, 755-770.

Fu, Y., Zhang, H., Dong, W., & Yuan, W. (2014). Comparison of phenology models for predicting the onset of growing season over the Northern Hemisphere. *Plos ONE*, **9**(10), e109544, https://doi.org/10.1371/journal.pone.0109544.

Gentry, B., Briantais, J.-M., & Baker, N.R. (1989). The relationship between the quantum yield of photosynthetic electron transport and quenching of chlorophyll fluorescence. *Biochem. Biophys. Acta, Bioenerg.*, **990**(1), 87-92, https://doi.org/10.1016/S0304-4165(89)80016-9.

Glatthor, N., Höpfner, M., Baker, I.T., Berry, J.A., Campbell, J.E., Kawa, S.R., ... von Clarmann, T. (2015). Tropical sources and sinks of carbonyl sulfide observed from space. *Geophys. Res. Lett.*, **42**, 10,082-10,090, https://doi.org/10.1002/2015GL066293.

Groenendijk, M., Dolman, A.J., Ammann, C., Arneth, A., Cescatti, A., Dragoni, D., *dots* Wohlfahrt, G. (2011). Seasonal variation of photosynthetic model parameters and leaf area index from global fluxnet eddy covariance data. *Journal of Geophysical Research: Biogeosciences*, **116**(G4), https://doi.org/10.1029/2011JG001742.

Gu, L., Post, W.M, Baldocchi, D., Black, T.A., Verma, S.B., Vesala, T., & Wofsy, S.C. (2003) Phenology of vegetation photosynthesis. In *Phenology: An Integrative Environmental Science*, edited by M.D. Schwartz, 566 pp., Kluwer Academic Publishers, Dordrecht, The Netherlands.

Guillemot, J., Francois, C., Hmimina, G., Dufrêne, E., Martin-StPaul, N.K., Soudani, K., ... Delpierre, N. (2017). Environmental control of carbon allocation matters for modelling forest growth. *New Phytol.*, **214**, 180-193, https://doi.org/10.1111/nph.14320.

Gurney, K.R., Law, R.M., Denning, A.S., Rayner, P.J., Baker, D., Bousquet, P., ... Yuen, C.-W. (2002). Towards robust regional estimates of CO_2 sources and sinks using atmospheric transport models. *Nature*, **415**, 626-630, https://doi.org/10.1038/415626a.

Hanan, N.P., Berry, J.A., Verma, S.B., Walter-Shea, E.A., Suyker, A.E., Burba, G.G., & Denning, A.S. (2005). Testing a model of CO_2, water and energy exchange in Great Plains tallgrass prairie and wheat ecosystems. *Agric. For. Meteorol.*, **131**, 162-179.

Hanes, J.M., Richardson, A.D., & Klosterman, S. (2013). Mesic temperate deciduous forest phenology. In *Phenology: An Integrative Environmental Science, Second Edition*, edited by M.D. Schwartz, pp. 211-224, Springer, Dordrecht.

Harper, A., Baker, I.T., Denning, A.S., Randall, D.A., Dazlich, D., & Branson, M. (2014). Impact of Evapotranspiration on dry season climate in the Amazon forest. *J. Clim.*, bf 27(2), https://doi.org/10.1175/JCLI-D-13-00074.1.

Haynes, K.D., Baker, I.T., Denning, A.S., Stöckli, R., Schaefer, K., Lokupitiya, E.Y., & Haynes, J.M. (2019a). Representing grasslands using dynamic prognostic phenology

based on biological growth stages: 1. Implementation in the Simple Biosphere Model (SiB4). *J. Adv. Model. Earth Syst.*, 11, https://doi.org/10.1029/2018MS001540.

Haynes, K.D., Baker, I.T., Denning, A.S., Wolf, S., Wohlfahrt, G., Kiely, G., Minaya, R.C., & Haynes, J.M. (2019b). Representing grasslands using dynamic prognostic phenology based on biological growth stages. 2. Carbon Cycling. *J. Adv. Model. Earth Syst.*, 11, https://doi.org/10.1029/2018MS001541.

Hopkins, F., Gonzalez-Meler, M.A., Flower, C.E., Lynch, D.J., Czimczik, Tang, J., & Subke, J.-A. (2013). Ecosystem-level controls on root-rhizosphere respiration. *New Phytol.*, **199**, 339-351, https://doi.org/10.1111/nph.12271.

Houborg, R., Cescatti, A., Migliavacca, M., & Kustas, W.P. (2013). Satellite retrievals of leaf chlorophyll and photosynthetic capacity for improved modeling of GPP. *Agric. For. Meteorol.*, **177**, 10-23, http://dx.doi.org/10.1016/j.agrformet.2013.04.006.

Huntzinger, D.N., Post, W.M., Wei, Y., Michalak, A.M., West, T.O., Jacobson, A.R., ... Cook, R. (2012). North American Carbon Program (NACP) regional interim synthesis: Terrestrial biospheric model intercomparison. *Ecological Modelling*, **232**, 144-157, https://doi.org/10.1016/j.ecolmodel.2012.02.004.

Ise, T., Litton, C.M., Giardina, C.P., & Ito, A. (2010). Comparison of modeling approaches for carbon partitioning: impact on estimates of global net primary production and equilibrium biomass of woody vegetation from MODIS GPP. *J. Geophys. Res.*, **115**, G04025, https://doi.org/10.1029/2010JG001326.

Iversen, C.M. (2010). Digging deeper: fine-root responses to rising atmospheric CO_2 concentration in forested ecosystems. *New Phytol.*, **186**, 346-357.

Jackson, R.B., Canadell, J., Ehleringer, J.R., Mooney, H.A., Sala, O.E., & Schulze, E.D. (1996), A global analysis of root distributions for terrestrial biomes, *Oecologia*, **108**, 389-411.

Jarvis, P.G. (1976). The interpretation of the variations in leaf water potential and stomatal conductance found in canopies in the field. *Phil. Trans. Soc. Lond. B*, **273**, 593-610.

Jeong, S.-J., Schimel, D., Frankenberg, C., Drewry, D.T., Fisher, J.B., Verma, M., Berry, J.A., Lee, J.-E., & Joiner, J. (2016). Application of satellite solar-induced chlorophyll fluorescence to understanding large-scale variations in vegetation phenology and function over northern high latitude forests. *Remote Sensing of Environment*, **190**, 178-187, https://dx.doi.org/10.1016/j.rse.2016.11.021.

Joiner, J., Yoshida, Y., Vasilkov, A.P., Corp, L.A., & Middleton, E.M. (2011). First observations of global and seasonal terrestrial chlorophyll fluorescence from space. *Biogeosciences*, **8**(3), 637-651, https://doi.org/10.5194/bg-8-637-2011.

Joiner, J., Yoshida, Y., Vasilkov, A.P., Schaefer, K., Jung, M., Guanter, L., ... Marchesini, B. (2014). The seasonal cycle of satellite chlorophyll observations and its relationsh9p to

vegetation phenology and ecosystem-atmosphere carbon exchange. *Remote Sens. Environ.*, **152**, 375-391.

Jolly, W.M., Nemani, R., & Running, S.W. (2005). A generalized, bioclimatic index to predict foliar phenology in response to climate. *Global Change Biol.*, **11**, 619-632.

Jones, C., Robertson, E., Arora, V., Friedlingstein, P., Shevliakova, E., Bopp, L., ... Tjiputra, J. (2013). Twenty-First-Century compatible CO_2 emissions and airborne fraction simulated by CMIP5 Earth system models under four representative concentration pathways. *J. Clim.*, **26**, 4398-4414, https://doi.org/10.1175/JCLI-D-12-00554.1.

Kaduk, J.D. & Los, S.O. (2011). Predicting the time of green up in temperate and boreal biomes. *Climatic Change*, **107**, 277-304, https://doi.org/10.1007/s10584-010-9951-1.

Kang, L., Han, X., Zhang, Z., & Sun, O.J. (2007). Grassland ecosystems in China: A review of current knowledge and research advancement. *Phil. Trans. Soc. B*, **362**, 997-1008, https://doi.org/10.1098/rstb.2007.2029.

Keenan, T.F., Baker, I., Barr, A., Ciais, P., Davis, K., Dietze, M., ... Richardson, A.D. (2012) Terrestrial biosphere model performance for inter-annual variability of land-atmosphere CO_2 exchange. *Glob. Chang. Biol.*, https://doi.org/10.1111/j.1365-2486.2012.02678.x.

Kim, Y., Moorcroft, P.R., Aleinov, I., Puma, M.J., & Kiang, N.Y. (2015). Variability of phenology and fluxes of water and caxrbon with observed and simulated soil moisture in the Ent Terrestrial Biosphere Model (Ent TBM version 1.0.1.0.0). *Geosci. Model Dev.*, **8**, 3837-3865, https://doi.org/10.5194/gmd-8-3837-2015.

Kitajima, M. & Butler, W. (1975). Quenching of chlorophyll fluorescence and primary photochemistry in chloroplasts by dibromothy-monquinone. *Biochem. Biophys. Acta, Bioenerg.*, **376**(1), 105-115, https://doi.org/10.1016/0005-2728(75)90209-1.

Klein, T. & Hoch, G. (2015). Tree carbon allocation dynamics determined using a carbon mass balance approach. *New Phytol.*, **205**, 147-159, https://doi.org/10.1111/nph.12994.

Knapp, A.K., Hoover, D.L., Blair, J.M., Buis, G., Burkepile, D.E., Chamberlain, A., ... Zinn, A. (2012). A test of two mechanisms proposed to optimize grassland aboveground primary productivity in response to grazing. *J. Plant Ecol.*, **5**(4), 357-365, https://doi.org/10.1093/jpe/rts020.

Koerner, S.E., Burkepile, D.E., Fynn, R.W.S., Burns, C.E., Eby, S., Govender, N., ... Smith, M.D. (2014). Plant community response to loss of large herbivores differs between North American and South American savanna grasslands. *Ecology*, **95**(4), 808-816.

Krause, G.H. & Weis, E. (1991). Chlorophyll fluorescence and photosynthesis: the basics. *Annu. Rev. Plant Physol. Plant Mol. Biol.*, **42**, 313-349.

Krinner, G., Viovy, N., Noblet-Ducoudré, N., Ogée, J.P., Friedlingsten, P., Ciais, P., Stitch, S., & Prentice, C. (2005). A dynamic global vegetation model for studies of the coupled atmosphere-biosphere system. *Glob. Biogeochem. Cycles*, **19**, GB1015, https://doi.org/10.1029/2003GB002199.

Kuai, L., Worder, J.R., Campbell, J.E., Kulawik, S.S., Li, K.F., Lee, M. ... Yung, Y.L. (2015). Estimate of carbonyl sulfide tropical oceanic surface fluxes using Auro Tropospheric Emission Spectrometer observations. *J. Geophys. Res. Atmos.*, **120**, https://doi.org/10.1002/2015JD023493.

Larcher, W. (2002) Plants under stress. In *Physiological Plant Ecology: Ecophysiology and Stress Physiology of Functional Groups*, edited by W. Larcher, pp. 345-450, Springer, Berlin, Germany.

Lauvaux, T., Schuh, A.E., Uliasz, M., Richardson, S., Miles, N., Andrews, A.E., ... Davis, K.J. (2012). Constraining the CO_2 budget of the maize belt: exploring uncertainties from the assumptions in a mesoscale inverse system. *Atmos. Chem. Phys.*, **12**, 337-354, https://doi.org/10.5194/acp-12-337-2012.

Law, R.M., Peters, W., Rödenbeck, C., Aulagnier, C., Baker, I.T., Bergmann, D.J., ... Zhu, Z. (2008). TransCom model simulations of hourly atmospheric CO_2: Experimental overview and diurnal cycle results for 2002. *Glob. Biogeochem. Cycles*, **22**, GB3009, https://doi.org/10.1029/2007GB003050.

Lawrence, D.M. & Slater, A.G. (2008). Incorporating organic soil into a global climate model. *Clim. Dyn.*, **30**, 145-160, https://doi.org/10.1007/s00382-007-0278-1.

Lawrence, D.M., Oleson, K.W., Flanner, M.G., Thornton, P.E., Swenson, S.C., Lawrence, P.J., ... Slater, A.G. (2011). Parameterization improvements and functional and structural advances in version 4 of the Community Land Model. *J. Adv. Model. Earth Syst.*, **3**, M03001, https://doi.org/10.1029/2011MS000045.

Lawrence, P.J. & Chase, T.N. (2007). Representing a new MODIS consistent land surface in the Community Land Model (CLM 3.0). *J. Geophys. Res.*, **112**, G01023, https://doi.org/10.1029/2006JG000168.

Lawrence, P.J., Fisher, R., Koven, C., Oleson, K., Swenson, S., & Vertenstein, M. (2018). Technical Description of version 5.0 of the Community Land Model (CLM). National Center for Atmospheric Research (NCAR) Release, Boulder, CO, USA.

Lee, J.-E., Berry, J.A., van der Tol, C., Yang, X., Guanter, L., Damm, A., Baker, I., & Frankenberg, C. (2015). Simulations of chlorophyll fluorescence incorporated into the Community Land Model version 4. *Glob. Change Biol.*, **12948**, https://doi.org/10.1111/gcb.12948.

Li, R. & Arora, V.K. (2012). Effect of mosaic representation of vegetation in land surface schemes on simulated energy and carbon balances. *Biogeosciences*, **9**, 593-605, https://doi.org/10.5194/bg-9-593-2012.

Liang, L. & He, K.S. (2017). Call for Content for Special Issue: Patterns, Trends, and Ecological Applications of Phenology. *Remote Sens. Ecol. Conserv. Blog*, https://rsecjournalblog.wordpress.com/2017/05/03/call-for-content-for-special-issue-patterns-trends-and-ecological-applications-of-phenology/

Lokupitiya, R.S., Zupanski, D., Denning, A.S., Kawa, S.R., Gurney, K.R., & Zupanski, M. (2008). Estimation of global CO_2 fluxes at regional scale using the maximum likelihood ensemble filter. *J. Geophys. Res.*, **113**, D20110, https://doi.org/10.1029/2007JD009679.

Lokupitiya, E., Denning, A.S., Paustian, K., Baker, I.T., Schaefer, K., Verma, S., ... Fischer, M. (2009). Incorporation of crop phenology in Simple Biosphere Model (SiBcrop) to improve land-atmosphere carbon exchanges from croplands. *Biogeosciences*, **6**, 969-986.

Lokupitiya, E., Denning, A.S., Schaefer, K., Ricciuto, D., Anderson, R., Arain, M.A., ... Xue, Y. (2016). Carbon and energy fluxes in cropland ecosystems: a model-data comparison. *Biogeochemistry*, https://doi.org/10.1007/s10533-016-0219-3.

Lu, L., Denning, A.S., da Silva-Dias, M.A., da Silva-Dias, P., Longo, M., Freitas, S.R., & Saatchi, S. (2005). Mesoscale circulations and atmospheric CO_2 variations in the Tapajós Region, Pará, Brazil. *J. Geophys. Res.*, **110**, D21102, https://doi.org/10.1029/2004JD005757.

Malhi, Y., Doughty, C., & Galbraith, D. (2011). The allocation of ecosystem net primary productivity in tropical forests. *Phil. Trans. R. Soc. B*, **366**, 3225-2345, https://doi.org/10.1098/rstb.2011.0062.

McCormack, M.L., Adams, T.S., Smithwick, E.A.H., & Eissenstat, D.M. (2014). Variability in root production, phenology, and turnover rate among 12 temperate tree species. *Ecology*, **95**(8), 2224-2235.

Medvigy, D., Wofsy, S.C., Munger, J.W., Hollinger, D.Y., & Moorcroft, P.R. (2009). Mechanistic scaling of ecosystem function and dynamics in space and time: Ecosystem Demography model version 2. *J. Geophys. Res.*, **114**, 1-21, https://doi.org/10.1029/2008JG000812.

Meir, P., Metcalfe, D.B., Costa, A.C.L., & Fisher, R.A. (2008). The fate of assimilated carbon during drought: impacts on respiration in Amazon rainforests. *Phil. Trans. R. Soc. B*, **363**, 1849-1855, https://doi.org/10.1098/rstb.2007.0021.

Melaas, E.K., Friedl, M.A., & Richardson, A.D. (2016). Multiscale modeling of spring phenology across deciduous forests in the eastern United States. *Glob. Chang. Biol.*, **22**, 792-805, https://doi.org/10.1111/gcb.13122.

Meroni, M., Rossini, M., Guanter, L., Alonso, L., Rascher, U., Colombo, R., & Moreno, J. (2009). Remote sensing of solar-induced shlorophyll fluorescence: Review of methods and applications. *Remote Sens. Environ.*, **113**(110), 2037-2051, https://doi.org/10.1016/j.rse.2009.05.003.

Migliavacca, M., Sonnentag, O., Keenan, T.F., Cescatti, A., O'Keefe, J., & Richardson, A.D. (2012). On the uncertainty of phenological responses to climate change, and implications for a terrestrial biosphere model. *Biogeosciences*, **9**, 2063-2083, https://doi.org/10.5194/bg-9-2063-2012.

Molchanov, A.G. (2009). Effect of moisture availability on photosynthetic productivity and autotrophic respiration of an oak stand. *Russ. J. Plant Physiol.*, **56**(6), 769-779, https://doi.org/10.1134/S1021443709060065.

Morellato, L.P.C., Alberton, B., Alvarado, S.T., Borges, B., Buisson, E., Camargo, M.G.G., ... Peres, C.A. (2016). Linking plant phenology to conservation biology. *Biological Conservation*, **195**, 60-72, https://doi.org/10.1016/j.biocon.2015.12.033.

Negrón-Juárez, R.I., Koven, C.D., Riley, W.J., Knox, R.G. & Chambers, J.Q. (2015). Observed allocations of productivity and biomass, and turnover times in tropical forests are not accurately represented in CMIP5 Earth system models. *Environ. Res. Lett.*, **10**, 064017, https://doi.org/10.1088/1748-9326/10/6/064017.

Nicholls, M., Denning, A.S., Prihodko, L., Vidale, P.-L., Baker, I.T., Davis, K., & Bakwin, P. (2003). A multiple-scale simulation of variations in atmospheric carbon dioxide using a coupled biosphere-atmospheric model. *J. Geophys. Res.*, **109**, D18117, https://doi.org/10.1029/2003JD004482.

Ogle, S.M., Davis, K., Lauvaux, T., Schuh, A., Cooley, D., West, T.O., ... Denning, A.S. (2015). An approach for verifying biogenic greenhouse gas emissions inventories with atmospheric CO_2 concentration data. *Environ. Res. Lett.*, **10**, 034012, https://doi.org/10.1088/1748-9326/10/3/034012.

Oleson, K.W., Emery, W.J., & Maslanik, J.A. (2000). Evaluating land surface parameters in the Biosphere-Atmosphere Transfer Scheme using remotely sensed data sets. *J. Geophys. Res.*, **105**(D6), 7275-7293, https://doi.org/10.1029/1999JD901041.

Ostle, N.J., Smith, P., Fisher, R., Woodward, F.I., Fisher, J.B., Smith, J.U., ... Bardgett, R.D. (2009). Integrating plant-soil interactions into global carbon cycle models *J. Ecology*, **97**, 851-863. https://doi.org/10.1111/j.1365-2745.2009.01547.x.

Parazoo, N.C., Denning, A.S., Kawa, S.R., Corbin, K.D., Lokupitiya, R.S., & Baker, I.T. (2008). Mechanisms for synoptic variations of atmospheric CO_2 in North America, South America, and Europe. *Atmos. Chem. Phys.*, **8**, 7239-7254.

Parazoo, N.C., Denning, A.S., Kawa, S.R., Pawson, S., & Lokupitiya, R. (2012). CO_2 flux estimation errors associated with moist atmospheric processes. *Atmos. Chem. Phys.*, **12**, 6405-6416, https://doi.org/10.5194/acp-12-6405-2012.

Patra, P.K., Law, R.M., Peters, W., Rödenbeck, C., Takigawa, M., Aulagnier, C., ... Zhu, Z. (2008). TransCom model simulations of hourly atmospheric CO_2: Analysis of synoptic-scale variations for the period 2002-2003. *Glob. Biogeochem. Cycles*, **22**, GB4013, https://doi.org/10.1029/2007GB003081.

Pau, S., Wolkovich, E.M., Cook, B.I., Davies, J., Kraft, N.J., Bolmgren, K., Betancourt, J.L., & Cleland, E.E. (2011). Predicting phenology by integrating ecology, evolution, and climate science. *Glob. Chang. Biol.*, **17**, 3633-3643, https://doi.org/10.1111/j.1365-2486.2011.02515.x.

Picard, G., Quegan, S., Delbart, N., Lomas, M.R., Le Toan, T., & Woodward, F.I. (2005). Bud-burst modelling in Siberia and its impact on quantifying the carbon budget. *Glob. Chang. Biol.*, bf 11, 2164-2176. https://doi.org/10.1111/j.1365-2486.2005.01055.x

Poorter, H., Jagodzinski, A.M., Ruiz-Peinado, R., Kuyah, S., Luo, Y., Oleksyn, J., ... Sack, L. (2015). How does biomass distribution change with size and differ among species? An analysis for 1200 plant species from five continents. *New Phytol.*, **208**, 736-749, https://doi.org/10.1111/nph.13571.

Potter, C.S., Randerson, J.T., Field, C.B., Matson, P.A., Vitousek, P.M., Mooney, H.A., & Klooster, S.A. (1993). Terrestrial ecosystem production: A process model based on global satellite and surface data. *Glob. Biogeochem. Cycles*, **7**(4), 811-841.

Prentice, I.C., Liang, X., Medlyn, B.E., & Wang, Y.-P. (2015). Reliable, robust, and realistic: the three R's of next-generation land surface modelling. *Atmos. Chem. Phys.*, **15**, 5987-6005, https://doi.org/10.5194/acp-15-5987-2015.

Raich, J.W. & Nadelhoffer, K.J. (1989). Belowground carbon allocation in forest ecosystems: global trends. *Ecology*, **70**(5), 1346-1354.

Raich, J.W., Rastetter, E.B., Melillo, J.M., Kicklighter, D.W., Steudler, P.A., & Peterson, B.J. (1991). Potential net primary productivity of South America: Application of a global model. *J. Atmos. Sci.*, **46**, 1943-1970.

Raich, J.W. & Schlesinger, W.H. (1992). The global carbon dioxide flux in soil respiration and its relationship to vegetation and climate. *Tellus B*, **44**, 81-99, https://doi.org/10.1034/j.1600-0889.1992.t01-1-00001.x.

Randall, D.A., Dazlich, D.A., Zhang, C., Denning, A.S., Sellers, P.J., Tucker, C.J., ... Fung, I.Y. (1996). A revised land surface parameterization (SiB2) for GCMs. Part III: The greening of the Colorado State University General Circulation Model. *J. Clim.*, **9**, 738-763.

Randerson, J.T., Thompson, M.V., Malmstrom, C.M., Field, C.B., & Fung, I.Y. (1996). Substrate limitations for heterotrophs: Implications for models that estimate the seasonal cycle of atmospheric CO_2. *Glob. Biogeochem. Cycles*, **10**(4), 585-602.

Reed, B.C., White, M., & Brown, J.F. (2003). Remote Sensing Phenology. In *Phenology: An Integrative Environmental Science*, edited by M.D. Schwartz, pp. 365-378, Springer, Dordrecht.

Reichstein, M., Falge, E., Baldocchi, D., Papale, D., Aubinet, M., Berbigier, P., ... Valentini, R. (2005). On the separation of net ecosystem exchange into assimilation and

ecosystem respiration: review and improved algorithm. *Glob. Chang. Biol.*, **11**, 1424-1439, https://doi.org/10.1111/j.1365-2486.2005.001002.x.

Restrepo-Coupe, N., da Roucha, H.R., Hutyra, L.R., da Araujo, A.C., Borma, L.S., Christoffersen, B., ... Saleska, S.R. (2013). What drives the seasonality of photosynthesis across the Amazon basin? A cross-site analysis of eddy flux tower measurements from the Brasil flux network. *Agricultural and Forest Meteorology*, **182-183**, 128-144, https://doi.org/10.1016/j.agrformet.2013.04.031.

Richardson, A.D., Black, T.A., Ciais, P., Delbart, N., Friedl, M.A., Gobron, N., ... Varlagin, A. (2010). Influence of spring and autumn phenological transitions on forest ecosystem productivity. *Phil. Trans. R. Soc. B*, **365**, 3227-3246, https://doi.org/10.1098/rstb.2010.0102.

Richardson, A.D., Anderson, R.S., Arain, M.A., Barr, A.G., Bohrer, G., Chen, G., ... Xue, Y. (2012). Terrestrial biosphere models need better representation of vegetation phenology: results from the North American Carbon Program site synthesis. *Glob. Chang. Biol.*, **18**, 566-584, https://doi.org/10.1111/j.1365-2486.2011.02562.x.

Richardson, A.D., Keenan, T.F., Migliavacca, M., Ryu, Y., Sonnentag, O. & Toomey, M. (2013). Cliamte change, phenology, and phenological control of vegetation feedbacks to the climate system. *Agric. For. Meteorol.*, **169**, 156-173, https://dx.doi.org/10.1016/j.agrformet.2012.09.012.

Richardson, A.D., Weltzin, J.F., & Morisette, J.T. (2017). Integrating multiscale seasonal data for resource management. *Eos*, **98**, https://doi.org/10.1029/2017EO065709.

Ryan, M.G. (1991). A simple method for estimating gross carbon budgets for vegetation in forest ecosystems. *Tree Physiol.*, **9**, 255-266.

Ryan, M.G. & Law, B.E. (2005). Interpreting, measuring, and modeling soil respiration. *Biogeochem.*, **73**, 3-27, https://doi.org/10.1007/s10533-004-5167-7.

Saleska, S., Wu, J., Guan, K., Araujo, A., Huerte, A., Nobre, A., & Restrepo-Coupe, N. (2014). Dry-season greening of Amazon forests. *Nature*, **531**, https://doi.org/10.1038/nature16457.

Sato, N., Sellers, P.J., Randall, D.A., Schneider, E.K., Shukla, J., Kinter III, J.L., Hou, Y.-T., & Albertazzi, E. (1989a). Effects of implementing the Simple Biosphere Model in a general circulation model. *J. Atmos. Sci.*, **46** (18), 2757-2782.

Sato, N., Sellers, P.J., Randall, D.A., Schneider, E.K., Shukla, J., Kinter III, J.L., Hou, Y.-T., & Albertazzi, E. (1989b). Implementing the Simple Biosphere Model (SiB) in a General Circulation Model: Methodologies and Results. *NASA Contractor Report 185509*.

Schaefer, K., Denning, A.S., Suits, N., Kaduk, J., Baker, I.T., Los, S., & Prihodko, L. (2002). Effect of climate on interannual variability of terrestrial CO_2 fluxes. *Glob. Biogeochem. Cycles*, **16**(4), 1102, https://doi.org/10.1029/2002GB001928.

Schaefer, K., Collatz, G.J., Tans, P., Denning, A.S., Baker, I.T., Berry, J., Prihodko, L., Suits, N., & Philpott, A. (2008). Combined Simple Biosphere/Carnegie-Ames-Stanford Approach terrestrial carbon cycle model. *J. Geophys. Res*, **113**, G03034, https://doi.org/10.1029/2007JG000603.

Schaefer, K., Zhang, T., Slater, A.G., Lu, L., Etringer, A., & Baker, I.T. (2009). Improving simulated soil temperatures and soil freeze/thaw at high-latitude regions in the Simple Biosphere/Carnegie-Ames-Stanford Approach model. *J. Geophys. Res.*, **114**, F02021, https://doi.org/10.1029/2008JF001125.

Schaefer, K., Zhang, T., Bruhwiler, L., & Barrett, A.P. (2011). Amount and timing of permafrost carbon release in response to climate warming. *Tellus*, **63B**, 165-180, https://doi.org/10.1111/j.1600-0889.2011.00527.x.

Schaefer, K. & Jafarov, E. (2016). A parameterization of respiration in frozen soils based on substrate availability. *Biogeosciences*, **13**, 1991-2001, https://doi.org/10.5194/bg-13-1991-2016.

Scheifinger, H., Menzel, A., Koch, E., Peter, C., & Ahas, R. (2002). Atmospheric mechanisms governing the spatial and temporal variability of phenological phases in central Europe. *Int. J. Climatol.*, **22**, 1739-1755, https://doi.org/10.1002/joc.817.

Schuh, A.E., Denning, A.S., Corbin, K.D., Baker, I.T., Uliasz, M., Parazoo, N., Andrews, A.E., & Worthy, D.E.J. (2010). A regional high-resolution carbon flux inversion of North America for 2004. *Biogeosciences*, **7**, 1625-1644, https://doi.org/10.5194/bg-7-1625-2010.

Schuh, A.E., Lauvaux, T., West, T.O., Denning, A.S., Davis, K.J., Miles, N., ... Ogle, S. (2013). Evaluating atmospheric CO_2 inversions at multiple scales over a highly inventoried agricultrual landscape. *Glob. Chang. Biol.*, **19**, 1424-1439, https://doi.org/10.1111/gcb.12141.

Seibt, J., Wingate, L., Lloyd, J., & Berry, J.A. (2006). Diurnally variable $\delta^{18}O$ signatures of soil CO_2 fluxes indicate carbonic anhydrase activity in a forest soil. *J. Geophys. Res.*, **111**, G04005, https://doi.org/10.1029/2006JG000177.

Seibt, U., Kesselmeier, J., Sandoval-Soto, L., Kuhn, U. & Berry, J.A. (2010). A kinetic analysis of leaf uptake of COS and its relation to transpiration, photosynthesis and carbon isotope fractionation. *Biogeosciences*, **7**(1), 333-341.

Sellers, P.J. (1985). Canopy reflectance, photosynthesis, and transpiration. *Int. J. Rem. Sens.*, **6**:8, 1335-1372, https://doi.org/10.1080/01431168508948283.

Sellers, P.J., Mintz, Y., Sud, Y.C., & Dalcher, A. (1986). A Simple Biosphere Model (SiB) for use withing general circulation models. *J. Atmos. Sci*, **43**(6), 505-531.

Sellers, P.J. (1987). Canopy reflectance, photosynthesis, and transpiration. II. The role of biophysics in the linearity of their interdependence. *Remote Sens. Eviron.*, **21**, 143-183.

Sellers, P.J., Shuttleworth, J.W., Dorman, J.L., Dalcher, A., & Roberts, J.M. (1989). Calibrating the simple biosphere model (SiB) for Amazonian tropical forest using field and remoste sensing data. Part I: Average calibration with field data. *J. Appl. Meteor.*, **28**, 727-759.

Sellers, P.J., Berry, J.A., Collatz, G.J., Field, C.B., & Hall, F.G. (1992). Canopy reflectance, photosynthesis, and transpiration. III. A reanalysis using improved leaf models and a new canopy integration scheme. *Remote Sens. Environ.*, **42**, 187-216.

Sellers, P.J., Randall, D.A., Collatz, G.J., Berry, J.A., Field, C.B., Dazlich, D.A., ... Buonoua, L. (1996a). A revised land surface parameterization (SiB2) for atmospheric GCMs. *J. Clim.*, **9**, 676-705.

Sellers, P.J., Los, S.O., Tucker, C.J., Justice, C.O., Dazlich, D.A., Collatz, G.J., & Randall, D.A. (1996b). A revised land surface parameterization (SiB2) for Atmospheric GCMs. Part II: The generation of global fields of terrestrial biophysical parameters from satellite data. *J. Clim.*, **9**, 706-737.

Sellers, P.J., Dickinson, R.E., Randall, D.A., Betts, A.K., Hall, F.G., Berry, J.A., ... Henderson-Sellers, A. (1997). Modeling the exchanges of energy, water, and carbon between continents and the atmosphere. *Science*, **275**, 502-509.

Smith, D.C., Denning, A. S., Smith, M., O'Dell, C., & Kummerow, C. (2018). Using Remotely Sensed Fluorescence and Soil Moisture to Better Understand the Seasonal Cycle of Tropical Grasslands. Master's Thesis, available from Colorado State University Theses and Dissertations database, https://hdl.handle.net/10217/185785.

Stimler, K., Montzka, S.A., Berry, J.A., Rudich, Y., & Yakir, D. (2010). Relationships between carbonyl sulfide (COS) and CO_2 during leaf gas exchange. *New Phytol.*, **186**(4), 869-878.

Stimler, K., Berry, J.A., & Yakir, D. (2012). Effects of carbonyl sulfide and carbonic anhydrase on stomatal conductance. *Plant Physiol.*, **158**(1), 524-530.

Stöckli, R., Rutishauser, T., Dragoni, D., O'Keefe, J., Thornton, P.E., Jolly, M., Lu, L., & Denning, A.S. (2008). Remote sensing data assimilation for a prognostic phenology model. *J. Geophys. Res.*, bf 113, G04021, https://doi.org/10.1029/2008JG000781.

Stöckli, R., Rutishauser, T., Baker, I.T., Liniger, M.A., & Denning, A.S. (2011). A global reanalysis of vegetation phenology. it J. Geophys. Res., bf 116, G03020, https://doi.org/10.1029/2010JG001545.

Suits, N.S., Denning, A.S., Berry, J.A., Still, C.J., Kaduk, J., Miller, J.B., & Baker, I.T. (2005). Simulation of carbon isotope discrimination of the terrestrial biosphere. *Glob. Biogeochem. Cycles*, **19**, GB1017, https://doi.org/10.1029/2003GB002141.

Sulman, B., Desai, A.R., Schroeder, N.M., Ricciuto, D., Barr, A., Richardson, A.D., ... Weng, E. (2012). Impact of hydrological variations on modeling of peatland CO_2 fluxes:

Results from the North American Carbon Program site synthesis. *J. Geophys. Res.*, **117**, G01031, https://doi.org/10.1029/2011JG001862.

Van Diest, H. & Kesselmeier, J. (2008). Soil atmosphere exchange of carbonyl sulfide (COS) regulated by diffusivity depending on water-filled pore space. *Biogeosciences*, **5**(2), 475-483.

van der Tol, C., Verhoef, W., & Rosema, A. (2009). A model for chlorophyll fluorescence and photosynthesis at leaf scale. *Agric. For. Meteorol.*, **149**)(1), 96-105.

van der Tol, C., Berry, J.A., Campbell, P.K.E., & Rascher, U. (2014). Models of fluorescence and photosynthesis for interpreting measurements of solar-induced chlorophyll fluorescence. *J. Geophys. Res. Biogeosci.*, **119**, https://doi.org/10.1002/2014JG002713.

van der Velde, I.R., Miller, J.B., Schaefer, K., van der Werf, G.R., Krol, M.C., & Peters, W. (2014). Terrestrial cycling of $^{13}CO_2$ by photosynthesis, respiration, and biomass burning in SiBCASA. *Biogeosciences*, **11**, 6553-6571, https://doi.org/10.5194/bg-11-6553-2014.

Vidale, P.L. & Stöckli, R. (2005). Prognostic canopy air space solutions for land surface Exchanges. *Theor. Appl. Climatol.*, **80**, 245-257, https://doi.org/10.1007/s00704-004-0103-2.

Wang, J.-W., Denning, A.S., Lu, L., Baker, I.T., Corbin, K.D., & Davis, K.J. (2007). Observations and simulations of synoptic, regional, and local variations in atmospheric CO_2. *J. Geophys. Res.*, **112**, D04108, https://doi.org/10.1029/2006JD007410.

Wang, Y., Deutscher, N.M., Palm, M., Warneke, T., Notholt, J., Baker, I.T., ... Kremser, S. (2016). Towards understanding the variability in biospheric CO_2 fluxes: using FTIR spectrometry and a chemical transport model to investigate the sources and sinks of carbonyl sulfide and its link to CO_2. *Atmos. Chem. Phys.*, **16**, 2123-2138, https://doi.org/10.5194/acp-16-2123-2016.

Wei, W., Jiang, F., & Oikawa, T. (2009). Contribution of root and microbial respiration to soil CO_2 efflux and their environmental controls in a humid temperate grassland of Japan. *Pedosphere*, **19**(1), 31-39.

White, M.A., Thornton, P.E., & Running, S.W. (1997). A continental phenology model for monitoring vegetation responses to interannual climatic variability. *Glob. Biogeochem. Cycles*, **11**, 2, 217-234.

Whittaker, R.H. (1956). Vegetation of the Great Smoky Mountains. *Ecol. Monogr.*, **26**, 1-80.

Williams, C.A., Hanan, N.P., Baker, I.T., Collatz, G.J., Berry, J., & Denning, A.S. (2008). Interannual variability of photosynthesis across Africa and its attribution. *J. Geophys. Res.*, **113**, G04015, https://doi.org/10.1029/2008JG000718.

Williams, C.A. & Hanan, N.P. (2011). ENSO and IOD teleconnections for African ecosystems: evidence of destructive interference between climate oscillations. *Biogeosciences*, **8**, 27-40, https://doi.org/10.5194/bg-8-27-2011.

Wilson, K.B. & Baldocchi, D.D. (2000). Estimating annual net ecosystem exchange of carbon over five years at a deciduous forest in the southern United States. *Agric. For. Meteorol.*, **100**, 1-18.

Wingate, L., Seibt, U., Maseyk, K., Ogee, J., Almeida, P., Yakir, D., Pereira, J.S., & Mencuccini, M. (2008). Evaporation and carbonic anhydrase activity recorded in oxygen isotope signatures of net CO_2 fluxes from a Mediterranean soil. *Global Change Biol.*, **14**(9), 2178-2193.

Wohlfahrt, G., Bahn, M., Haslwanter, A., Newesely, C., & Cernusca, A. (2005). Estimation of daytime ecosystem respiration to determine gross primary production of a mountain meadow. *Agric. For. Meteorol.*, **130**, (1-2), 13-25.

Wu, J., Albert, L., Lopes, A., Restrepo-Coupe, N., Hayek, M., Wiedermann, K., ... Saleska, S. (2016). Leaf development and demography explain photosynthetic seasonality in Amazon evergreen forests. *Science*, **351**(6276), 13-25, https://doi.org/10.1126/science.aad5068.

Wullschleger, S.D., Epstein, H.E., Box, E.O., Euskirchen, E.S., Goswami, S., Iversen, C.M., ... Xu, X. (2014). Plant functional types in Earth System Models: past experiences and future directions for application of dynamic vegetation models in high-latutitude ecosystems. *Ann. Bot.*, **114**, 1-16.

Xia, J., Yuan, W., Wang, Y-P., & Zhang, Q. (2017). Adaptive carbon allocation by plants enhances the terrestrial carbon sink. *Scientific Reports*, **7**, 3341, https://doi.org/10.1038/s41598-017-03574-3.

Xu, X., Medvigy, D., Wright, J.S., Kitajima, K., Wu, J., Albert, L.P., ... Pacala, S.W. (2017). Variations of leaf longevity in tropical moist forests predicted by a trait-driven carbon optimality model. *Ecology Letters*, **20**(9), 1097-1106, https://doi.org/10.1111/ele.12804.

Yan, L., Zhou, G., & Zhang, F. (2013). Effects of different grazing intensities on grassland production in China: A meta-analysis. *PloS ONE*, **8** (12), e81466, https://doi.org/10.1371/journal.pone.0081466.

Yang, X., Tang, J., Mustard, J.F., Lee, J.-E., Rossini, M., ... Joiner, J. (2015). Solar-induced chlorophyll fluorescence that correlates with canopy photosynthesis on diurnal and seasonal scales in a temperate deciduous forest. *Geophys. Res. Lett.*, **42**, 2977-2987.

Yi, Z.G., Wang, X.M., Sheng, G.Y., Zhang, D.Q., Zhou, G.Y., & Fu, J.M. (2007). Soil uptake of carbonyl sulfide in subtropical forests with different successional stages in south China. *J. Geophys. Res.*, **112**, D08302, https://doi.org/10.1029/2006JD008048.

Zarco-Tejada, P.J., Morales, A., Testi, L., & Villalobos, F.J. (2013). Spatio-temporal patterns of chlorophyll fluorescence and physiological and structural indices acquired from hyperspectral imagery as compared with carbon fluxes. *Remote Sens. Environ.*, **133**, 102-115.

Zhang, X., Friedl, M.A., Schaaf, C.B., Strahler, A.H., Hodges, J.C.F., Gao, F., Reed, B.C., & Huete, A. (2003). Monitoring vegetation phenology using MODIS. *Remote Sens. Environ.*, **84**, 471-475, https://doi.org/10.1016/S0034-4257(02)00135-9.

Zhang, Y., Guanter, L., Berry, J.A., Joiner, J., Tol, C., Huete, A., Gitelson, A., Voigt, M., & Kohler, P. (2014). Estimation of vegetation photosynthetic capacity from space-based measurements of chlorophyll fluorescence for terrestrial biosphere models. *Global Change Biol.*, **20**(12), 3727-3742.

Zhou, Y., Ju, W., Sun, X., Hu, Z., Han, S., Black. T.A., Jassal, R.S., & Wu, X. (2014). Close relationship between spectral vegetation indices and V_{cmax} in deciduous and mixed forests. *Tellus B: Chemical and Physical Meteorology*, **66**:1, 23279, https://doi.org/10.3402/tellusb.v66.23279.

Zupanski, D., Denning, A.S., Uliasz, M., Zupanski, M., Schuh, A.E., Rayner, P.J., Peters, W., & Corbin, K.D. (2007). Carbon flux bias estimation employing Maximum Likelihood Ensemble Filter (MLEF). *J. Geophys. Res.*, **112**, D7107, https://doi.org/10.1029/2006JD008371.

Acknowledgements

SiB4 Version 4.2 is available at https://gitlab.com/kdhaynes/sib4v2_corral.
The National Aeronautics and Space Administration (NASA) funded this research with contributions from four contracts: Terrestrial Ecology, NNX11AB87G; Carbon Monitoring System Program, NNX12AP86G; Science Team for the OCO-2 Missions, NNX15AG93G; and Carbon Cycle Science, NNX14AI52G.
The Department of Energy Project DE-SC00014438 also contributed funding.

Appendix A: Input Data and Parameters

Table A1: Meteorological Drivers.

Name	Definition	Units
LW_{Dwn}	Surface Incident Longwave Radiation	W/m^2
Pr_{cu}	Cumulus Precipitation Rate	mm/s
Pr_{ls}	Stratiform Precipitation Rate	mm/s
P_s	Surface Pressure	hPa
Sh	Mixed Layer Water Vapor Mixing Ratio	kg/kg
$Spdm$	Wind Speed	m/s
SW_{Dwn}	Surface Incident Shortwave Radiation	W/m^2
T_m	Mixed Layer Temperature	K
PCO_{2m}	Mixed Layer CO_2 Partial Pressure	Pa
$PCOS_m$	Mixed Layer COS Partial Pressure	Pa

Table A2: Fire Emissions.

Name	Definition	Units
$Fire_C$	Fire Carbon Loss	mol C/m^2/s
$Fire_{CO2}$	Fire CO_2 Respiration	mol C/m^2/s

Table A3: Structural Properties.

Name	Definition	Units
PFT_{Area}	PFT Fractional Coverage (per grid cell)	-
PFT_{Ref}	PFT Reference Number	-
$Clay_{Frac}$	Soil Clay Fraction	-
$Sand_{Frac}$	Sand Clay Fraction	-
$Soref_{Vis}$	Soil Shortwave Reflectance	-
$Soref_{NIR}$	Soil Longwave Reflectance	-

Table A4: Aerodynamic Parameters.

Name	Definition	Units
RbC	Coefficient for Canopy to CAS Aerodynamic Resistance	-
RdC	Coefficient for Ground to CAS Aerodynamic Resistance	-
Z_0	Canopy Roughness Coefficient	-
Zp_{Disp}	Zero Plane Displacement	-

Table A5: Physiological Parameters.

Name	Definition	Range	Units
A_{Theta}	Coupling Parameter	0.8 to 0.98	-
B_{Theta}	Coupling Parameter	0.95	-
B_{Inter}	Conductance-Photosynthesis Intercept	0.01 to 0.04	mol C/m^2/s
Chi_l	Leaf Angle Distribution Factor	-0.3 to 0.25	-
Eff_{Con}	Quantum Efficiency	0.05 to 0.08	mol CO_2/mol quanta
FC_{Min}	Field Capacity Minimum	0.3 to 1	m^{-3}
$Flag_{C4}$	C4 Flag	T or F	-
$Flag_{Graze}$	Grazing Flag	T or F	-
$FPAR_{Sat}$	Saturation FPAR (Fraction of Photosynthetically Active Radiation)	≤ 1	-
G_{Meso}	Mesophyll Conductance	4000	mol C/m^2/s
$Grad_m$	Conductance-Photosynthesis Slope Parameter	4 to 9	-
hfti	Half-Point of Frost Inhibition	267 to 269	K
hhti	Half-Point of High-Temp Inhibition	303 to 317	K
hlti	Half-Point of Low-Temp Inhibition	268 to 281	K
K_{Root}	Root Density Extinction Coefficient	1.7 to 5.5	-
LAI_{Min}	Minimum *LAI*	0.05 to 0.15	m^2/m^2
LAI_{Sat}	Saturation *LAI*	0 to 8.5	m^2/m^2
Ref	Leaf Reflectance (Shortwave/Longwave and Green/Brown)	0.07 to 0.48	-
$Root_D$	Maximum Rooting Depth	3.5 to 10	m
SLA	Specific Leaf Area	10 to 210	cm^2 Leaf Area/g Leaf
sfti	Slope of Frost Inhibition	0.35 to0.6	K^{-1}
shti	Slope of High-Temp Inhibition	0.3 to 0.35	K^{-1}
slti	Slope of Low-Temp Inhibition	0.2 to 0.95	K^{-1}
Tran	Leaf Transmittance (Shortwave/Longwave and Green/Brown)	0.05 to 0.375	-
WP_{Min}	Wilting Point Minimum	0.16 to 1	m^{-3}
WSSP	Water Stress Shape Parameter	0.1 to 0.2	-
Z_1	Canopy Bottom	0.1 to 12	m
Z_2	Canopy Top	1 to 35	m

Table A6: Dynamic Phenology Parameters.

Name	Definition	Range	Units
AllocP (nlpool,nstage)	Phenology-Specific allocation fractions (per live pools and per phenology stage)	0 to 1	-
AL_{RL}	Assimilation Potential Running-Mean Length	10	days
AL_{RV}	Assimilation Potential Threshold	0.1	-
CL_C	Climatological LAI Coefficient	0.6 to 2.4	-
CL_G	Climatological LAI Maximum Offset	0.6 to 5.2	-
CL_L	Climatological LAI Minimum Offset	-0.4 to 3.2	-
$ClimP_A$	Climatological Suitability (*ClimP*) Exponential Adjustment	0 to 0.1	-
$ClimP_B$	*ClimP* Exponential Adjustment Base	0 to 800	-
$ClimP_C$	*ClimP* Multiplicative Adjustment Coef	0 to 3	-
$ClimP_D$	*ClimP* Multiplicative Adjustment Offset	0 to 0.6	-
$ClimP_{Min}$	*ClimP* Minimum Value	0.05 to 0.6	-
$ClimP_{Max}$	*ClimP* Maximum Value	1 to 2	-
CWA_{Type}	Climatological Ssuitability Water Availability Type 1 = Convective Precipitation 2 = Total Precipitation 3 = Root-Weighted Plant Available Water 4 = Root-Weighted Total Available Water	1 to 4	-
GL_{MinI}	Minimum Day Length for GSS (increasing day length)	10 to 24	hr
GL_{OffD}	Minimum Day Length for GSS (decreasing day length)	-13 to 4	hr
GT_{Len}	Valid Temperature Days for GSS	4 to 7	days
GT_{Min}	Minimum Temperature for GSS	268 to 288	K
GT_{Max}	Maximum Temperature for GSS	298 to 312	K
GW_{Len}	Days of Water Availability for GSS	4 to 6	days
GW_{Min}	Minimum Water Availability for GSS	0.12	-
LP_{Tran} *(nstage)*	Phenology-based Leaf (LAI) Transfer (per phenology stage)	0 to 0.5	Pool Fraction
nstage	Number of Phenological Stages	5	-

PI_{Thresh} *(nstage-1)*	Thresholds Between Phenology Stages (per phenology stage change)	0 to 1	-
PSD_{Ref}	Day Lenth Potential Reference	-1 to 2	hr
PSD_{Min}	Day Length Potential Minimum	0.38 to 1	-
PSD_{Mul}	Day Length Potential Daily Change	0 to 0.14	-
PSG_{Min}	Growth Potential Minimum	0.25 to 0.5	-
$PSWX_{Type}$	$PSWX$ type 1 = PAW_{FTop}, 2 = PAW_{FZW} 3 = $PAW_{FZW} \cdot 2$, 4 = No Stress for $PAW_{FZW} > 0$ 5 = TAW_{FTop}, 6 = TAW_{FZW} 7 = F_{RZ}, 8 = F_E	1 to 8	-
V_{Max} *(nstage)*	Rubisco Velocity (per phenology stage)	$0.1e^{-4}$ to $1.8e^{-4}$	$mol/m^2/s$

Table A7: Defined Phenology Parameters.

Name	Definition	Range	Units
AllocP (nlpool,nstage)	Phenology-Specific allocation fractions (per live pools and per phenology stage)	0 to 1	-
AL_{RL}	Assimilation factor running-mean length	7 to 10	days
AL_{RV}	Assimilation factor threshold to reset growing season	0.05 to 0.1	-
GL_{MinI}	Minimum Day Length for GSS (increasing day length)	10 to 24	hr
GL_{OffD}	Minimum Day Length for GSS (decreasing day length)	-13 to 4	hr
GP_{Aft}	Days After Max Precip for GSS	10 to 90	days
GP_{Bef}	Days Before Max Precip for GSS	70 to 90	days
GP_{Len}	Precip Running-Mean Length for GSS	30	days
GT_{Len}	Valid Temperature Days for GSS	4 to 7	days
GT_{Min}	Minimum Temperature for GSS	268 to 288	K
GT_{Max}	Maximum Temperature for GSS	298 to 312	K
GW_{Len}	Days of Water Availability for GSS	4 to 6	days
GW_{Min}	Minimum Water Availability for GSS	0.12	-
GDD_{TBase}	Growing Degree Day (GDD) base temperature	42 to 50	F
GDD_{TMax}	GDD Maximum Temperature	78 to 90	F
GPD	Crop Season Length Identifier (GDD or DAPD)	1 or 2	-
GSL_{Max}	Maximum Growing Season Length	140 to 260	day
Hrv_{Tran} *(ndpool + 2)*	Harvest Transfer Fractions (resp,rem,dp)	0 to 1	-
LP_{Tran} *(nstage)*	Phenology-based leaf pool (LAI) transfer (per phenology stage)	0 to 0.5	Pool Fraction
nstage	Number of phenological stages	10	-
PI_{Thresh} *(nstage-1)*	Thresholds between phenology stages (per phenology stage change)	0 to 1	-
$Seed_C$	Carbon Contained in Seed	2	g C
$Seed_R$	Daily Seed Carbon Released	0.2	g C
V_{Max} *(nstage)*	Rubisco Velocity (per phenology stage)	$0.1e^{-4}$ to $1.8e^{-4}$	$mol/m^2/s$

Table A8: Fire Parameters.

Name	Definition	Value
$FireF_C$	Coarse Dead Fraction	0.2
$FireF_L$	Leaf Fire Emission Fraction	0.3
$FireF_{ML}$	Metabolic Litter Fire Emission Fraction	0.2
$FireF_{SL}$	Structural Litter Fire Emission Fraction	0.2
$FireF_W$	Wood Fire Emission Fraction	0.1

Note: All parameters are unitless and a single value is specified for all PFTs.

Table A9: Grazing Parameters.

Name	Definition	Value
$Flag_{PFT}$	Grazing Flag Per PFT	T or F
Grz_{CFracP}	Fraction of Canopy C Grazed Daily (productive)	0.008
Grz_{CFracD}	Fraction of Canopy C Grazed Daily (sparse/non-productive)	0.003
Grz_{MLAI}	Minimum LAI for Grazing	0.7
Grz_{SLAI}	LAI Sparse/Productive Grazing Threshold	1.0
Grz_{Tran} *(ndpool+2)*	Grazing transfer fractions (per dead pool with remove and respire)	0 to 1

Note: All parameters are unitless and a single value is specified for all PFTs except for $Flag_{PFT}$.

Table A10: Allocation Parameters.

Name	Definition	Units
Adj_{Moist}	Use Moisture Adjust Allocations	T or F
Adj_{Temp}	Use Temperature Adjust Allocations	T or F

Table A11: Autotrophic Respiration Parameters.

Name	Definition	Range	Units
CR_{AMH}	Canopy resp assimilation high multiplier	0 to 4	-
CR_{AML}	Canopy resp assimilation low multiplier	0 to 1	-
CR_{AMax}	Canopy resp assimilation maximum	1 to 2	-
CR_{AMin}	Canopy resp assimilation minimum	0.4 to 1	-
CR_{FMin}	Canopy resp freeze inhibition minimum	0 to 0.3	-
CR_{FMul}	Canopy resp freeze inhibition multiplier	0 to 0.1	-
CR_{FRef}	Canopy resp freeze inhibition ref temperature	274 to 278	K
CR_{HMax}	Canopy resp high temperature maximum	1 to 3	-
CR_{HQ10}	Canopy resp high temperature Q10 base	1 to 2.2	-
CR_{HRef}	Canopy resp high temperature reference	295 to 313	K
E_{LP} *(nlpool)*	Respiration efficiency for live pools (per live pools)	0.3 to 0.95	-
GR_{Frac} *(nlpool)*	Growth respiration fraction (per live pools)	0.1 to 0.4	-
RRT_{AMH}	Root resp/transfer assim high multiplier	2 to 4	-
RRT_{AML}	Root resp/transfer assim low multiplier	0.6 to 1.5	-
RRT_{AMax}	Root resp/transfer assim maximum	1 to 1.2	-
RRT_{AMin}	Root resp/transfer assim minimum	0.6 to 1	-
RRT_{FMin}	Root resp/transfer freeze inhibit minimum	0.4 to 1	-
RRT_{FMul}	Root resp/transfer freeze inhibit multiplier	0.1 to 1	-
RRT_{FRef}	Root resp/transfer freeze inhibit ref temp	270 to 278	K
RRT_{HMax}	Root resp/transfer hot maximum	1 to 3	-
RRT_{HQ10}	Root resp/transfer hot Q10 base	1.8 to 2.2	-
RRT_{HRef}	Root resp/transfer hot ref temperature	293 to 311	K
RRT_{LMin}	Root resp/transfer LAI ratio minimum	1	-
RRT_{LMax}	Root resp/transfer LAI ratio maximum	1	-
τ *(nlpool)*	Pool turnover time (per live pool)	0.1 to 320	yr

Table A12: Senescence Parameters.

Name	Definition	Range	Units
LT_{DC}	Leaf transfer day length coefficient	0 to 0.0008	-
LT_{DMax}	Leaf transfer day length max (fraction per day)	0 to 0.08	-
LT_{DR}	Leaf transfer day length reference	0 to 6	hr
LT_{FMax}	Leaf transfer freeze max (fraction per day)	0 to 0.1	-
LT_{FQ10}	Leaf transfer freeze Q10 base	2.2	-
LT_{FR}	Leaf transfer freeze reference temperature	274 to 278	K
LT_{WB}	Leaf transfer water deficiency exponential base	0 to 0.07	-
LT_{WC}	Leaf transfer water deficiency coefficient	0 to 0.005	-
LT_{WMax}	Leaf transfer water deficiency max (fraction per day)	0 to 0.08	-
LT_{WR}	Leaf transfer water deficiency reference	0 to 0.12	-
TF *(nlpool,ndpool)*	Transfer Fraction (from live pool lp to dead pool dp)	0 to 1	-

Table A13: Heterotrophic Respiration Parameters.

Name	Definition	Range	Units
E_{DP} *(ndpool,ndpool2)*	Respiration efficiency for dead pools (from dead pool dp to dead pool dp2)	0.4 to 0.95	-
$HRT_{Sfc,AMH}$	Surface pool het resp/transfer assim high multiplier	0 to 2	-
$HRT_{Sfc,AML}$	Surface pool het resp/transfer assim low multiplier	0 to 0.6	-
$HRT_{Sfc,AMax}$	Surface pool het resp/transfer assim maximum	1 to 1.2	-
$HRT_{Sfc,AMin}$	Surface pool het resp/transfer assim minimum	0.1 to 1	-
$HRT_{Sfc,FMin}$	Surface pool het resp/transfer freeze minimum	0.1 to 1	-
$HRT_{Sfc,FMul}$	Surface pool het resp/transfer freeze multiplier	0.1 to 1	-
$HRT_{Sfc,FRef}$	Surface pool het resp/transfer freeze ref temp	274 to 278	K
$HRT_{Sfc,HMax}$	Surface pool het resp/transfer hot maximum	1 to 3	-
$HRT_{Sfc,HQ10}$	Surface pool het resp/transfer hot Q10 base	1.6 to 2.2	-
$HRT_{Sfc,HRef}$	Surface pool het resp/transfer hot ref temp	283 to 300	K
$HRT_{Sfc,PMin}$	Sfc pool het resp/trans precip inhibit min	0.1 to 1	-
$HRT_{Sfc,PML}$	Sfc pool het resp/trans precip inhibit multiplier	0.8 to 1	-
$HRT_{Soil,AMH}$	Soil het resp/transfer assim high multiplier	2	-
$HRT_{Soil,AML}$	Soil het resp/transfer assim low multiplier	0.6	-
$HRT_{Soil,AMax}$	Soil het resp/transfer assim maximum	1 to 1.2	-
$HRT_{Soil,AMin}$	Soil het resp/transfer assim minimum	0.6 to 1	-
$HRT_{Soil,FMin}$	Soil het resp/transfer freeze minimum	0.1 to 1	-
$HRT_{Soil,FMul}$	Soil het resp/transfer freeze multiplier	0.1 to 0.2	-
$HRT_{Soil,FRef}$	Soil het resp/transfer freeze ref temp	274	K
$HRT_{Soil,HMax}$	Soil het resp/transfer hot maximum	1 to 3	-
$HRT_{Soil,HQ10}$	Soil het resp/transfer hot Q10 base	1.6 to 2.2	-
$HRT_{Soil,HRef}$	Soil het resp/transfer hot ref temp	283 to 300	K
$HRT_{Soil,MMin}$	Soil het resp/trans moisture inhibition min	0.02 to 1	-
$HRT_{Soil,PAWMin}$	Soil het resp/trans PAW inhibition min	0.2 to 1	-
τ *(ndpool)*	Pool turnover time (per dead pools)	0.1 to 320	yr
TF_{DP} *(ndpool,ndpool)*	Transfer Fraction (from dead pool dp1 to dead pool dp2)	0 to 1	-

Table A14: Physical Constants.

Name	Definition	Value	Units
amagat	Molar Volume Reciprocal	44.6	mol/m^3
$amagat_{wv}$	Water-Vapor Adjusted *Amagat*	44.032476	mol/m^3
bco_{2m}	Mixed Layer CO_2 Concentration	370.0	*ppm*
$bcos_m$	Mixed Layer COS Concentraiton	500.0	*ppt*
$cosz_{min}$	Minimum Cosize of Zenith Angle	-0.1045	*radians*
cpice	Specific Heat of Ice	2117.27	$J/deg/kg$
cpliq	Specific Heat of Water	4188.0	$J/deg/kg$
cv	Specific Heat of Water Vapor (constant pressure)	1952.0	$J/deg/kg$
cwlim	Canopy Water Storage Limit	0.001	kg/m^2
dec_{max}	Maximum Declination	23.441	-
denh2o	Density of Water	1000.0	kg/m^3
denice	Density of Ice	917.0	kg/m^3
eccn	Eccentricity	0.016715	-
eqnx	Day of Vernal Equinox	80	*day*
gas_const_R	Gas Constant for Dry Air	287.0	$J/kg/K$
grav	Earth Gravity	9.81	m/s^2
gwctog	Water Storage Adjustment	0.25	-
gwlim	Ground Water Storage Limit	10.	kg/m^2
h2ohc	Water Heat Capacity	4.186E^6	$J/deg/m^3$
leafhc	Leaf Heat Capacity	837.2	$J/deg/m^3$
lvap	Latent Heat of Vaporization	2.25E^6	J/kg
lfus	Latent Heat of Fusion	0.3336E^6	J/kg
lsub	Latent Heat of Sublimation	$lvap + lfus$	J/kg
mol_bmze	Convert: mol C/m^2 to bushels/acre	4.248 (corn)	-
mol_bsoy	Convert: mol C/m^2 to bushels/acre	3.965 (soy)	-
mol_bwwt	Convert: mol C/m^2 to bushels/acre	3.965 (wheat)	-
mol_dw	Convert: mol C/m^2 to g DW/m^2	24.0	-
mol_mg	Convert: mol C/m^2 to Mg C/ha	0.12	-
mol_umol	Convert: mol C/m^2 to umol C/m^2	1.E6	-
mol_pmol	Convert: mol C/m^2 to pmol C/m^2	1.E12	-
$molc_{h2o}$	Moles per Liter of Water	55.36	mol/l
mwc	Molecular Weight of Carbon	12.0	g/mol
$NH_{Solstice}$	NH Longest Day of Year	172	*day*

po_{2m}	Mixed Layer O_2 Concentration	20900.0	ppm
$phmin$	Minimum Soil Potential	-1E^8	mm
π	Pi	3.1415926535897932384	-
π_{day}	Zenith Angle Constant	0.0172142	-
π_{peri}	Zenith Angle Constant	1.7924530506134	-
psb	PBL Mass Depth	50	hPa or mb
$psref$	Reference Pressure	1013.246	hPa
$p0_{sfc}$	Surface Pressure	1E^5	Pa
rv	Water Vapor Gas Constant	4.61E^2	-
$rstar$	Universal Gas Constant	8.3143	$m^3\ Pa/mol/K$
$Solar\_Const$	Solar Constant	1367.0	W/m^2
$SH_{Solstice}$	SH Longest Day of Year	355	Day
$snomel$	Latent Heat of Fusion of Ice	3.705185E^8	J/m^3
$spec\_heat\_cp$	Specific Heat at Constant Pressure	1005.0	$J/kg/K$
ssi	Irreducible Water Fraction of Snow	0.033	-
$stefan$	Stefan Boltzmann Constant	5.67E^{-8}	$W/m^2/K^4$
TF_{frz}	Freezing Temperature	32.0	F
TK_{air}	Thermal Conductivity of Air	0.023	$W/m/K$
TK_{wat}	Thermal Conductivity of Water	0.6	$W/m/K$
TK_{ice}	Thermal Conductivity of Ice	2.29	$W/m/K$
Ts_{ref}	Reference Temperature	373.15	K
T_{ref}	Reference Temperature	273.15	K
T_{ice}	Freezing Temperature of Water	273.15	K
Tbg_{min}	Minimum Snow Temperature	253.15	K
Tbg_{max}	Maximum Snow Temperature	273.15	K
Ti_{min}	Lowest Ice Temperature	173.16	K
Ti_{max}	Highest Ice Temperature	273.16	K
Tw_{min}	Lowest Water Temperature	173.16	K
Tw_{max}	Highest Water Temperature	373.16	K
$vkrmn$	Von Karmann Constant	0.35	-
$wimp$	Water Impermeability Level	0.05	-
$wpot_{fc}$	Water Potential At Field Capacity	-15.	J/kg
$wpot_{wp}$	Water Potential At Wilting Point	-1500.	J/kg
$wtfact$	High Water Table Areal Fraction	0.3	-
$zlnd$	Roughness Length for Land	0.01	m

Table A15: Specified Constants.

Name	Definition	Value	Units
$aadjustmin$	Phenology allocation adjustment minimum	0.02	-
$bstabl$	Surface Flux Constant	8.0	-
$bunstabl_M$	Surface Flux Constant	10.0	-
$bunstabl_T$	Surface Flux Constant	15.0	-
$cstabl$	Surface Flux Constant	10.0	-
$cunstabl_M$	Surface Flux Constant	75.0	-
$cunstabl_T$	Surface Flux Constant	75.0	-
$Clim_{Len}$	Climtological averaging length	3650	days
$CO2_{CASMin}$	CAS Depth Minimum for CO_2	4	m
COS_{CASMin}	CAS Depth Minimum for COS	10	m
COS_{ksoil}	COS Soil Decay Rate	1.2E^4	s^{-1}
$lftit$	Leaf Adjustment Reference Temperature	273.0	K
$lftif$	Leaf Adjustment Factor	1.3	-
$lgrw_{min}$	Leaf Growth Minimum	0.6	-
$moist_{mul}$	Moisture Adjustment Multiplier	2.8	-
rad_{c1}	Radiation Parameter	580.	-
rad_{c2}	Radiation Parameter	464.	-
rad_{c3}	Radiation Parameter	499.	-
rad_{c4}	Radiation Parameter	963.	-
rad_{c5}	Radiation Parameter	1160.	-
RH_{AStart}	Humidity stress curvature start	0.5	-
RH_{Exp}	Humidity stress curvature	2.2	-
$RH_{Exp,Crop}$	Humidity stress crop exponent	0.7	-
$RH_{NForest}$	Humidity stress min for needle forests	0.7	-
RH_{Tundra}	Humidity stress min for tundra	0.6	-
RST_{max}	Maximum Stomatal Resistance	5E^6	s/m
$RT_{moist,exp}$	Moisture Resp/Transfer Scalar Exponent	30.0	-
$RT_{moist,range}$	Moisture Resp/Transfer Scalar Range	0.98	-
$Seas_{Len}$	Seasonal averaging length	10	days
$Seas_{Len,Precip}$	Seasonal precipitation averaging length	18	days
SIF_{mu}	SIF Aerosol Optical Depth Parameter	-0.6	-
SIF_{perih}	SIF TOA Solar Parameter	1.7963	-

SIF_{a1}	SIF Parameter	1.93	-
SIF_{a2}	SIF Parameter	10.0	-
SIF_{kf0}	SIF Parameter	0.05	-
SIF_{kn0}	SIF Parameter	5.01	-
SIF_{kp0}	SIF Parameter	4.0	-
$snow_{c2}$	Snow Compaction Parameter	$23E^{-3}$	m^3/kg
$snow_{c3}$	Snow Compaction Parameter	$2.77E^{-6}$	s^{-1}
$snow_{c4}$	Snow Compaction Parameter	0.04	K^{-1}
$snow_{c5}$	Snow Compaction Parameter	2.0	-
$snow_{dm}$	Compaction Limit	100.0	kg/m^3
$snow_{eta0}$	Viscosity Coefficient	$9E^5$	kg/m^3
Tc_{bot}	Minimum Canopy Temperature	253.15	K
wftit	Wood/Stem Adjustment Reference Temperature	278.0	K
wftif	Wood/Stem Adjustment Factor	1.3	-
$wsat_{default}$	Default Water Saturation Fraction	0.95	-

Appendix B: Variables

Table B1: Soil Structure.

Name	Definition	Units
Dz *(nsoil+nsnow)*	Prognostic Soil/Snow Thickness (per soil/snow layer)	m
$Layer_z$ *(nsoil+nsnow)*	Soil/Snow Layer Interface Depth (per soil/snow layer)	m
$Node_z$ *(nsoil+nsnow)*	Soil/Snow Layer Node Depth (per soil/snow layer)	m

Table B2: Soil Properties.

Name	Definition	Range	Units
BD_{Dry}	Bulk Density of Dry Soil Material	-	kg/m^{-3}
Bee	Exponent	-	-
C_{Solid}	Heat Capacity (Soil Solids)	-	$J/m^3/K$
FC	Field Capacity (Volumetric)	0 to 1	m^{-3}
K_{Sat}	Hydraulic Conductivity at Saturation	-	m/s
PH_{Sat}	Tension at Saturation	-	m
$Poros$	Porosity	0 to 1	-
TK_{Dry}	Thermal Conductivity (Dry Soil)	-	W/m/K
$TK_{Mineral}$	Thermal Conductivity (Soil Minerals)	-	W/m/K
TK_{Sat}	Thermal Conductivity (Saturated Soil)	-	W/m/K
W_{Exp}	Combined Soil Moisture Exponent	0 to 1	-
W_{Opt}	Optimal Soil Moisture Saturation Fraction	0 to 1	-
W_{Sat}	Saturated Soil Moisture Saturation Fraction	0 to 1	-
WP	Wilting Point (Volumetric)	0 to 1	m^{-3}
Z_m	Texture-Based Constant	0 to 1	-

Table B3: Vegetation Properties.

Name	Definition	Units
cc1	Bulk boundary layer resistance coefficient	$(s/m)^{1/2}$
cc2	Ground to canopy air space resistance	-
$Clim_{LAI}$	Climatolotical LAI	m^2/m^2
FPAR	Fraction of absorbed fraction of photosynthetic radiation	-
gmudmu	Time-mean leaf projection	-
green	Green fraction of LAI	-
LAI	Leaf area index	m^2/m^2
LAI_T	Canopy total LAI (with dead grass)	m^2/m^2
RootF (nsoil)	Rooting Vertical Distribution (fraction per soil layer)	-
VCover	Fraction of vegetation cover	-
V_{Max}	Rubisco Velocity	$mol/m^2/s$
Z_0	Canopy snow-adjusted roughness length	m
Z_{0D}	Canopy roughness length	m
ZP_{DispD}	Zero-plane displacement	m
ZPD_{Adj}	Snow-adjusted zero-plane displacement	m
ZZ_{Temp}	Temperature height for mass flux	m
ZZ_{Wind}	Wind height for mass flux	m

Table B4: Prognostic Variables

Name	Definition	Units
C *(nlpool+ndpool, nsoil)*	Pool Carbon (per pool, soil layer)	$mol\ C\ m^{-2}$
$capacc_{liq}$	Canopy Surface Liquid	kg/m^2
$capacc_{snow}$	Canopy Surface Snow	kg/m^2
capacg	Ground Surface Liquid	kg/m^2
e_a	CAS Water Vapor Pressure	hPa
$pco2_a$	CAS CO_2 Partial Pressure	Pa
rst	Stomatal resistance	s/m
T_c	Canopy Temperature	K
T_a	Canopy Air Space (CAS) Temperature	K
nsl	Number of Snow Layers	-
Dz *(nsoil+nsnow)*	Soil/Snow Thickness (per soil/snow layer)	m
T_D *(nsoil+nsnow)*	Soil/Snow Temperature (per soil/snow layer)	K
WWW_{Liq} *(nsoil+nsnow)*	Soil/Snow Liquid Water (per soil/snow layer)	kg/m^2
WWW_{Ice} *(nsoil+nsnow)*	Soil/Snow Ice (per soil/snow layer)	kg/m^2

Table B5: Radiation Variables

Name	Definition	Units
$albedo_{VisB}$	Visible beam albedo	-
$albedo_{VisD}$	Visible diffuse albedo	-
$albedo_{NIRB}$	Near-Infrared (NIR) beam albedo	-
$albedo_{NIRD}$	NIR diffuse albedo	-
radc3c	Absorbed radiation by canopy	W/m^2
radc3g	Absorbed radiation by ground	W/m^2
$radfacc_{1,1}$	Canopy radiation absorption factor (visible, beam)	-
$radfacc_{1,2}$	Canopy radiation absorption factor (visible, diffuse)	-
$radfacc_{2,1}$	Canopy radiation absorption factor (NIR, beam)	-
$radfacc_{2,2}$	Canopy radiation absorption factor (NIR, diffuse)	-
$radfacg_{1,1}$	Ground radiation absorption factor (visible, beam)	-
$radfacg_{1,2}$	Ground radiation absorption factor (visible, diffuse)	-
$radfacg_{2,1}$	Ground radiation absorption factor (NIR, beam)	-
$radfacg_{2,2}$	Ground radiation absorption factor (NIR, diffuse)	-
radtc	Canopy net radiation	W/m^2
radtg	Ground net radiation	W/m^2
radts	Snow net radiation	W/m^2
radvbc	Visible beam radiation	W/m^2
radvdc	Visible diffuse radiation	W/m^2
radnbc	NIR beam radiation	W/m^2
radndc	NIR beam radiation	W/m^2
tsfc	Surface temperature	K

Table B6: Flux Variables

Name	Definition	Units
ct	Thermal transfer coefficient	-
cu	Momentum transfer coefficient	-
$drag$	Drag	kg/m^2/s
e_a	Canopy Air Space (CAS) water vapor pressure	hPA or mb
E_C	Canopy latent heat flux	J/m^2
E_{CI}	Latent heat flux, canopy interception (Puddles)	J/m^2
E_{CT}	Latent heat flux, canopy transpiration	J/m^2
E_G	Ground latent heat flux	J/m^2
E_{GI}	Latent heat flux, ground interception	J/m^2
E_{GS}	Latent heat flux, ground evaporation	J/m^2
E_S	Snow latent heat flux	J/m^2
fss	CAS sensible heat flux	W/m^2
fws	CAS latent heat flux	W/m^2
$hcap_C$	Canopy heat capacity	J/m^2/K
$hcap_{CAS}$	CAS heat capacity	J/m^2/K
H_C	Canopy sensible heat flux	J/m^2
H_G	Ground sensible heat flux	J/m^2
H_S	Snow sensible heat flux	J/m^2
r_a	CAS to mixed layer resistance	s/m
r_b	Canopy to CAS resistance	s/m
r_c	Bulk leaf to canopy resistance	s/m
r_d	Ground to CAS resistance	s/m
r_soil	Soil surface resistance	s/m
sh_{CAS}	CAS water vapor mixing ratio	kg/kg
$Stor_{HC}$	Canopy heat storage flux	W/m^2
$Stor_{HG}$	Ground heat storage flux	W/m^2
T_C	Canopy temperature	K
T_{CAS}	CAS temperature	K
TC_{Min}	Frost Canopy Temperature	K
TKE_{CAS}	CAS turbulent kinetic energy	J/kg
$u*$	Friction velocity	m/s
$VCap_{CAS}$	CAS vapor capacity	J/m2/hPa
$ventmf$	Ventilation mass flux	kg/m^2/s

Table B7: Photosynthesis Variables

Name	Definition	Units
$APAR$	Absorbed photosynthetically active radiation	mol/m^2/s
$APAR_{KK}$	Factor for scaling of leaf radiation	-
$assim$	Gross assimilation rate	mol C/m^2/s
$assim_D$	Daily assimilation rate	mol C/m^2/s
$assim_{OMC}$	Rubisco-limited assimilation	mol C/m^2/s
$assim_{OME}$	Light-limited assimilation	mol C/m^2/s
$assim_{OMS}$	Sink-limited assimilation	mol C/m^2/s
$assimfac_1$	Assimilation rate rubisco-limited stress factor	-
$assimfac_2$	Assimilation rate light-limited stress factor	-
$assimfac_3$	Assimilation rate sink-limited stress factor	-
$assimfac_4$	Total Assimilation rate stress factor	-
$assimpot$	Potential top leaf photosynthesis	mol C/m^2/s
$assimpot_{OMC}$	Potential rubisco-unlimited assimilation	mol C/m^2/s
$assimpot_{OME}$	Potential light-unlimited assimilation	mol C/m^2/s
$assimpot_{OMS}$	Potential sink-unlimited assimilation	mol C/m^2/s
F_{LH}	Leaf surface relative humidity potential ($rstfac_1$)	-
F_{RZ}	Rootzone water potential ($rstfac_2$)	-
F_T	Temperature potential ($rstfac_3$)	-
F_E	Environmental Photosynthetic Potential ($rstfac_4$)	-
$gamma$	CO_2 photocompensation point	Pa
PAR	Photosynthetically active radiation	mol/m^2/s
PAR_{NS}	Non-scattered PAR	mol/m^2/s
$PCO2_C$	Chloroplast CO_2 partial pressure	Pa
$PCO2_A$	CAS CO_2 partial pressure	Pa
$PCO2_I$	Leaf internal CO_2 partial pressure	Pa
$PCO2_S$	Leaf surface CO_2 partial pressure	Pa
rst	Prognostic stomatal resistance	s/m
$Soil_{Frz}$	Soil freeze function	-
$Soil_{FrzTG}$	Soil freeze function for top soil layer	-
$Soil_{FrzTD}$	Soil freeze function for second soil layer	-
$V_{Max,SS}$	Stressed rubisco velocity	mol/m^2/s

Table B8: Hydrology Variables (Surface or Single-Value)

$Clim_{PAWFRW}$	Climatological root-weighted PAW fraction	-
$Clim_{TAWFRW}$	Climatological root-weighted TAW fraction	-
infil	Water infiltrated into the top soil layer	mm
nsl	Prognostic number of snow layers	-
PAW_{FRW}	Root-weighted PAW	-
PAW_{FZW}	Soil layer thickness weighted PAW	-
PAW_{FTop}	Mean PAW fraction in top 3 soil layers	-
p0	Ground surface precipitation	mm
$pcpg_{rain}$	Ground surface rain precipitation	mm/s
$pcpg_{snow}$	Ground surface snow precipitation	mm/s
roff	Total subsurface runoff from soil layers	mm
roffo	Overland runoff	mm
S_c	Canopy wetness storage limit	kg/m^2
S_g	Ground wetness storage limit	kg/m^2
$snow_{gdepth}$	Depth of snow on ground	m
$snow_{gmass}$	Mass of snow on ground	kg/m^2
$snow_{cvfc}$	Snow vertical cover fraction	-
$snow_{gvfc}$	Snow ground cover fraction	-
TAW_{FRW}	Root-weighted TAW	-
TAW_{FTop}	Mean TAW fraction in top 3 soil layers	-
wetfracc	Canopy wetness fraction	-
wetfracg	Ground wetness fraction	-

Table B9: Hydrology Variables (Column)

Name	Definition	Units
eff_{poros} *(nsoil+nsnow)*	Soil/snow liquid effective porosity (per soil/snow layer)	-
PAW *(nsoil)*	Plant Available Water (per soil layer)	kg/m^3
rootr *(nsoil)*	Effective rooting fraction (per soil layer)	-
satfrac *(nsoil)*	Fraction of water saturation (per soil layer)	-
shcap *(nsoil+nsnow)*	Soil/Snow total heat capacity (per soil/snow layer)	J/m^2/K
TAW *(nsoil)*	Total Available Water (per soil layer)	kg/m^3
T_D *(nsoil+nsnow)*	Prognostic Soil/Snow Temperature (per soil/snow layer)	K
TK_{soil} *(nsoil+nsnow)*	Soil/Snow thermal conductivity (per soil/snow layer)	W/m/K
vol_{ice} *(nsoil)*	Soil ice water volume (per soil layer)	kg/m^3
vol_{liq} *(nsoil)*	Soil liquid water volume (per soil layer)	kg/m^3

Table B10: Solar-Induced Fluorescence (SIF) Variables

Name	Definition	Units
ϕ_D	Heat Dissipation Yield	-
ϕ_F	SIF Yield	-
ϕ_N	NPQ Yield	-
ϕ_P	Photosynthetic Yield	-
sif_{je}	Electron Transport	-
sif_{jo}	Max Electron Transport	-
sif_{jejo}	Fractional Transport (je/jo)	-
sif_{Kd}	Heat Dissipation Probability	-
sif_{Kf}	SIF Probability	-
sif_{Kn}	Non-photochemical quenching (NPQ) Probability	-
sif_{Kp}	Photosynthesis Probability	-
SIF	Solar-Induced Fluorescence (SIF)	W m^{-2} sr^{-1} nm^{-1}

Table B11: Carbonyl Sulfide (COS) Variables

Name	Definition	Units
$assim_{COS}$	COS Assimilation	mol/m^2/s
$grnd_{COS}$	COS Soil Uptake	mol/m^2/s
$flux_{COS}$	Canopy Air Space (CAS) COS Flux	mol/m^2/s
cos_{cap}	Air Capacity for COS Exchange	mol air/m^2
cos_{CAS}	CAS COS	mol COS/mol air
cos_i	Leaf Internal COS	mol COS/mol air
cos_s	Leaf Surface COS	mol COS/mol air
g_{COS}	Apparent Mesophyll Conductance and Biochemical Activity	mol/m^2/s
gt_{COS}	Total COS Conductance	mol/m^2/s
lru_{COS}	COS Leaf Relative Uptake	-
V_{MaxT}	Temperature-Adjusted Maximum Rubisco Velocity	mol/m^2/s

Table B12: Dynamic Phenology Variables

Name	**Phenology Variable**	**Units**	**Min**	**Max**
$AssimRM$	Running-Mean Assimilation	mol C/m^2/s	0	
$AssimSM$	Seasonal Maximum Mean Assimilation	mol C/m^2/s	0	
$Clim_{Cupr}$	Climatological Convective Precipitation	mm/s	0	
$Clim_{Pr}$	Climatological Precipitation	mm/s	0	
$Clim_{PAWFRW}$	Climatological Root-Weighted PAW	-	0	1
$Clim_{TAWFRW}$	Climatological Root-Weighted TAW	-	0	1
$ClimLAI_{Max}$	Maximum Climatological LAI	m^2/m^2	0	
$ClimLAI_{Min}$	Minimum Climatological LAI	m^2/m^2	0	
$ClimP$	Climatological Suitability	-	CP_{Min}	CP_{Max}
$ClimW$	Climatological Water Availability	-	0	1
$FlagA$	Assimilation Flag	T or F		
$FlagG$	Growing Season Flag	T or F		
Name	**Diagnostic Potential**	**Units**	**Min**	**Max**
PF_A	Running-Mean Assimilation Potential	-	0	1
PF_E	Running-Mean Environmental Potential	-	0	1
PF_{WA}	Running-Mean Water Availability Potential	-	0	1
PF_{Wx}	Mean Weather Potential	-	0	1
$PF_{Wx,SM}$	Mean Weather Potential Seasonal Maximum	-	0	1
PI	Phenology Stage Index	-	0	1
PI_{Stage}	Phenology Stage	-	1	$nstage$
PS_{DayL}	Phenology Stage Day Length Potential	-	0	1
PS_{Grw}	Phenology Stage Growth Potential	-	0	1
PS_{Wx}	Phenology Stage Weather Potential	-	0	1
Name	**Environmental Variables**	**Units**	**Min**	**Max**
$DayL$	Day Length	hr	0	24
$DayL_{dt}$	Change in Day Length	hr	0	0.1
$DayL_{Max}$	Maximum Day Length	hr	0	24
TM_D	Daily Mean Temperature	K		
Name	**Water Availability Metrics**	**Units**	**Min**	**Max**
F_E	Environmental Potential	-	0	1
F_{RZ}	Root-Zone Soil Moisture Potential	-	0	1
PAW_{FTop}	Root-Weighted PAW in Top Three Layers	-	0	1
PAW_{FZW}	Soil Layer Thickness-Weighted PAW	-	0	1
TAW_{FTop}	Root-Weighted TAW in Top Three Layers	-	0	1
TAW_{FZW}	Soil Layer Thickness-Weighted TAW	-	0	1

Table B13: Defined Phenology Variables

Name	**Crop Variable**	**Units**
DAPD	Days After Planting Date	days
DAPDAF	Days After Planting Date Above Freezing	days
FlagG	Growing Season Flag	T or F
FlagP	Precipitation Flag	T or F
GDD	Growing Degree Days	-
PF_{Pr}	Running-Mean Precipitation	mm/day
$PF_{Pr,SM}$	Seasonal Maximum Precipitation	mm/day
$PF_{Pr,SDOY}$	Day of Seasonal Maximum Precipitation	DOY
$PF_{Pr,CDOY}$	Climatological Mean Day of Seasonal Max Precip	DOY
PI	Phenology Stage Index	-
PI_{Stage}	Phenology Stage	-
TM_{DF}	Daily Mean Temperature	Degrees F
Name	**Pool Variable**	**Units**
$Gain_{Seed,lp}$ *(nlpool)*	Seed Carbon Gain to Live Pools (per live pool)	mol C/m^2
Hrv_C	Total Harvested Carbon	mol C/m^2
$Gain_{Hrv,dp}$ *(ndpool)*	Harvested Carbon Gain to Dead Pools (per dead pool)	mol C/m^2
$Loss_{Hrv,lp}$ *(nlpool)*	Harvested Carbon Loss from Live Pools (per live pool)	mol C/m^2
$Resp_{Hrv}$	Harvested Carbon Respired	mol C/m^2
$Rmvd_{Hrv}$	Harvested Carbon Removed	mol C/m^2
$Seed_{Pool}$	Seed Pool Carbon	Mol C/m^2

Table B14: Fire Variables

Name	**Fire Variables**	**Units**
nd_{Fire}	Number of Days Burned	days
Name	**Pool Variables**	**Units**
$Loss_{Fire}$ *(npool)*	Fire Carbon Loss from Live and Dead Pools (per pool)	mol C/m^2
$Resp_{Fire}$	Fire Respiration	mol C/m^2/s
$Rmvd_{Fire}$	Fire Respired But Not Removed	mol C/m^2

Table B15: Grazing Variables

Name	**Grazing Variables**	**Units**
nd_{Grz}	Number of Days Grazed	days
Name	**Pool Variables**	**Units**
$Gain_{Grz,dp}$ *(ndpool)*	Grazed Carbon Gain to Dead Pools (per dead pool)	mol C/m^2
$Loss_{Grz,cp}$ *(ncpool)*	Grazed Carbon Loss from Canopy Pools (per canopy pool)	mol C/m^2
$Resp_{Grz}$	Grazed Carbon Respired	mol C/m^2/s
$Rmvd_{Grz}$	Grazed Carbon Removed	mol C/m^2

Table B16: Allocation Variables

Name	**Allocation Variables**	**Units**
$Alloc_{lp}$ *(nlpool)*	Allocation Fractions (per live pool)	-
$AllocA_{lp}$ *(nlpool)*	Weather-Based Allocation Adjustment (per live pool)	-
$AllocAM_{lp}$ *(nlpool)*	Soil Moisture Allocation Adjustment (per live pool)	-
$AllocAT_{lp}$ *(nlpool)*	Temperature Allocation Adjustment (per live pool)	-
$Assim_{Day}$	Daily Assimilation	mol C/m^2/day
$TMin_{Day}$	Daily Minimum Temperature	K
Name	**Environmental Potentials**	**Units**
AF_{LeafF}	Leaf Freeze Allocation Adjustment Potential	-
AF_{Root}	Root Allocation Adjustment Potential	-
AF_{RZ}	Daily Mean Root-Zone Soil Moisture Potential	-
AF_{Wood}	Wood Allocation Adjustment Potential	-
AF_{WoodF}	Wood Freeze Allocation Adjustment Potential	-
AF_{WoodT}	Wood Temperature Allocation Adjustment Potential	-
Name	**Pool Variables**	**Units**
Distrib (nlpool, nsoil)	Soil Carbon Vertical Distribution (fraction per soil layer, per live pools)	-
$Gain_{A,lp}$ *(nlpool)*	Assimilated Carbon Gain to Live Pools (per live pool)	mol C/m^2

Table B17: Autotrophic Respiration Variables

Name	Autotrophic Respiration Variables	Units
$krate_r$ *(nlpool,nsoil)*	Scaled Maintenance Loss Rate (per live pool, per soil layer)	1/s
MCR_{Assim}	Canopy Assimilation Scalar	-
MCR_{Freeze}	Canopy Freeze Inhibition	-
MCR_{Hot}	Canopy High Temperature Exponential	-
MCR_{Scale}	Combined Canopy Respiration Scalar	-
MRR_{Assim}	Root-Weighted Root Assimilation Scalar	-
MRR_{Freeze}	Root-Weighted Root Freeze Inhibition	-
$MRR_{Freeze,Lay}$ *(nsoil)*	Root Freeze Inhibition (per soil layer)	-
MRR_{Hot}	Root-Weighted Root High Temperature Exponential	-
$MRR_{Hot,Lay}$ *(nsoil)*	Root High Temperature Exponential (per soil layer)	-
MRR_{Scale}	Root-Weighted Combined Root Respiration Scalar	-
$MRR_{Scale,Lay}$ *(nsoil)*	Combined Root Respiration Scalar (per soil layer)	-
Name	**Environmental Variables**	**Units**
$Clim_{Assim}$	Climatological Assimilation Rate	mol C/m^2/s
Name	**Pool Variables**	**Units**
$Loss_{GResp}$ *(nlpool)*	Growth Respiration Live Pool Loss (per live pool)	mol C/m^2
$Loss_{MResp}$ *(nlpool,nsoil)*	Maintenance Respiration Live Pool Loss (per live pool, per soil layer)	mol C/m^2
Name	**Respiration Rates**	**Units**
R_A	Autotrophic Respiration	mol C/m^2/s
R_G	Growth Respiration	mol C/m^2/s
R_{Leaf}	Leaf Respiration	mol C/m^2/s
R_M	Maintenance Respiration	mol C/m^2/s
R_{NVeg}	Non-Vegetation Respiration	mol C/m^2/s
R_{Root}	Root Respiration	mol C/m^2/s

Table B18: Senescence Variables

Name	**Senescence Variables**	**Units**
T_D	Litterfall Daylength Transfer Fraction	-
T_F	Litterfall Freezing Temperature Transfer Fraction	-
T_P	Litterfall Phenology Transfer Fraction	-
T_W	Litterfall Water Deprivation Transfer Fraction	-
Name	**Pool Variables**	**Units**
$Gain_{TL}$ *(ndpool,nsoil)*	Dead Pool Gain From Live Pools (per dead pool, per soil layer)	mol C/m^s
$Loss_{LF}$ *(nlpool)*	Litterfall Live Pool Loss (per live pool)	mol C/m^2
$Loss_T$ *(nlpool,nsoil)*	Turnover Live Pool Loss (per live pool, per soil layer)	mol C/m^2

Table B19: Heterotrophic Respiration Variables

Name	Heterotrophic Respiration Variables	Units
$krate_r$ *(ndpool,nsoil)*	Scaled Loss Rate (per dead pool, per soil layer)	1/s
$MH_{Sfc,Assim}$	Surface Pool Assimilation Scalar	-
$MH_{Sfc,Freeze}$	Surface Pool Freeze Inhibition	-
$MH_{Sfc,Hot}$	Surface Pool High Temperature Exponential	-
$MH_{Sfc,Precip}$	Surface Pool Precipitation Exponential	-
$MH_{Sfc,Scale}$	Combine Surface Pool Respiration Scalar	-
$MH_{Soil,Freeze}$ *(nsoil)*	Soil Pool Freeze Inhibition (per soil layer)	-
$MH_{Soil,Hot}$ *(nsoil)*	Soil Pool High Temperature Exponential (per soil layer)	-
$MH_{Soil,Moist}$ *(nsoil)*	Soil Pool Moisture Scalar (per soil layer)	-
$MH_{Soil,PAW}$ *(nsoil)*	Soil Pool PAW Scalar (per soil layer)	-
$MH_{Soil,Scalar}$ *(nsoil)*	Combined Soil Pool Respiration Scalar (per soil layer)	-
Name	**Environmental Variables**	**Units**
Pr_{Clim}	Climatological Precipitation Rate	mm/day
Pr_{Seas}	Seasonal Precipitation Rate	mm/day
Name	**Pool Variables**	**Units**
$Gain_{TD}$ *(ndpoolnsoil)*	Dead Pool Gain from Dead Pool Transfers (per dead pool, per soil layer)	mol C/m^2
$Loss_{HR}$ *(ndpool,nsoil)*	Heterotrophic Respiration Dead Pool Loss (per dead pool, per soil layer)	mol C/m^2
$Loss_{HT}$ *(ndpool,nsoil)*	Decay Dead Pool Loss (per dead pool, per soil layer)	mol C/m^2
Name	**Respiration Rates**	**Units**
R_H	Heterotrophic Respiration	mol C/m^2/s
R_{Soil}	Soil Respiration	mol C/m^2/s
R_{SoilNR}	Dead Soil Respiration (Without Roots)	mol C/m^2/s